To the Graduate Council:

I am submitting herewith a dissertation written by Bryan Lamar Broadhead entitled "A Nuclear Data Adjustment Methodology Utilizing Resonance Parameter Sensitivities and Uncertainties." I have examined the final copy of this dissertation for form and content and recommend that it be accepted in partial fulfillment of the requirements for the degree of Doctor of Philosophy, with a major in Nuclear Engineering.

H.L. Dodds, Jr., Major Professor

We have read this dissertation
and recommend its acceptance.

Accepted for the Council:

Vice Chancellor
Graduate Studies and Research

A NUCLEAR DATA ADJUSTMENT METHODOLOGY UTILIZING RESONANCE PARAMETER SENSITIVITIES AND UNCERTAINTIES

A Dissertation

Presented for the

Doctor of Philosophy

Degree

The University of Tennessee, Knoxville

Bryan Lamar Broadhead

June 1983

ACKNOWLEDGMENTS

The author wishes to express his sincere appreciation for the encouragement and support of his major professor, Dr. H.L. Dodds, Jr., and the dissertation committee members at the University of Tennessee, Dr. G. deSaussure, Dr. F.W. Stallman, Dr. R.B. Perez, and Dr. P.F. Pasqua. The author is also indebted to the many helpful comments and suggestions by Mr. N.M. Greene, Dr. J. Barhen, and Dr. M.L. Williams of the Oak Ridge National Laboratory.

Appreciation is also expressed to the Computer Sciences and Engineering Physics Divisions of the Oak Ridge National Laboratory for their funding of this work and to my wife, Kathy, without whose help and encouragement this work would not have been possible.

ABSTRACT

This work presents the development and demonstration of a Nuclear Data Adjustment Method that allows inclusion of both energy and spatial self-shielding into the adjustment procedure. The resulting adjustments are for the basic parameters (i.e. resonance parameters) in the resonance regions and for the group cross sections elsewhere. The majority of this development effort concerns the production of resonance parameter sensitivity information which allows the linkage between the responses of interest and the basic parameters.

The resonance parameter sensitivity methodology developed herein usually provides accurate results when compared to direct recalculations using existing and well-known cross section processing codes. However, it has been shown in several cases that self-shielded cross sections can be very non-linear functions of the basic parameters. For this reason caution must be used in any study which assumes that a linear relationship exists between a given self-shielded group cross section and its corresponding basic data parameters.

The study also has pointed out the need for more approximate techniques which will allow the required sensitivity information to be obtained in a more cost effective manner.

TABLE OF CONTENTS

LIST OF TABLES

LIST OF FIGURES

CHAPTER I

INTRODUCTION

The Nuclear Data Adjustment procedure developed and demonstrated in this dissertation is a next generation of the current cross section adjustment procedures. Current generation cross section adjustment procedures involve the combination of differential nuclear data measurements (i.e. evaluated cross sections such as ENDF/B) with integral data measurements (i.e. k_{eff}, fission ratios, central worths, etc.) to obtain "newly evaluated" or "adjusted" cross section data and integral data. This combination procedure is the so-called Least Squares Adjustment procedure (see Appendix A). The steps required to perform such an analysis are generally (1) processing of uncertainty information about the differential nuclear data, (2) calculating detailed sensitivity information which will allow propagation of the differential data uncertainties to the integral data values, and (3) the calculation of the integral data values with the differential nuclear data values. Thus, the differential data measurements and the integral data measurements are "combined" with this procedure to produce the "best" estimates of each in the least squares sense. The mathematics of this technique are founded on Bayes Theorem and are detailed in Chapter III as well as many other places[1-4]. However, current generation Cross Section Adjustment Procedures have some inherent limitations. All techniques to date assume that the so-called shielding factors (both energy and spatial) have no uncertainty. The impact on the cross section adjustment is the implication that the infinitely dilute cross section can be changed

without affecting the shielding factors. While this approximation is good outside the resonance range, near resonances it breaks down. Greenspan[5] has shown that the uncertainty in the energy shielding factors is only about 10% of that due to the infinitely dilute cross sections in the unresolved region. Therefore, most of the adjustment studies done to date have been for fast reactors in which the primary region of interest is in the unresolved region.

In the resolved resonance range, the primary region of interest for thermal reactors, Greenspan has shown that uncertainties in the energy shielding factors are in some cases equal to the uncertainty in the infinitely dilute cross sections. Thus, it would appear that the inclusion of self-shielding effects in an Uncertainty Analysis and Data Adjustments for thermal reactors is very important.

The Nuclear Data Adjustment technique presented herein will allow for several improvements over current technology. First, the remaining approximations in the region of fast reactor interest (unresolved region) can be removed. The use of adjustment techniques will also now be feasible for use on thermal and intermediate reactors (LWR, HWR, HTGR,etc.). These techniques can be used either to obtain adjustments in the energy self-shielding factors or to obtain adjustments in the resonance parameters. Both procedures adjust the group cross sections outside the resonance region and produce the same results although in a slighty different form. Also new in this work is the representation of the uncertainties in the spatial self-shielding effect.

This work has been divided into several sections. The Sensitivity

Coefficients to the Basic Nuclear Data Methodology is described in Chapter II. The Generalized Data Adjustment Methodology using a Bayes Theorem approach is presented in Chapter III. Chapter IV describes the calculation of TRX-1 spectrum and integral values. This new technique requires two types of sensitivity coefficients. The first type is the conventional cross section sensitivity which relates changes in the integral values to changes in the group cross sections. The second type of sensitivity information is the resonance parameter sensitivity which will be developed in this dissertation and relates changes in the group cross sections to changes in the individual resonance parameters. The calculations of the conventional sensitivities, the resonance parameter sensitivities, and the parameter covariance information are detailed in Chapters V-VII, respectively. Chapter VIII shows how all the input to the adjustment procedure should be assembled and presents the results of a demonstration adjustment. Conclusions and Recomendations for Future Work are presented in Chapters IX and X, respectively.

CHAPTER II

SENSITIVITY COEFFICIENTS OF BASIC NUCLEAR DATA METHODOLOGY

Several methods have been outlined for the calculation of basic nuclear data sensitivities.[5] These include the consistent bilinear method, where a Generalized Perturbation Theory approach is utilized, and the consistent flux method where either direct perturbations are made or analytical methods are utilized. The method employed in this work falls into the consistent flux class with several improvements over previous work.[6] Further discussion of this method will consider the resolved and unresolved regions separately.

In the resolved region the following Single Level Breit-Wigner (SLBW) equations represent the point-wise infinitely-dilute cross sections at zero degrees K:[7]

$$\sigma_t(E) = \sum_{\ell} \sigma_t^{\ell}(E) = \text{total cross section} , \qquad \text{II-1}$$

where

$$\sigma_t^{\ell}(E) = (2\ell + 1)\frac{4\pi}{k^2}\sin^2\phi_\ell + \frac{\pi}{k^2}\sum_J g_J \sum_\lambda \frac{N_\lambda}{D_\lambda} ,$$

$$N_\lambda = \Gamma^2_{n\lambda}\cos 2\phi_\ell - 2\Gamma_{n\lambda}(\Gamma_{\gamma\lambda}+\Gamma_{f\lambda})\sin^2\phi_\ell + 2(E-E'_\lambda)\Gamma_{n\lambda}\sin 2\phi_\ell ,$$

$$D_\lambda = (E-E'_\lambda)^2 + (1/4)\Gamma^2_\lambda ;$$

$$\sigma_c(E) = \sum_{\ell} \sigma_c^{\ell}(E) = \text{capture cross section} , \qquad \text{II-2}$$

where

$$\sigma_c^{\ell}(E) = \frac{\pi}{k^2} \sum_J g_J \sum_\lambda \frac{N_\lambda^c}{D_\lambda} \quad ,$$

$$N_\lambda^c = \Gamma_{n\lambda}\Gamma_{\gamma\lambda} \; ;$$

$$\sigma_f(E) = \sum_{\ell} \sigma_f^{\ell}(E) = \text{fission cross section,} \qquad \text{II-3}$$

where

$$\sigma_f(E) = \frac{\pi}{k^2} \sum_J g_J \sum_\lambda \frac{N_\lambda^f}{D_\lambda} \; ,$$

$$N_\lambda^f = \Gamma_{n\lambda}\Gamma_{f\lambda} \; ;$$

$$\sigma_e(E) = \sum_{\ell} \{\sigma_t^{\ell}(e) - \sigma_c^{\ell}(E) - \sigma_f^{\ell}(E)\} = \text{elastic cross section,} \qquad \text{II-4}$$

where

$$g_J = \frac{2J+1}{2(2I+1)} \quad ,$$

$$\Gamma_{n\lambda} = \frac{P_{\ell}(E)\Gamma_{n\lambda}^{\circ}}{P_{\ell}(E_\lambda)} = \text{the neutron width for resonance } \lambda \; ,$$

$\Gamma_\lambda = \Gamma_{n\lambda} + \Gamma_{\gamma\lambda} + \Gamma_{f\lambda}$ = the total width for resonance λ ,

E_λ = the resonance energy of resonance λ ,

$\Gamma_{\gamma\lambda}$ = the capture width for resonance λ ,

$\Gamma_{f\lambda}$ = the fission width for resonance λ ,

$\Gamma_{n\lambda}^{\circ} = \Gamma_{n\lambda}(E_\lambda)$,

J = the spin of the compound nucleus ,

I = the spin of the target nucleus ,

$$E'_\lambda = E_\lambda + \frac{S_{\ell}(E_\lambda) - S_{\ell}(E)}{2P_{\ell}(E_\lambda)} \Gamma_{n\lambda}(E_\lambda) \; ,$$

$$k = 2.196771 \times 10^{-3} \, A/(A+1.0) \, \sqrt{E} \quad ,$$

A = ratio of mass of particular isotope to that of a neutron ,

S_ℓ = the shift factor ,

P_ℓ = the penetration factor ,

$\phi_\ell = \phi_\ell(\hat{a})$ = the phase shift,

$\hat{a}$ = the effective scattering radius.

The initial objective is to analytically obtain the partial derivatives of the above equations to the basic parameters, $\Gamma_{\gamma\lambda}$, $\Gamma_{f\lambda}$, $\Gamma_{n\lambda}{}^{\circ}$, σ_o, and $\hat{a}$. The equations for the capture cross section derivatives follow:

$$\frac{\partial \sigma_c{}^{\ell}(E)}{\partial \Gamma_{\gamma\lambda}} = \frac{\pi}{k^2} g_J \left[\frac{\Gamma_{n\lambda}}{D_\lambda{}^c} - \frac{\Gamma_{n\lambda}\Gamma_{\gamma\lambda}\Gamma_\lambda}{2D_\lambda{}^{c\ 2}}\right] , \qquad \text{II-5}$$

$$\frac{\partial \sigma_c{}^{\ell}(E)}{\partial \Gamma_{f\lambda}} = -\frac{\pi}{k^2} g_J \left[\frac{\Gamma_{n\lambda}\Gamma_{\gamma\lambda}\Gamma_\lambda}{2D_\lambda{}^{c\ 2}}\right] , \qquad \text{II-6}$$

$$\frac{\partial \sigma_c{}^{\ell}(E)}{\partial \Gamma_{n\lambda}{}^{\circ}} = \frac{\pi}{k^2} g_J \left[\frac{Y\Gamma_{\gamma\lambda}}{D_\lambda} - \frac{\Gamma_{n\lambda}\Gamma_{\gamma\lambda}}{D_\lambda{}^2}\{2(E-E'_\lambda)Z + .5\Gamma_\lambda Y\}\right] , \qquad \text{II-7}$$

$$\frac{\partial \sigma_c{}^{\ell}(E)}{\partial \sigma_o} = \frac{\partial \sigma_c{}^{\ell}(E)}{\partial \hat{a}} = 0 , \qquad \text{II-8}$$

where

$Y = P_\ell(E)/P_\ell(E_\lambda)$,

$Z = \partial E'_\lambda / \partial \Gamma_{n\lambda}{}^{\circ}$.

The equations for fission cross sections are of the same form with Γ_γ replaced by Γ_f. The equations for the total cross sections take on a slightly different form as shown below.

$$\frac{\partial \sigma_t^{\ell}(E)}{\partial \Gamma_{x\lambda}} = \frac{\pi}{k^2} g_J \left[\frac{\Gamma_{n\lambda}\cos 2\phi_\ell}{D_\lambda} - \frac{2N_\lambda \Gamma_\lambda}{D_\lambda^2}\right] \quad , x = \gamma \text{ or } f \ , \qquad \text{II-9}$$

$$\frac{\partial \sigma_t^{\ell}(E)}{\partial \Gamma_{n\lambda^\circ}} = \frac{\pi}{k^2} g_J \left[\frac{X\cos 2\phi_\ell + 2Y\sin 2\phi_\ell (E-E'_\lambda) - 2\Gamma_{n\lambda}\sin 2\phi_\ell Z}{D_\lambda}\right.$$

$$\left. - \frac{N_\lambda}{D_\lambda^2}\{2(E'_\lambda - E)Z + .5\Gamma_\lambda Y\}\right] , \qquad \text{II-10}$$

$$\frac{\partial \sigma_t^{\ell}(E)}{\partial \hat{a}} = \frac{4\pi}{k^2}(2\ell+1)2\sin\phi_\ell \cos\phi_\ell V$$

$$+ \frac{\pi}{k^2} \sum_J g_J \sum_\lambda \left[\frac{-2\Gamma_{n\lambda}\Gamma_\lambda \sin 2\phi_\ell + 4\Gamma_{n\lambda}\cos 2\phi_\ell (E-E'_\lambda)}{D_\lambda}\right] V \ , \qquad \text{II-11}$$

where

$$X = (\Gamma_{n\lambda} + \Gamma_\lambda)Y \ ,$$

$$V = \partial\phi_\ell / \partial \hat{a} \ .$$

The elastic cross section derivatives are similar to the total but in most cases have additional terms.

The next step is to Doppler broaden these point-wise derivatives. We begin by writing the free-gas model equation for Doppler broadening.[8]

$$\sigma_x(E,T_2) = \frac{1}{2E}\sqrt{\alpha/\pi} \int_0^\infty dE_r \, E_r^{1/2} \, \sigma_x(E,T_1)$$

$$\cdot \left[e^{-\alpha(E^{1/2}-E_r^{1/2})^2} - e^{-\alpha(E^{1/2}+E_r^{1/2})^2}\right] \ , \qquad \text{II-12}$$

with

$$\alpha = A/k(T_2 - T_1) \ ,$$

E_r = relative energy .

By differentiating equation II-12 with respect to the resonance parameter of interest, q_k, we obtain:

$$\frac{\partial \sigma_x(E,T_2)}{\partial q_k} = \frac{1}{2E}\sqrt{\alpha/\pi}\int_0^\infty dE_r\, E_r^{1/2}\,\frac{\partial \sigma_x(E_r,T_1)}{\partial q_k} \cdot \left[e^{-\alpha(E^{1/2}-E_r^{1/2})^2} - e^{-\alpha(E^{1/2}+E_r^{1/2})^2}\right] . \qquad \text{II-13}$$

The method used to solve equation II-13 is similar to that used in the MINX[9] cross section processing code. The method involves assuming a linear interpolation between tabulated values of the derivative (see Appendix B). This approach differs from that of Greenspan who uses psi and chi type formalism to perform the Doppler broadening. This method is more accurate than Greenspan's approach especially in the wings of the resonance where large errors can occur using the psi and chi functions.

The next step in the development of the Resonance Parameter Sensitivities is to group average and resonance self-shield the Doppler broadened point values. This is accomplished via the so-called Bondarenko method,[10] where the weighting function for cross section averaging process is represented as:

$$\phi(E,T,\sigma_0) = \frac{C(E)}{\sigma_t(E,T) + \sigma_0} , \qquad \text{II-14}$$

where C(E) is a continuous slowly varying function (normally 1/E), and σ_0 is the background cross section used to incorporate varying degrees

of resonance self-shielding. The value for the group cross section using this weight function is then:

$$\sigma_{xg}(\sigma_o,T) = \frac{\int_g \phi(E,T,\sigma_o)\sigma_x(E,T)dE}{\int_g \phi(E,T,\sigma_o)dE} = \frac{N_g}{D_g} \qquad \text{II-15}$$

Now taking derivatives of the above equation with respect to the resonance parameters results in the following equation:

$$\frac{\partial\sigma_{xg}(\sigma_o,T)}{\partial q_k} = \frac{1}{D_g}\left[\int_g \{\phi(E,T,\sigma_o)\frac{\partial\sigma_x(E,T)}{\partial q_k} + \sigma_x(E,T)\frac{\partial\phi(E,T,\sigma_o)}{\partial q_k}\}dE \right. \qquad \text{II-16}$$

$$\left. - \sigma_{xg}(\sigma_o,T)\int_g \frac{\partial\phi(E,T,\sigma_o)}{\partial q_k}dE\right] .$$

In practice the σ_o and T dependence are usually represented in a so-called f-factor, where

$$f_{xg}(\sigma_o,T) = \frac{\sigma_{xg}(\sigma_o,T)}{\sigma_{xg}(\infty,T)} , \qquad \text{II-17}$$

where $\sigma_{xg}(\sigma_o,T)$ is the shielded group cross section, and $\sigma_{xg}(\infty,T)$ is the infinitely dilute group cross section. Thus, the following expression is obtained:

$$\frac{q_k}{f_{xg}(\sigma_o,T)}\cdot\frac{\partial f_{xg}(\sigma_o,T)}{\partial q_k} = \frac{q_k}{\sigma_{xg}(\sigma_o,T)}\cdot\frac{\partial\sigma_{xg}(\sigma_o,T)}{\partial q_k}$$

$$- \frac{q_k}{\sigma_{xg}(\infty,T)}\cdot\frac{\partial\sigma_{xg}(\infty,T)}{\partial q_k} . \qquad \text{II-18}$$

These f-factor sensitivities (eq. II-18) are tabulated at various values of σ_o (i.e. 10^{-1}, 10^0, 10^1, 10^2, 10^3, 10^6, 10^{10}). The sen-

sitivities corresponding to a given value of σ_0 for a particular system being modelled can then be interpolated using methods similar to the methods utilized for the cross sections. The most promising of these appears to be a power method interpolation scheme developed by N. M. Greene.[11]

The unresolved resonance region offers a considerable amount of complexity due to the statistical nature of the cross section representation. We begin our development by rewriting equation II-15, the equation for Bondarenko weighted group-averaged cross sections, with energy limits E_1 to E_2 and E^* some value in that range.

$$\sigma_x(E^*,\sigma_0) = \frac{\int_{E_1}^{E_2}\phi(E,T,\sigma_0)\sigma_x(E,T)dE}{\int_{E_1}^{E_2}\phi(E,T,\sigma_0)dE} = \frac{N^x(E^*)}{D(E^*)} \qquad \text{II-19}$$

If we write equation II-19 explicitly in terms of many resonances, λ, and resonance sequences, s,

$$\sigma_x(E^*,\sigma_0) = \frac{N_r^x(E,E^*)}{D(E,E^*)} + \sigma_{x_f}(E^*) + \sigma_p(E^*)\delta_{xe} \quad , \qquad \text{II-20a}$$

where

$$N_r^x(E,E^*) = \int_{E_1}^{E_2} \frac{\sum_s \sum_\lambda \sigma_{x\lambda}^s(E,E^*)dE}{\sum_s \sum_\lambda \sigma_{t\lambda}^s(E,E^*)+\sigma_p} \quad , \qquad \text{II-20b}$$

$$D(E,E^*) = \int_{E_1}^{E_2} \frac{dE}{\sum_s \sum_\lambda \sigma_{t\lambda}^s(E,E^*)+\sigma_p} \quad , \qquad \text{II-20c}$$

$$\sigma_x(E,E^*,T) = \sum_s \sum_\lambda \frac{\sigma_{0\lambda}^s(E^*)\Gamma_{x\lambda}^s(E^*)}{\Gamma_\gamma^s(E^*)} \psi(\zeta_\lambda^s,\chi_\lambda^s)$$

$$+ \sigma_{x_f}(E^*) + \sigma_p(E^*)\delta xe \quad , \qquad \text{II-20d}$$

$\sigma_{o\lambda}^{s}(E^*)$ = peak cross section for resonance λ in sequence s,

$\psi(\zeta,\chi)$ = Doppler broadened line shape function,

$\zeta_\lambda^s = \Gamma_\gamma^s(E^*)/(4E^*kT/M)^{1/2}$,

$\chi_\lambda^s = 2(E-E_\lambda^s)/\Gamma_\lambda^s(E^*)$,

k = boltzmann constant ,

M = atomic weight ratio for target nucleus ,

$(4E^*kT/M)^{1/2}$ = Doppler width at E^* ,

$\sigma_p(E^*)$ = potential scattering cross section at E^* ,

$\sigma_{x_f}(E^*)$ = file 3 cross section value at E^* ,

$\sigma_p = \sigma_p(E^*) + \sigma_{f_f}(E^*) + \sigma_{c_f}(E^*) + \sigma_{e_f}(E^*) + \sigma_o$.

Since many resonances occur in the interval (E_2-E_1) we can treat them statistically as,[9]

$$\frac{1}{N_s}\sum_{\lambda} f_\lambda^s \rightarrow \int_0^\infty P_n(y)P_m(z)f^s(y,z)dy\,dz = \langle f^s \rangle \quad , \qquad \text{II-21}$$

with

N_s = number of resonances,

D_s = average resonance width .

We now desire to treat the numerator and denominator of equation II-20 in this manner. First, rearranging the numerator, and neglecting overlap effects, we can write

$$NUM = \sum_s \sum_\lambda \int_{E_1}^{E_2} \frac{\sigma_{x\lambda}^s(E,E^*)}{\sigma_{t\lambda}^s(E,E^*)+\sigma_p} \left[1 - \sum_{s'\neq s} \sum_{\lambda'} \frac{\sigma_{t\lambda'}^{s'}(E,E^*)}{\sigma_{t\lambda'}^{s'}(E,E^*)+\sigma_p}\right]dE \qquad \text{II-22}$$

inserting equation II-20d into equation II-22 and omitting the s and λ dependence of ζ and ψ

$$NUM = \sum_s \sum_\lambda \frac{\Gamma_{x\lambda}^s(E^*)}{\Gamma_\gamma^s(E^*)} \int_{E_1}^{E_2} \frac{\psi(\zeta,x)}{\psi(\zeta,x)+\beta} \left[1 - \sum_{s'\neq s} \sum_{\lambda'} \frac{\psi(\zeta,x)}{\psi(\zeta,x)+\beta}\right] dE \ , \qquad \text{II-23}$$

with

$$\beta = \sigma_p/\sigma_{o\lambda}^s(E^*) \ .$$

Defining the usual J function as

$$J(\zeta,\beta) = \int_0^\infty \frac{\psi(\zeta,x)dx}{\psi(\zeta,x)+\beta} \ , \qquad \text{II-24}$$

performing the above statistical integration on equation II-23, we obtain:

$$NUM = (E_2-E_1) \sum_s \frac{\langle \Gamma_x^s(E^*) J(\zeta,\beta)\rangle}{D_s} \left[1 - \sum_{s'\neq s} \frac{\langle \Gamma^{s'}(E^*) J(\zeta,\beta)\rangle}{D_{s'}}\right] . \qquad \text{II-25}$$

Performing similar operations on the denominator, we can now write the cross section for reaction x at E^* as

$$\sigma_x(E^*,\sigma_o) = \sigma_p \sum_s a_x^s \left(1 - \sum_{s'\neq s} b^{s'}\right) / \left[1 - \sum_s b^s \left(1 - \sum_{s'\neq s} b^{s'}\right)\right]$$

$$+ \sigma_{x_f} + \sigma_p \delta_{xe} \ , \qquad \text{II-26}$$

where

$$a_x^s = \langle \Gamma_x^s J^s\rangle / D_s \ ,$$

$$b^s = \langle \Gamma^s J^s\rangle / D_s \ .$$

We now take derivatives of equation II-25 with respect to the resonance parameters, $q_k{}^s$. First looking only at the D_s derivatives,

$$\frac{\partial \sigma_x(E^*,\sigma_o)}{\partial D_s} = \sigma_p\{\frac{1}{DEN_s}[-\frac{a_x{}^s}{D_s}(1-\sum_{s'\neq s} b^{s'}) - \sum_{s''\neq s} a_x{}''(-\frac{b^s}{D_s})]$$

$$+ \frac{NUM_s}{DEN_s{}^2}[-\frac{b^s}{D_s}(1-\sum_{s'\neq s} b^{s'}) - \sum_{s''\neq s} b^{s''}(-\frac{b^s}{D_s})]\} \qquad \text{II-27}$$

Similarly for $\Gamma_f(E^*)$, $\Gamma_\gamma(E^*)$, $\Gamma_n(E^*)$,

$$\frac{\partial \sigma_x(E^*,\sigma_o)}{\partial q_k{}^s} = \sigma_p\{\frac{1}{DEN_s}[\frac{\partial a_x{}^s}{\partial q_k{}^s}(1-\sum_{s'\neq s} b^{s'}) - \sum_{s''\neq s} a_x{}''(\frac{\partial b_s}{\partial q_k{}^s})]$$

$$+ \frac{NUM_s}{DEN_s{}^2}[\frac{\partial b^s}{\partial q_k{}^s}(1-\sum_{s'\neq s} b^{s'}) - \sum_{s''\neq s} b^{s''}(\frac{\partial b^s}{\partial q_k{}^s})]\} \qquad \text{II-28}$$

where

$$NUM_s = \sum_s a_x{}^s(1 \mp \sum_{s'\neq s} b^{s'}) \quad ,$$

$$DEN_s = 1 - \sum_s b^s\ (1 \mp \sum_{s'\neq s} b^{s'}) \ .$$

We now evaluate the terms,

$$\frac{\partial a_x{}^s}{\partial q_k{}^s} \ , \ \frac{\partial b^s}{\partial q_k{}^s} \ .$$

Once again excluding D_s from q_k,

$$\frac{\partial a_x{}^s}{\partial q_k{}^s} = \frac{\partial}{\partial q_k{}^s}\frac{\langle \Gamma_x{}^s J\rangle}{D_s} = \frac{1}{D_s}\frac{\partial \langle \Gamma_x{}^s J\rangle}{\partial q_k{}^s} \quad , \qquad \text{II-29}$$

$$\frac{\partial b^s}{\partial q_k{}^s} = \frac{\partial}{\partial q_k{}^s}\frac{\langle \Gamma^s J\rangle}{D_s} = \frac{1}{D_s}\frac{\partial \langle \Gamma^s J\rangle}{\partial q_k{}^s} \ . \qquad \text{II-30}$$

We can write symbolically $\langle \Gamma_x{}^s J\rangle$ as follows,

$$\langle \Gamma_X J \rangle = \int_0^\infty P_\mu(\Gamma_X) d\Gamma_X \int_0^\infty P_\nu(\Gamma_Y) \Gamma_X J(\Gamma_X, \Gamma_Y) d\Gamma_Y \quad , \qquad \text{II-31}$$

with

$$P_\mu(\Gamma_X) d\Gamma_X = \frac{\mu}{2\Gamma(\mu/2)} \left[\frac{\mu\Gamma_X}{2\Gamma_X(E^*)}\right]^{\mu/2-1} \exp\left[-\frac{\mu\Gamma_X}{2\Gamma_X(E^*)}\right] d\Gamma_X \quad .$$

Thus

$$\frac{\partial \langle \Gamma_X J \rangle}{\partial \Gamma_X(E^*)} = \int_0^\infty P_n(\Gamma_Y) d\Gamma_Y \int_0^\infty \frac{\partial P_\mu(\Gamma_X)}{\partial \Gamma_X(E^*)} \Gamma_X J(\Gamma_X, \Gamma_Y) d\Gamma_X \quad , \qquad \text{II-33}$$

$$\frac{\partial \langle \Gamma_X J \rangle}{\partial \Gamma_Y(E^*)} = \int_0^\infty \frac{\partial P_\mu(\Gamma_Y)}{\partial \Gamma_Y(E^*)} d\Gamma_Y \int_0^\infty P_\mu(\Gamma_X) \Gamma_X J(\Gamma_X, \Gamma_Y) d\Gamma_X \quad , \qquad \text{II-33}$$

with

$$\frac{\partial P_\mu(\Gamma_X)}{\partial \Gamma_X(E^*)} = \left[\frac{\mu\Gamma_X - (\mu-2)\Gamma_X(E^*)}{2\Gamma_X(E^*)^2}\right] P_\mu(\Gamma_X) \quad .$$

A special case occurs for Γ_γ which requires additional development. Further details are given in Appendix C.

Before proceeding further, we now shall describe briefly the application of the above procedure to the MC^2-2 algorithm[12]. The equation used by MC^2-2 for the capture cross section for sequence s, is,

$$\sigma_X^s(E^*, \sigma_0) = \frac{\sigma_p \{\frac{1}{D_s} \langle \Gamma_X^s J(\beta_s, \xi_s, a_s, 0) \rangle - O_X^s\}}{\cos 2\delta_\ell \{1 - [\frac{1}{D_s} \langle \Gamma^s J(\beta_s, \xi_s, a_s, b_s) \rangle - O_s^t]\}} \quad , \qquad \text{II-34}$$

with

$$J(\beta_s, \xi_s, a_s, b_s) = \frac{1}{2} \int_{-\infty}^{\infty} \frac{\psi + b_s \chi}{\beta_s + \psi + a_s \chi} \, dx \quad ,$$

$$O_X^S = \frac{1}{D_S}\left\langle \frac{\Gamma_X^S}{2}\int_{-\infty}^{\infty}\omega(\delta)\frac{d\delta}{D_S}\int_{-\infty}^{\infty}\frac{\psi_S}{\beta_S+\psi_S}\frac{A_{S'}\psi_{S'}dx_S}{\beta_S+\psi_S+A_{S'}\psi_{S'}}\right\rangle_{S,S'} ,$$

$$A_S = \frac{N_{S'}\sigma_{OS'}}{N_S\sigma_{OS}} ,$$

where $\omega(\delta)$ is the probability of finding a resonance s' at $\delta = (E_{OS}-E_{OS'})$. Taking once again derivatives of σ_X^S with respect to q_k and D_S separately and equation II-34 as NUM/DEN,

$$\frac{\partial\sigma_X^S}{\partial D_S} = \frac{1}{DEN}\sigma_p\{-\frac{1}{D_S^2}\langle\Gamma_X^S J\rangle - \frac{\partial O_X^S}{\partial D_S}\}$$

$$+ \frac{NUM}{DEN^2}\cos 2\delta_\ell\{-\frac{1}{D_S^2}\langle\Gamma_t^S J\rangle - \frac{\partial O_t^S}{\partial D_S}\} , \qquad \text{II-35}$$

$$\frac{\partial\sigma_X^S}{\partial q_k^S} = \frac{1}{DEN}\sigma_p\{\frac{1}{D_S}\frac{\partial\langle\Gamma_X^S J\rangle}{\partial q_k^S} - \frac{\partial O_X^S}{\partial q_k^S}\}$$

$$+ \frac{NUM}{DEN^2}\cos 2\delta_\ell\{\frac{1}{D_S}\frac{\partial\langle\Gamma_t^S J\rangle}{\partial q_k^S} - \frac{\partial O_t^S}{\partial q_k^S}\} . \qquad \text{II-36}$$

The $\langle\Gamma_X^S J\rangle$ derivative terms are very similar to the terms in equation II-33 and are evaluated in the same manner. The O_X^S derivative terms have been omitted from this analysis with little or no consequences.

The final step is that of group averaging the cross sections and their derivatives. Without development (see ref. 12) we present the equation for group averaging cross sections in the unresolved resonance region,

$$\sigma_{Xg}(T,\sigma_o) = \frac{\int_g \frac{\sigma_X(T,\sigma_o,E^*)C(E)}{\sigma_o + \sigma_t(T,\sigma_o,E^*)}dE}{\int_g \frac{C(E)}{\sigma_o + \sigma_t(T,\sigma_o,E^*)}dE} = \frac{NUM_g}{DEN_g} . \qquad \text{II-37}$$

thus,

$$\frac{\partial \sigma_{xg}(T,\sigma_o)}{\partial q_k{}^s} = \frac{1}{DEN_g} \int_g C(E)dE \left[\frac{1}{\sigma_o+\sigma_t(T,\sigma_o,E^*)} \frac{\partial \sigma_x(\sigma_o,T,E^*)}{\partial q_k{}^s} \right.$$

$$\left. - \frac{\sigma_x(T,\sigma_o,E^*)}{\{\sigma_o+\sigma_t(T,\sigma_o,E^*)\}^2} \frac{\partial \sigma_t(T,\sigma_o,E^*)}{\partial q_k{}^s} \right]$$

$$+ \frac{NUM_g}{DEN_g{}^2} \int_g \frac{C(E)dE}{\{\sigma_o+\sigma_t(T,\sigma_o,E^*)\}^2} \frac{\partial \sigma_t(T,\sigma_o,E^*)}{\partial q_k{}^s} \quad . \qquad \text{II-38}$$

Thus, the group averaging of the sensitivities is very similar to that of the cross sections.

CHAPTER III

GENERALIZED DATA ADJUSTMENT METHODOLOGY

The Generalized Least Squares Data Adjustment procedure utilized in this dissertation is described in this chapter. First, a general approach to Generalized Least Squares is presented followed by the specific application to cross section adjustments.

Several methods exist for performing Least Squares Adjustments.[1-4] The method followed herein is similar to that of Perey.[3] This method has several advantages in that the underlying assumptions in the final result are clearly enumerated. We first derive the general equations, then we will apply them to cross section adjustments.

We begin by writing a definition of the commonly called conditional probabilities or loss functions[13] as:

$$P(B/A) = \frac{P(AB)}{P(A)} \quad , \quad P(A/B) = \frac{P(AB)}{P(B)} \quad , \qquad \text{III-1}$$

where P(A/B) is the probability of A given B is true. Rearranging, these definitions we obtain a form of Bayes Theorem,

$$P(A/B) = \frac{P(AB)}{P(B)} = \frac{P(B/A)P(A)}{P(B)} \; . \qquad \text{III-2}$$

Now, we let A_1, A_2, $\cdot\cdot$ A_n and B_1, B_2, $\cdot\cdot$ B_m be mutually exclusive states. Assume we know how A_i affects B_j, thus $P(B_j/A_i)$ is known for all i,j. Assume that we also know the "a priori" probabilities $P(A_i)$. Thus, we have some knowledge of the quantities A_i. Their probabilities

tell us to what extent they reflect the "true" values of A_i. We now want to improve on this knowledge of the A_i's. Thus, we perform measurements and determine that B_μ is true. We now need to determine the new probabilities of A_ν given the information B_μ, i.e. $P(A_\nu/B_\mu)$. Applying Bayes Theorem,

$$P(A_\nu/B_\mu) = \frac{P(B_\mu/A_\nu)P(A_\nu)}{P(B_\mu)} , \qquad \text{III-3}$$

with

$$P(B_\mu) = \sum_{i=1} P(A_i B_\mu) = \sum_{i=1} P(B_\mu/A_i)P(A_i) .$$

Thus equation III-3 allows us to update our knowledge of the A_i's by including results of measurements of the B_μ's. Equation III-3 holds for discrete values of A_i and B_j. For continuous values the form of Bayes Theroem is similar, but probability functions replace the probability measures in equation III-3.

We begin by defining a continuous probability function F(p) as,

$$P(p_0 \leq p \leq p_0+dp) = d(F(p_0)) = f(p_0)dp , \qquad \text{III-4}$$

where $f(p_0)$ is a probability density function (pdf). The variable p is here a scalar but this concept can easily be extended to vectors. The probability function and pdf for the variable r may be defined by $G(r_0)$ and $g(r_0)$ respectively. Using these definitions, conditional probability functions and pdf's can be defined as equation III-1. Bayes Theorem then assumes the form:

$$d(F(p_o/r_o)) = f(p_o/r_o) = \frac{d(G(r_o/p_o))d(F(p_o))}{\int_p d(G(r_o/p))d(F(p))} \qquad \text{III-5}$$

$$= \frac{g(r_o/p_o)f(p_o)dp}{\int_p g(r_o/p)f(p)dp} \quad ,$$

where now the new measurements, r_o, update our previous knowledge, p_o, with $f(p_o)$ the pdf of the p's and $g(r_o/p_o)$ the loss function or conditional probability function. Now assuming that $g(r_o/p_o)$ can be represented as a Gaussian distribution,

$$g(r_o/p_o) = c_r \exp[-1/2(r_o - r(p_o))^{+}V^{-1}(r_o - r(p_o))] \qquad \text{III-6}$$

with mean $r(p_o)$ and a variance-covariance matrix V which is independent of p_o. We assume that the function r(p) can be approximated locally by a linear function corresponding to the first term of a Taylor Series,

$$r(p+\delta p) = r(p) + G\delta p \qquad \text{III-7}$$

where G is the sensitivity matrix for r with respect to p.

The pdf for the parameter p (the a priori pdf f(p)) may also be given as a Gaussian;

$$f(p) = c_p \exp[-1/2(p-\bar{p})^{+}M^{-1}(p-\bar{p})] \quad , \qquad \text{III-8}$$

with mean $\bar{p}$ and variance-covariance matrix M. Using Bayes Theorem, III-5, we obtain,

$$f(p_o/r_o) = \frac{g(r_o/p_o)f(p_o)}{\int_p g(r_o/p)f(p)dp} \quad . \qquad \text{III-9}$$

Substituting III-7 for r(p) with $\bar{r} = r(\bar{p})$,i.e.

$$r(p) = \bar{r} + G(p - \bar{p}), \qquad \text{III-10}$$

formula III-9 assumes the form:

$$f(p/r_o) = c_p' \exp\left[-1/2(p-p')^{+}M'^{-1}(p-p')\right] , \qquad \text{III-11}$$

where p' is the adjusted best estimate for p given r_o and M' is the variance-covariance matrix for the adjusted parameter. Futher manipulations which are described in Appendix D yield:

$$p' = \bar{p} + MG^{+}(N+V)^{-1}(r_o-\bar{r}), \text{ and}$$

$$M' = M - MG^{+}(N+V)^{-1}GM ,$$

$$N = GMG^{+} .$$

These formulas can also be obtained as the result of a properly formulated least squares adjustment procedure.

In conventional cross section adjustments the vector r represents a series of measured integral parameters with uncertainties described by the covariance matrix V in equation III-6. The vector p represents quantities such as cross sections, bias factors, modelling parameters, etc. that are necessary to calculate the values of r(p). The variance-covariance matrix of these quantities is given by M. The matrix G contains the sensitivities of the various r values to each of the p values. Recent developments in the area of Generalized Perturbation Theory[1] have

made calculation of these sensitivities economical for many different responses (r values) to many parameters, p (namely multi-group cross sections). However, the inadequacy of methods to incorporate energy and spatial self-shielding into the variance-covariance matrix, M, has limited the use of Cross Section Adjustment Studies to Fast Reactors and responses fairly insensitive to self-shielding. The methods developed in this dissertation remove these limitations and allow either the energy and spatial self-shielding factor or the resonance parameters to be included in the p vector.

CHAPTER IV

TRX-1 INTEGRAL PARAMETER CALCULATIONS

The calculations described in this chapter include the flux spectrum and several integral parameters for the TRX-1 facility. One of these integral parameters, $^{28}\rho$, will be used in the demonstration adjustment in Chapter VIII.

The TRX-1 is a thermal reactor benchmark consisting of H_2O moderated 1.3% enriched fuel pins in a triangular array. Specifications are given in reference 14 and Table IV-1. The TRX-1 was chosen for this study since both energy and spatial self-shielding effects are extremely important in the accurate calculation of integral parameters. The $^{28}\rho$ response was chosen since we desired to concentrate on ^{238}U capture.

The cross sections used in this study were processed (see figure IV-1) from ENDF/B-V by the processing code NJOY[15] into 97 groups (62 fast and 35 thermal) with $\sigma_0 = 10^{10}$, 10^3, 10^2, 25, and 1 at a temperature of 300°K. NJOY uses a point-wise reconstruction method wherein successive points are linearly interpolated to within a specified tolerance. Doppler broadening follows a numerical procedure[15] after which thinning (a reduction in the number of cross section points) is performed. The subsequent group averaging is performed using analytical integration of the basic ENDF interpolation laws[7]. The weight function utilized by NJOY was the EPRI LWR spectrum[15]. The energy self-shielding was accomplished by the use of the BONAMI module of the AMPX[16] system. The Bondarenko formalism as shown in Chapter I is the method utilized in obtaining energy self-shielded nuclear cross sections for this study.

Table IV-1

Cylindricized Calculational Model of
TRX-1 Hexagonal Lattice

Region	Outer Radius(cm)	Isotope	Concentration atoms/barn-cm
Fuel	0.4915	^{235}U	6.253×10^{-4}
		^{238}U	4.721×10^{-4}
Void	0.5042	-	-
Clad	0.5753	Al	6.025×10^{-2}
Moderator	0.9482	^{1}H	6.676×10^{-2}
		^{16}O	3.338×10^{-2}

Total Buckling = 5.7×10^{-3} cm^{-2}

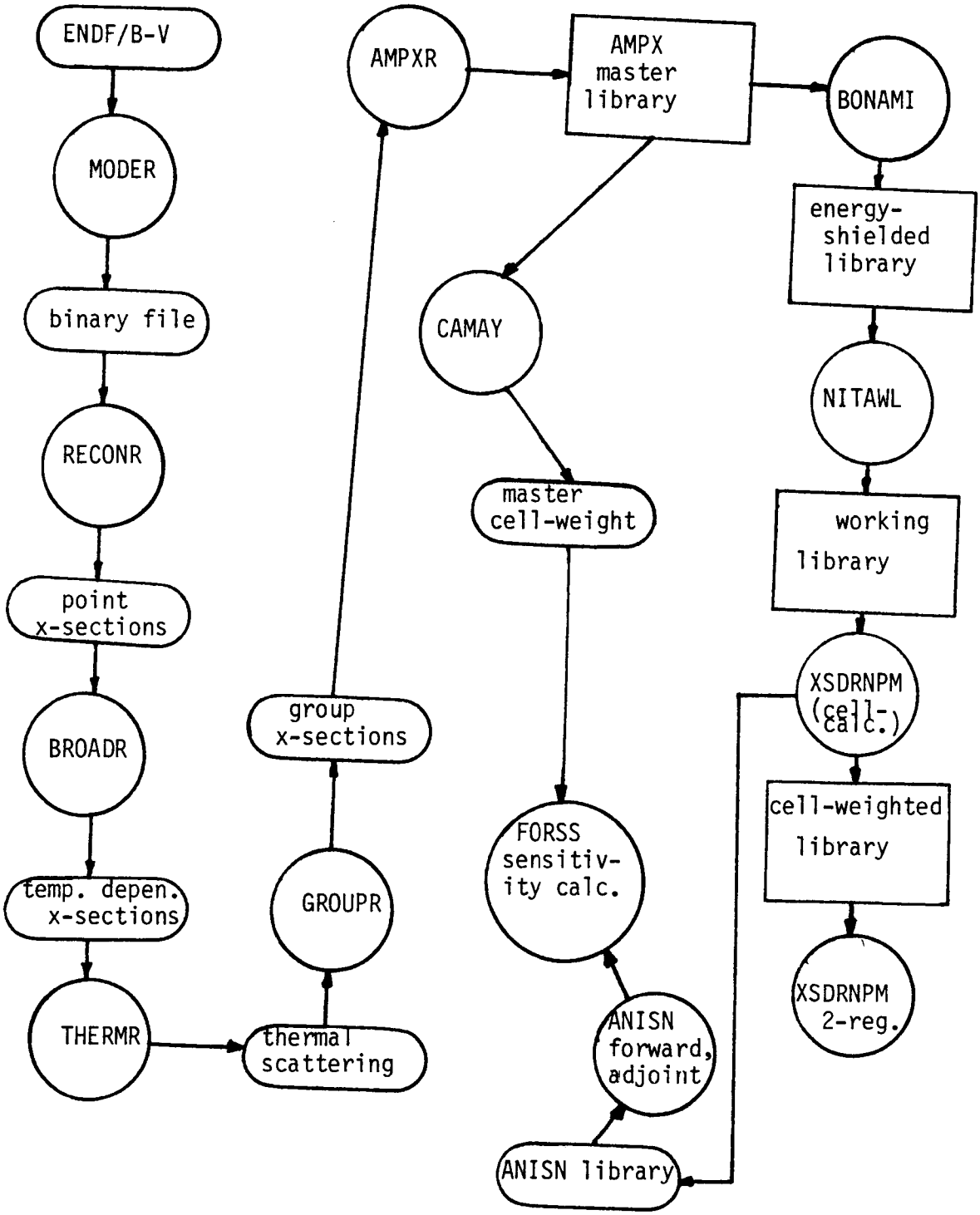

Figure IV-1. TRX-1 Cross Section Generation Flowpath

The NJOY processed cross sections are tabulated at various σ_0 values and various temperatures. The BONAMI code then calculates a σ_0 value corresponding to the given system and interpolates between values of the tabulated σ_0's to obtain self-shielded cross sections. The effects of nearby fuel pins are included in the σ_0 through an "escape" cross section as in EPRI-CELL.[17] The resulting cross sections are problem dependent since they have been energy self-shielded.

Spatial self-shielding of the cross sections by cell weighting and collapse was performed by the XSDRNPM module of the AMPX system. The model for the cell calculation consisted of 4 concentric cylinders of radii of .4915, .5042, .5753, and .94822 centimeters for the fuel pin, gap, clad, and moderator, respectively. Reflected boundary conditions were used at the center with a white boundary condition on the outer edge.

The governing equation for cell weighting the cross sections is given by:

$$\Sigma_{g_{cell}} = \frac{\int_g dE \int_V dr\ \Sigma(r,E)\phi(r,E)}{\int_g dE \int_V dr\ \phi(r,E)} \qquad \text{IV-1}$$

the actual equation used in XSDRNPM is,[18]

$$\sigma_G{}^{cell} = \frac{\sum_{j=1}^{IZM} N_j \sum_{i\epsilon j} \Delta V_i \sum_{g\epsilon G} \phi_g(i)\sigma_g(j)}{\left[\sum_j N_j \sum_{i\epsilon j} \Delta V_i\right]\left[1/V \sum_i^{IM} \Delta V_i \sum_{g\epsilon G} \phi_g(i)\right]}, \qquad \text{IV-2}$$

where IZM = number of zones and IM = number of intervals. Equation IV-2 is also used to collapse the cross sections, where G is the broad group

and g are the fine group indices. In our study, the 20 groups below 0.625 eV were collapsed to one group. This was done to reduce the number of groups for the remaining analysis and reduce the number of groups with upscatter.

The above equations apply only to an infinite reactor. The leakage can be accounted for in several ways. One such way is through a B_1 calculation with experimentally determined bucklings. The method utilized was a two-region calculation with the first cylindrical zone of XSDRNPM produced cell averaged cross section values extending to 26.2093 centimeters from the center, and followed by 20 centimeters of water reflector. The hydrogen and oxygen cross sections in the reflector were infinitely dilute with no cell weighting. The collapsing of the reflector cross sections was performed by the MALOCS module of the AMPX system using the same EPRI LWR spectrum employed by NJOY in the initial cross section generation.

These reflector cross sections were modified since XSDRNPM uses the total cross section to arrive at the value of D in the axial leakage correction DB^2. Thus, the axial leakage was zeroed out and a "fake" material with total and absorption cross sections set equal to DB^2, with $B^2 = 5.26 \times 10^{-4}$ cm^{-2} [14]. The D values were obtained[19] for both the core and reflector regions.

In Table IV-2, several integral values calculated as described above are shown and compared with other calculations using other methods. In order to obtain an independent calculation of the integral parameters, results for TRX-1 were calculated using EPRI-CELL. The

Table IV-2

Comparison of Various TRX-1 Integral Parameters

Response	TRX-1 Integral Parameters				
	This work		ORNL(20)	EPRI(21)	MEASURED
	XSDRNPM	EPRI-CELL	ANISN	HAMMER	VALUE
$^{28}\rho$	1.351	1.352	1.369	1.343	1.320 ±.021
$^{28}\delta$	0.0969	0.0967	0.0987	0.0986	0.0946 ±.0041
$^{25}\delta$	0.1004	0.0975	0.0993	0.0995	0.0987 ±.0010
CR	0.798	0.800	0.802	0.793	0.797 ±.008
k_{eff}	1.003	0.9950	0.9930	1.0002	1.00

$^{28}\rho$ - ratio of epithermal-to-thermal ^{238}U captures

28δ - ratio of ^{238}U fissions to ^{235}U fissions

25δ - ratio of epithermal-to-thermal ^{235}U fissions

CR - ratio of ^{238}U captures to ^{235}U fissions

XSDRNPM and EPRI-CELL values for $^{28}\rho$ are in excellent agreement. Both values are between the EPRI and ORNL values (see Table IV-2), while being about 3% higher than the experimental value. Both $^{28}\delta$ and CR agree well with the other quoted values as well as lie within the experimental uncertainties. However both $^{25}\delta$ and k_{eff} are somewhat high relative to the other calculations and the experiments. This discrepency is attributed to the fast leakage treatment where the measured bucklings and calculated diffusion coefficients were used to account for the axial leakage. This treatment allows too few fast neutrons to leak from the system and thus increases both $^{25}\delta$ and k_{eff}.

CHAPTER V

CALCULATION OF CROSS SECTION SENSITIVITIES

The calculation of the cross section sensitivities to be utilized in the demonstration adjustment in Chapter VIII is described in this chapter. These cross section sensitivities provide a means of relating changes in the group cross sections to changes in the corresponding integral parameters.

Cross Section Sensitivity Theory utilizing Generalized Perturbation Theory has been described in detail in several other studies.[1,22,23] The problem solved involves the integral parameter, R, of the form,

$$R = \frac{\int \phi^*(\xi)\, H_1[\Sigma(\xi)]\, \phi(\xi)\, d\xi}{\int \phi^*(\xi)\, H_2[\Sigma(\xi)]\, \phi(\xi) d\xi} \qquad \text{V-1}$$

where H_1 and H_2 are suitable cross section operators, ϕ^* and ϕ are the adjoint and forward fluxes, respectively. Derivatives of this general response are desired with respect to the cross sections, Σ, in equation V-1. These derivatives have been shown[1] to be

$$\frac{dR/R}{d\Sigma(\rho)/\Sigma(\rho)} = I_1 - I_2 + I_3 + I_4 \,, \qquad \text{V-2}$$

where

$$I_1 = \Sigma(\rho)\, \frac{\int \phi^*(\xi)\, \frac{dH_1[\Sigma(\xi)]}{d\Sigma(\rho)}\, \phi(\xi) d\xi}{\int \phi^*(\xi)\, H_1[\Sigma(\xi)] \phi(\xi) d\xi)} \,,$$

$$I_2 = \Sigma(\rho)\, \frac{\int \phi^*(\xi)\, \frac{dH_2[\Sigma(\xi)]}{d\Sigma(\rho)}\, \phi(\xi) d\xi}{\int \phi^*(\xi)\, H_2[\Sigma(\xi)] \phi(\xi) d\xi)} \,,$$

$$I_3 = \frac{\Sigma(\rho)}{R} \int \frac{\partial R}{\partial \phi(\xi)} \frac{d\phi(\xi)}{d\Sigma(\rho)} d\xi \quad ,$$

$$I_4 = \frac{\Sigma(\rho)}{R} \int \frac{\partial R}{\partial \phi^*(\xi)} \frac{d\phi^*(\xi)}{d\Sigma(\rho)} d\xi \quad .$$

For responses that do not involve the adjoint flux, the I_4 term vanishes. Thus, we are concerned only with the I_1, I_2, and I_3 terms. The I_1 and I_2 terms are the so-called direct effects and are easily evaluated. However the so-called indirect effect, I_3, requires the use of Generalized Perturbation Theory in order to calculate the $d\phi(\xi)/d\Sigma(\rho)$ term of I_3.

Writing the steady state Boltzmann equation as,

$$L[\Sigma(\xi)]\phi(\xi) = 0 \qquad \text{V-3}$$

and then differentiating with respect to $\Sigma(\rho)$, we obtain,

$$L[\Sigma(\rho)]\frac{d\phi(\xi)}{d\Sigma(\rho)} + \frac{dL[\Sigma(\xi)]}{d\Sigma(\rho)}\phi(\xi) = 0 \qquad \text{V-4}$$

$$L[\Sigma(\rho)]\frac{d\phi(\xi)}{d\Sigma(\rho)} = -\frac{dL[\Sigma(\xi)]}{d\Sigma(\rho)}\phi(\xi) \quad .$$

Writing this symbolically,

$$L[\Sigma(\xi)]\psi(\xi,\rho) = Q(\xi,\rho) \quad , \qquad \text{V-5}$$

where $\psi(\xi,\rho)$ is the term in I_3 that we wish to calculate. However, if we write the adjoint to equation V-5 as;

$$L^*[\Sigma(\xi)]\Gamma^*(\xi) = S^* = \frac{\partial R}{\partial \phi(\xi)}, \qquad \text{V-6}$$

where $\Gamma^*(\xi)$ is the Generalized adjoint and multiply equation V-5 by Γ^* and equation V-6 by ψ and integrate over all phase space ξ, we obtain, using the definition of an adjoint operator:

$$\int \Gamma^*(\xi) Q(\xi,\rho) d\xi = \int \psi(\xi,\rho) \frac{\partial R}{\partial \phi(\xi)} d\xi = \frac{R}{\Sigma(\rho)} I_3 \quad . \qquad \text{V-7}$$

This allows us two ways of calculating I_3. The forward method requires the recalculation of ψ for every ρ, however the adjoint formulation requires only one Γ^* calculation for each response since it is not a function of ρ.

The response considered in this study is the reaction rate ratio of ^{238}U epithermal (E>.625 eV) to ^{238}U thermal (E<.625 eV) capture in the TRX-1 central interval. As seen above values for the forward flux ϕ, generalized adjoint source S^*, and the generalized adjoint flux Γ^* are needed. The same TRX-1 model discussed in Chapter IV was used in the calculation of the TRX-1 fluxes (with the exception of the mesh spacing). For the TRX-1 forward flux the mesh spacing was tightened to approximately .2 centimeters per mesh or 133 intervals in the core region and .5 centimeters per mesh or 59 intervals in the reflector. This was necessary since the flux must be calculated using the same mesh as the generalized adjoint flux (see next paragraph). The TRX-1 forward flux spectrum in the central interval is presented in Figure V-1.

The TRX-1 spectrum is characterized by a fission spectrum at high energies with an approximately 1/E shape in the epithermal range,

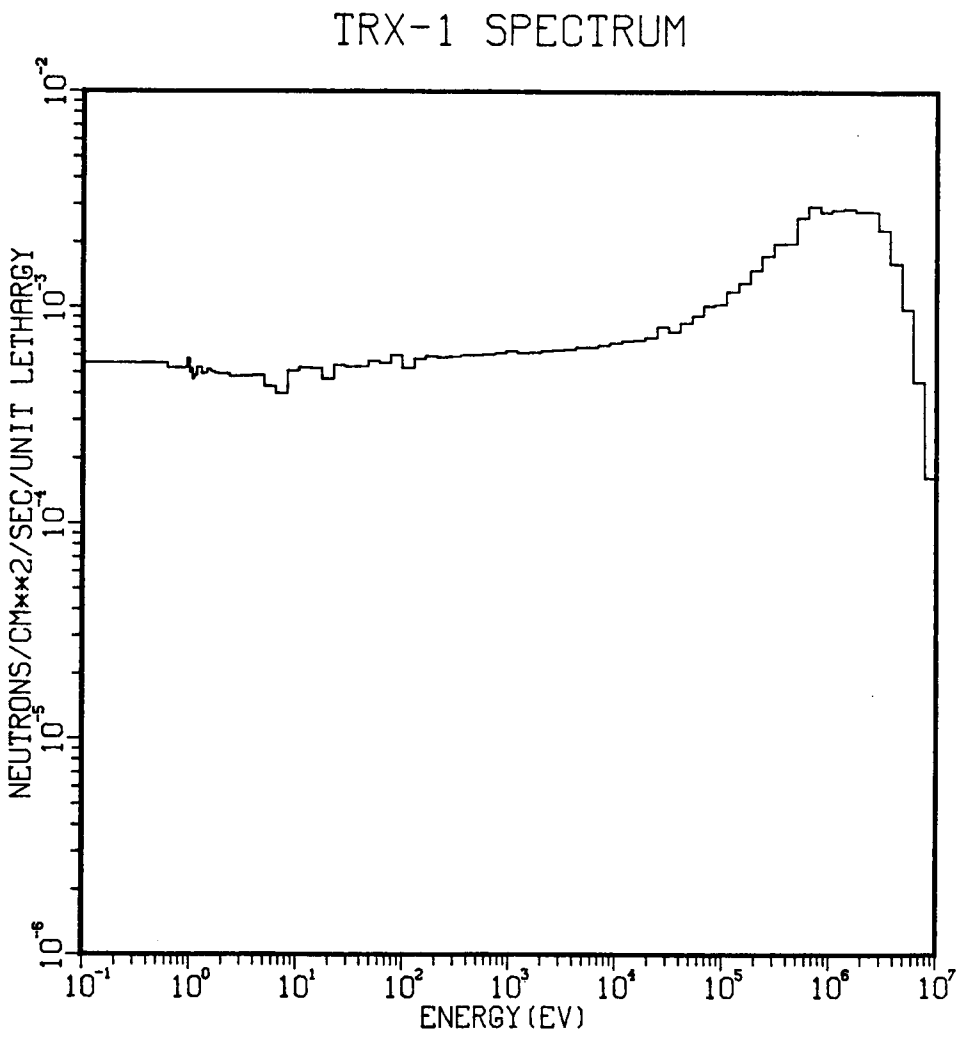

Figure V-1. TRX-1 Central Interval Flux Spectrum

followed by a maxwellian in the thermal range. The effect of the maxwellian is masked by the presence of only one thermal group, however an increase is clearly seen. Flux depressions and peaks are also clearly seen for the resonance peaks and minima of ^{238}U capture cross section. Several fluctuations in the spectrum are also seen in the 1-3 eV range corresponding to resonances in ^{235}U.

In order to perform the generalized adjoint calculation, the generalized source had to be calculated. For a reaction rate ratio response equation V-1 can be simplified to

$$R = \frac{\int \Sigma_1(\rho)\phi(\rho)d\rho}{\int \Sigma_2(\rho)\phi(\rho)d\rho} . \qquad \text{V-8}$$

Representing the energy dependence in group-wise form and for the central interval, ci.

$$R = \frac{\sum_g \Sigma_{g1}^{ci}\phi_g}{\sum_g \Sigma_{g2}^{ci}\phi_g} . \qquad \text{V-9}$$

We can now obtain the generalized source by differentiating equation V-9 with respect to the group flux in the central interval. Thus,

$$S_g^* = R\left[\frac{\Sigma_{g1}^{ci}}{\sum_g \Sigma_{g1}^{ci}\phi_g^{ci}} - \frac{\Sigma_{g2}^{ci}}{\sum_g \Sigma_{g2}^{ci}\phi_g^{ci}}\right] , \qquad \text{V-10}$$

for the central interval and equal to zero otherwise. The generalized adjoint source is shown in figure V-2.

The generalized adjoint flux is then calculated using the above source with the neutronics code in the adjoint mode. As can be seen

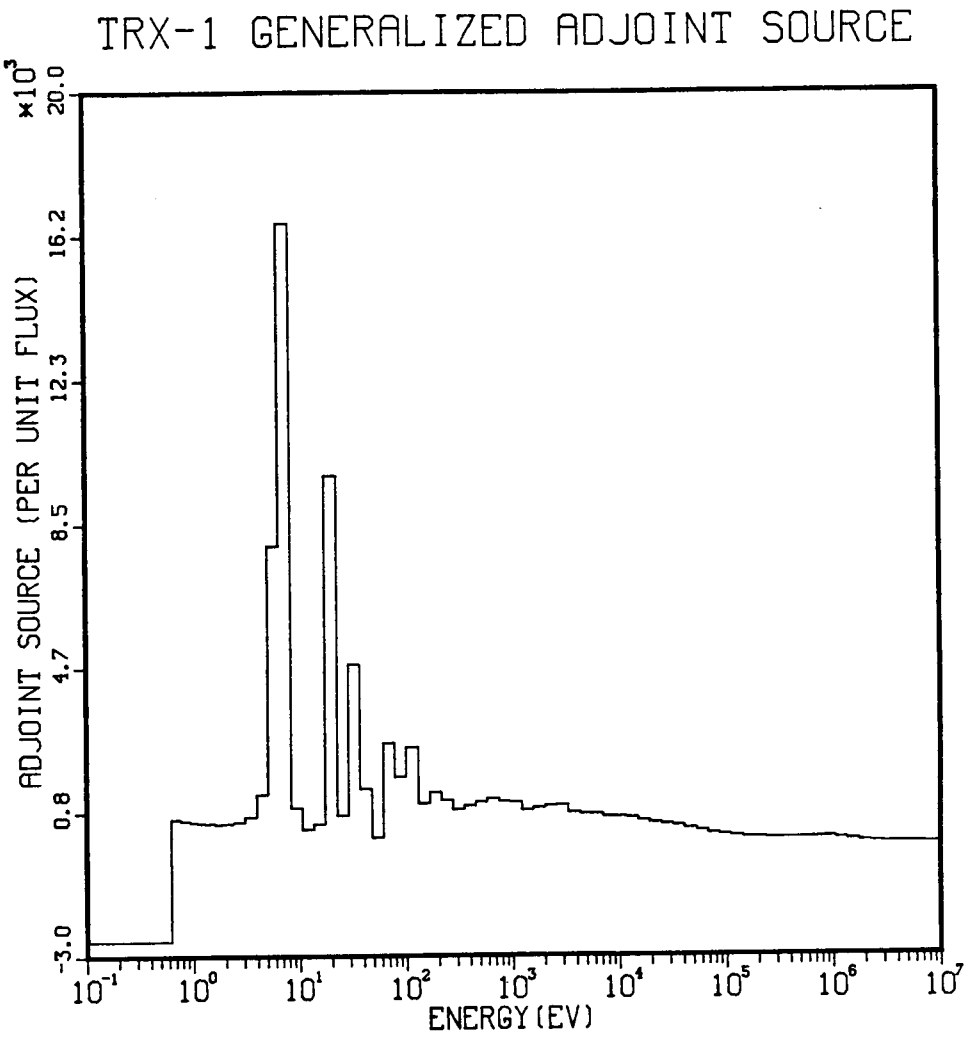

Figure V-2. TRX-1 Generalized Adjoint Source

from figure V-2 the generalized adjoint source becomes negative for the thermal group (E<.625 eV). Thus the generalized adjoint flux solution will also be both positive and negative. Much work has been performed on trying to guarantee that the flux solution in a transport theory code remains everywhere positive. For this reason the generalized adjoint calculations had to be performed using the linear diamond difference differencing scheme.[24] which permits negative fluxes. In order to prevent the diamond differencing scheme from breaking down, mesh points (see previous paragraph) were added to insure the accuracy of the solution. An interesting phenomenom in the solution is the inclusion of upscatter for the bottom 15 groups(1.9eV down). Thus with a negative source in the last group (first adjoint group), the adjoint solution consists of groups upscattering particles to a group where the flux is negative. The method of solution is also quite interesting since basically a fixed source is placed in a critical system. The method (see reference 1 for further details) involves sweeping out the fundamental mode "contamination" after every outer iteration until the remaining modes converge to the specified tolerance.

An anomaly was encountered in calculating the generalized adjoint flux, specifically, an oscillation occurred in the solution such that the outer iteration would not converge. It was discovered that upon turning off outer iteration rebalance[1] the oscillation vanished. However convergence was very slow and 23 outer were required for convergence. The generalized adjoint flux in the TRX-1 central interval is shown in figure V-3.

The generalized adjoint spectrum shows the importance of the

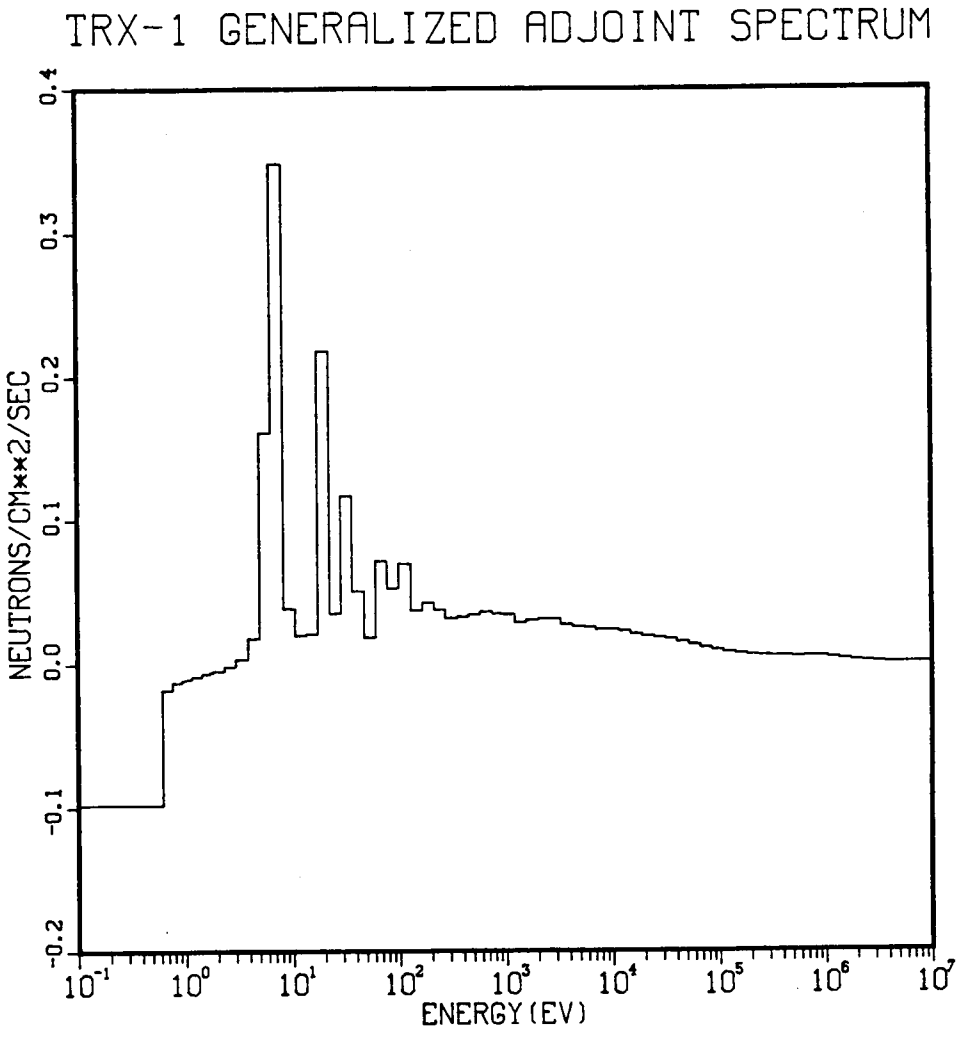

Figure V-3. TRX-1 Generalized Adjoint Spectrum

first few resolved resonances of ^{238}U to the $^{28}\rho$ response. The thermal value is also quite large indicating it's importance toward the $^{28}\rho$ response. The negative flux value results from the negative value of the source, since the thermal cross section is in the denominator of the $^{28}\rho$ response.

The final calculations of the TRX-1 $^{28}\rho$ sensitivities were performed using the ORNL FORSS[25] system. FORSS requires additional cross sections (i.e. partials) over the ones required in the neutronic analysis. Thus, an additional path was required (see figure IV-1) to obtain partial cross sections for input to the FORSS calculations. The module CAMAY is a new addition to the AMPX system which produced cell-weighted cross sections in an AMPX master format as required by FORSS.

Sensitivities were calculated for all significant reactions for the TRX-1 constituent materials; ^{238}U, ^{235}U, ^{1}H, ^{16}O, and ^{27}Al. Direct and indirect effects were evaluated for ^{238}U capture cross sections, with indirect effects only for all others. K-reset[1] effects were not considered.

Selected results for $^{28}\rho$ sensitivity to the most important material reactions are shown in figures V-4 to V-7.

Figure V-4 shows the relative sensitivity on a per unit lethargy basis of TRX-1 $^{28}\rho$ to elastic scattering in ^{1}H. As expected, the effects of ^{1}H scattering are pronounced since elastic scattering is the dominant slowing-down mechanism. Even at high energies the sensitivities are negative indicating the long range effects of ^{1}H slowing-down. The sensitivity curve traces the fission spectrum shape around 1 MeV indicating that the importance of a neutron to the

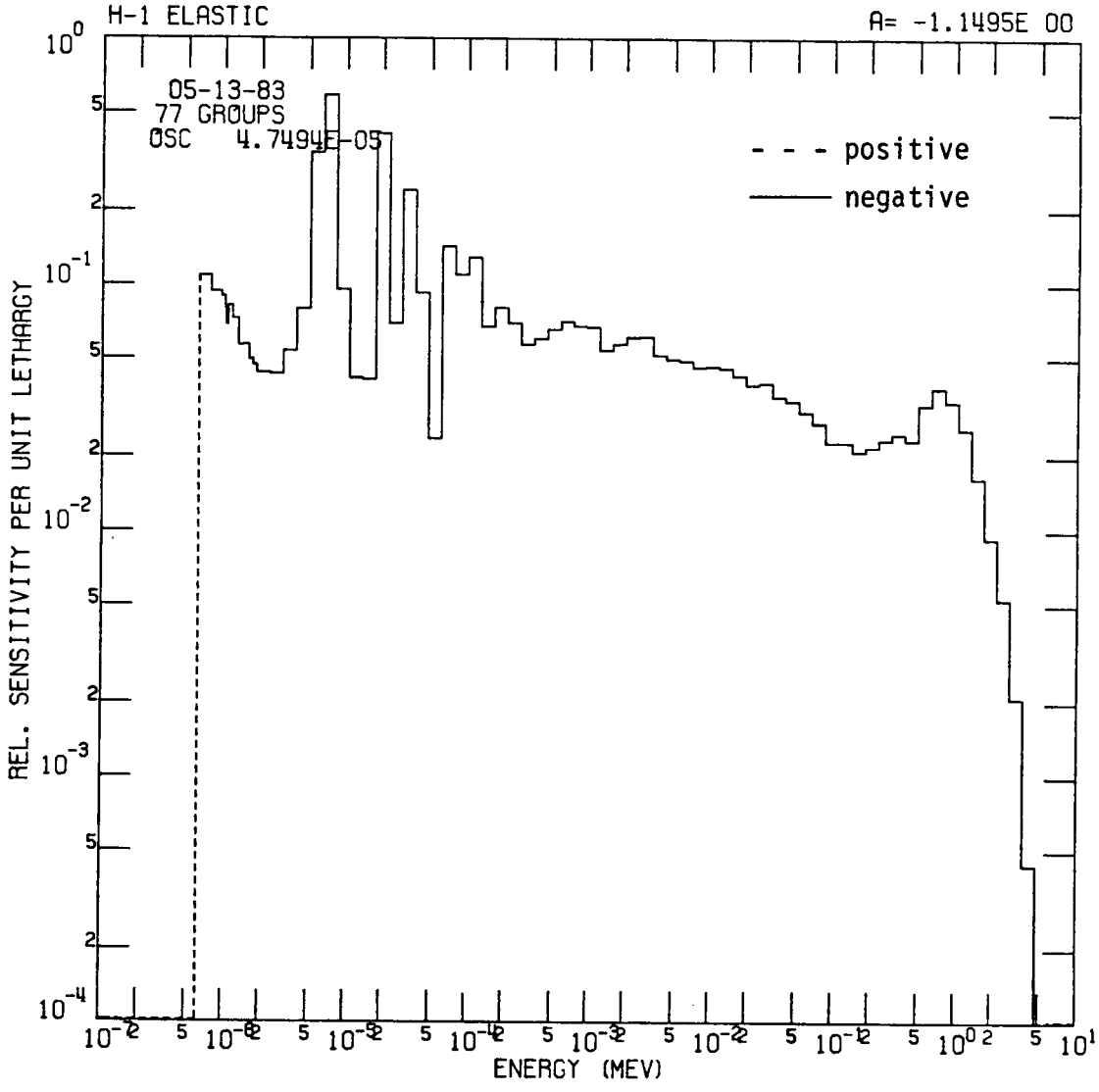

Figure V-4. Relative Sensitivity per unit lethargy of TRX-1 $^{28}\rho$ to Hydrogen Elastic Scattering Cross Section

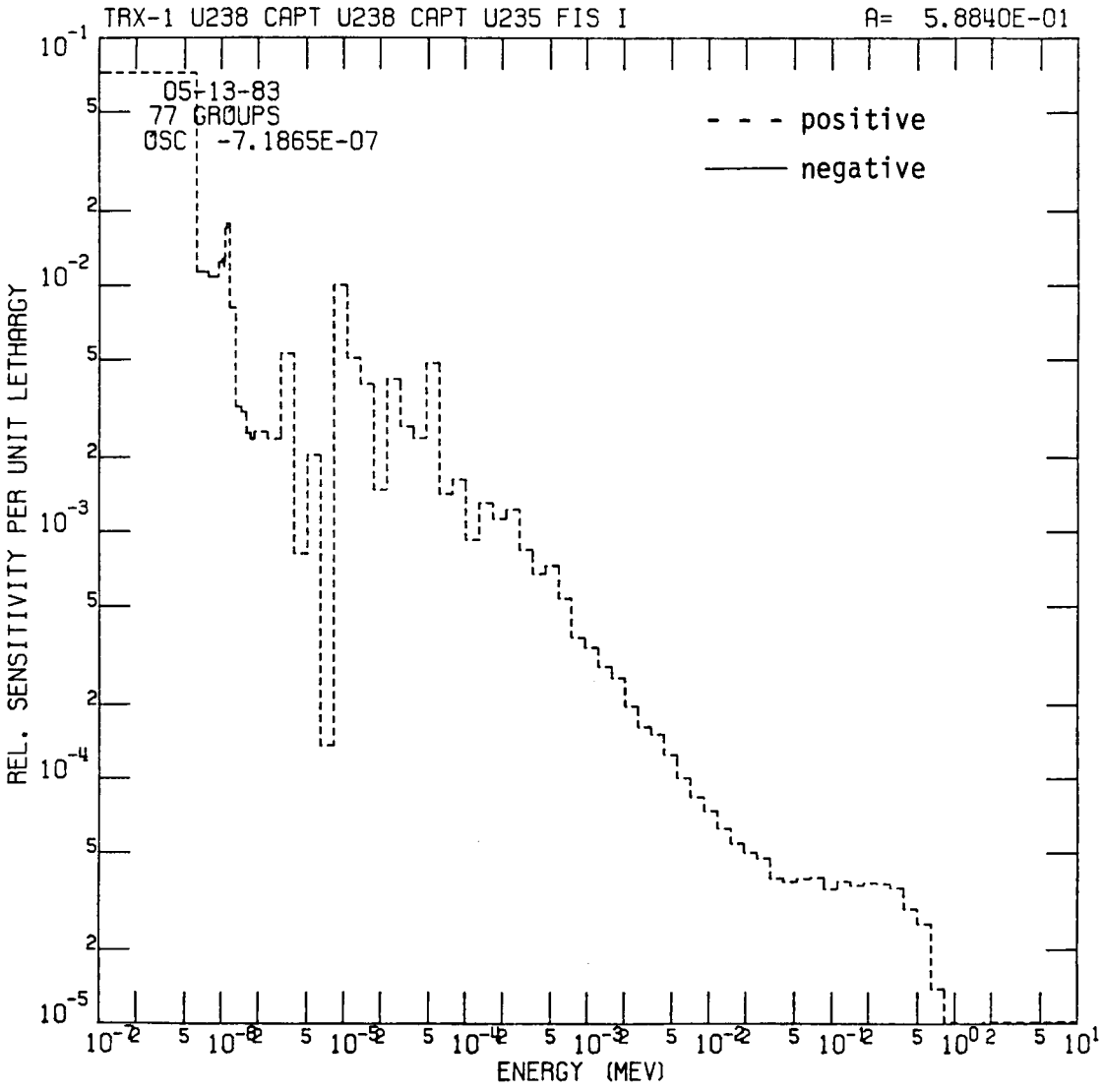

Figure V-5. Relative Sensitivity per unit lethargy of TRX-1 $^{28}\rho$ to U-235 Fission Cross Section

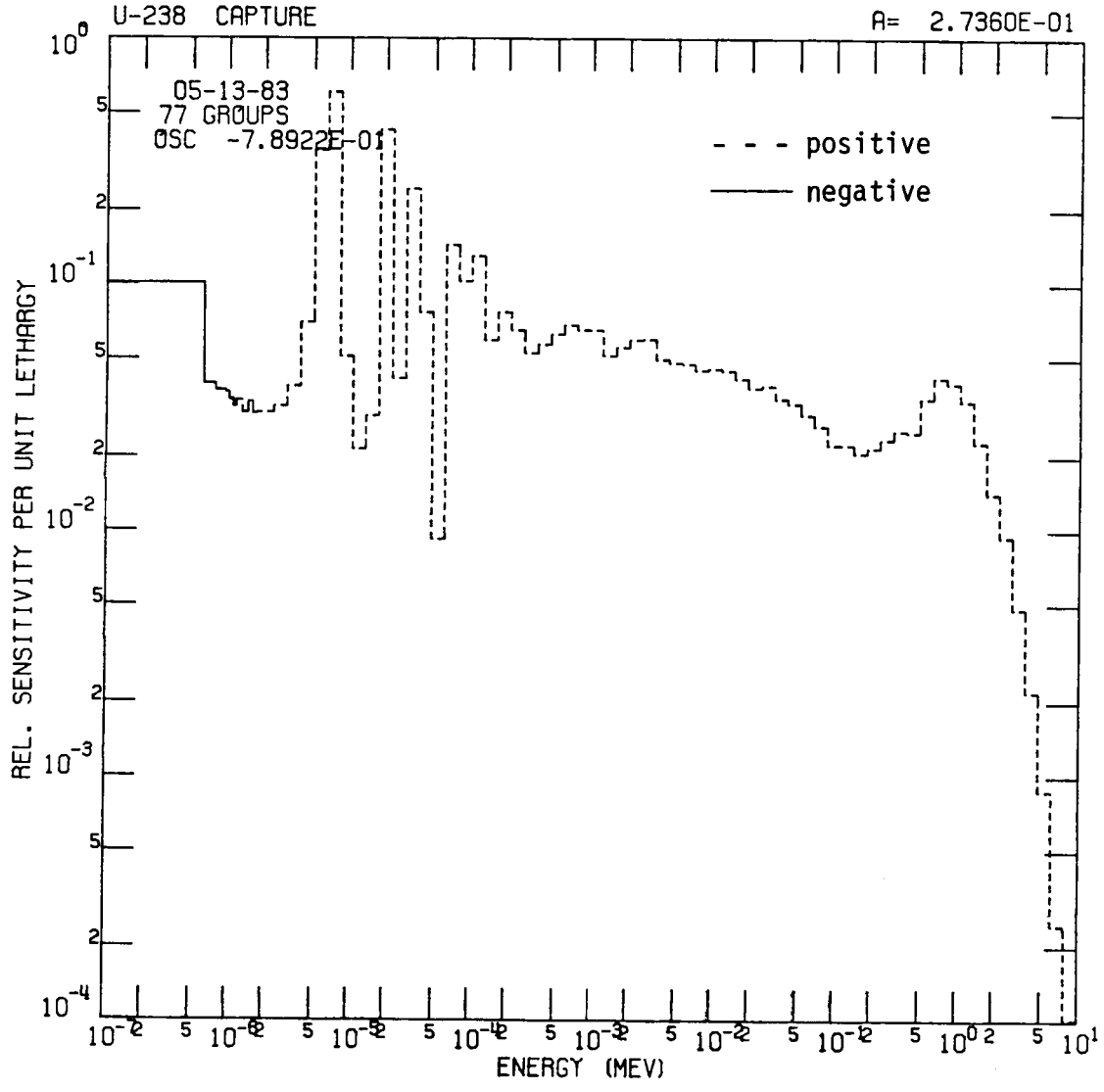

Figure V-6. Relative Sensitivity per unit lethargy of TRX-1 $^{28}\rho$ to U-238 Capture Cross Section (direct and indirect effects)

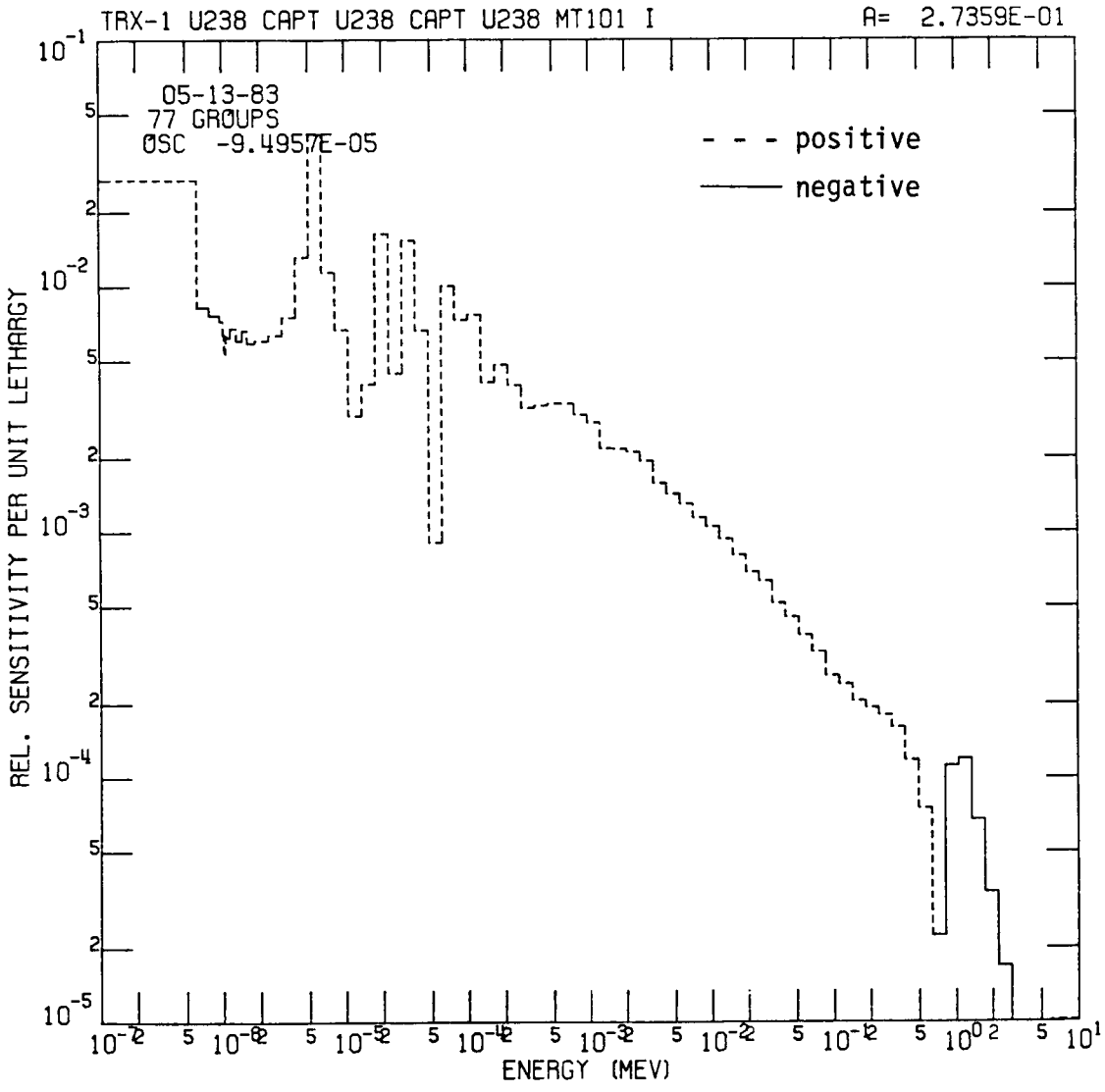

Figure V-7. Relative Sensitivity per unit lethargy of TRX-1 $^{28}\rho$ to U-238 Capture Cross Section (indirect effects only)

$^{28}\rho$ response is flat in the range and therefore dependent only upon the density of the neutron population. This situation changes as one tends toward lower energies as the neutron density increases in a 1/E fashion, while the neutron importance increases (in the negative direction) due to the higher probability that the neutron will be thermalized and contribute to the denominator term of $^{28}\rho$. Pronounced effects are seen for the first five or six resolved resonances as expected with very large peaks and valleys as in ^{238}U capture cross section. Once a neutron is thermalized (E<.625eV) the slowing down mechanism effect is nullified thus the sensitivity drops to near zero.

The ^{235}U fission sensitivity in figure V-5 shows quite a different behavior at high energies with a very small sensitivity at 1 MeV. Also since ^{235}U fission is a "source" of high energy neutrons, the sensitivity is positive over the entire range. Once again rapid variations are seen in the vicinity of the first few ^{238}U resolved resonances, while the influence of the first few ^{235}U resonances are also seen. The dominant effect is for the thermal group where, in effect, the fission event is a removal of the neutron from the thermal region and a source of neutrons in the fast range.

For ^{238}U capture as seen in figure V-6 the shape at high energy is very similar to that of ^{1}H elastic scattering. As expected, the sensitivity is positive above thermal and negative below thermal. Also, as before, the influence of the first few ^{238}U resolved resonances on TRX-1 $^{28}\rho$ is clearly seen.

An interesting effect is seen in figure V-7 which presents only the indirect contribution to the total ^{238}U capture sensitivity.

Surprisingly between .625 eV and 1 MeV the sensitivity is positive. This shows the importance of the capture cross section to the thermal flux (since an increase in the fast capture cross section has to decrease the fast flux). Thus the reduction in the thermal flux more than compensates for the decrease in the fast flux and a net positive effect results.

CHAPTER VI

CALCULATION OF RESONANCE PARAMETER SENSITIVITIES

As a test of the validity and usefulness of the resonance parameter sensitivity methodology, the theory described in Chapter II was programmed into a computer code DEFUNCT (see Appendix E). A description of methods employed in DEFUNCT for the calculation of resonance parameter sensitivities in first the resolved and then the unresolved region follows.

Coding Considerations

The first step in the Resolved Resonance Region involves reconstruction of the point cross sections and the point-wise resonance parameter sensitivities. DEFUNCT uses only a Single-Level-Breit-Wigner (SLBW) formula for reconstruction. Multilevel-Breit-Wigner nuclides are treated as SLBW materials.

The energy points for reconstruction are obtained in a similar way to the NPTXS[16] code. A factor R is defined as:

$$R = \frac{X_{i+1}}{X_i} , \qquad \text{VI-1}$$

where $X_i = 1/\{(E_i-E_0)^2 + 1/4\Gamma^2)^2\}$,

and E_0 is the resonance energy for a particular resonance under reconstruction. Then we solve for E_{i+1} ,

$$E_{i+1} = E_0 + R^{-1/2}[(E_i-E_0)^2 + 1/4(1-R^{1/2})\Gamma^2] \text{ , for } E_{i+1}>E_0 . \qquad \text{VI-2}$$

The value or values of R are set internally, however, they can be

changed for various problems. This scheme is used only over a portion of the energy range. This portion is determined by the value of SFACT as shown in figure VI-1.

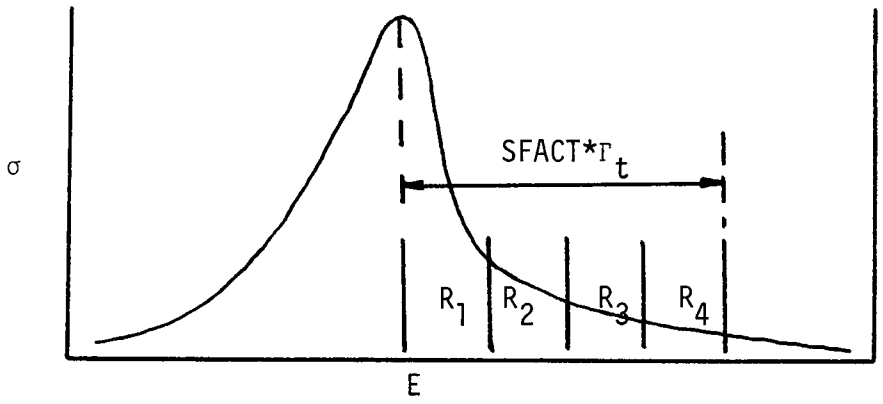

Figure VI-1: Resonance Region Energy Grid Scheme

Thus, the value of SFACT represents the number of total widths to which the above scheme applies. Also note this interval is divided into 4 equal regions each with its own value of R. A constant lethargy width of value, DU, is then used to add additional points between resonances.

The resulting point values of both cross sections and sensitivities are then Doppler broadened according to equations II-11 and II-12, respectively. No thinning is done after Doppler broadening. Upon completion of the Doppler broadening, the cross section values are unionized onto a single grid and the individual resonance contributions summed. The cross sections are then group averaged according to equation II-15 with the integration performed analytically on the basis of the interpolating formula. The sensitivities are then group averaged on the same unionized grid as the cross sections with interpolated values at

points not contained in the grid for that resonance only.

The unresolved resonance region calculations use the MINX code as a basis. Once again as in the resolved resonance region the cross sections and their sensitivities are calculated. Three options exist on calculating the cross sections, (1) the ETOX method[26] which involves only sequence-sequence overlap, (2) the MC^2-2 method[12] which involves both sequence-sequence and within sequence overlap effects, and (3) the UXS method[27] which contains a modified version of method 2. Sensitivities can be calculated for cross sections based on the ETOX method with sequence-sequence overlap taken into account(see equation II-26,27), and for methods 2 and 3 assuming no overlap effects(see equations II-35,36). Thus far, only minor differences have been observed between the two methods, and excellent agreement with direct calculations have been obtained. These tabulated cross sections and sensitivities are now ready for group averaging. This is performed using equations II-37,38 with linear interpolation between E^* points and Simpson's rule.

The problem of resolved region-unresolved region overlap sometimes occurs when processing cross sections as shown in figure VI-2.

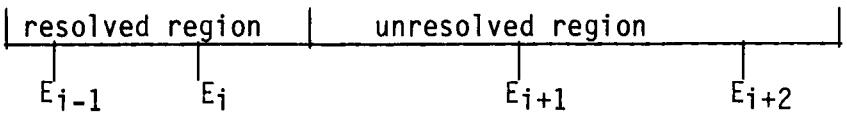

Figure VI-2: Resolved-Unresolved Overlap Model

In processing multigroup cross sections for the group which spans E_i to

E_{i+1} contributions are obtained from both the resolved and unresolved regions. In DEFUNCT the two regions are assumed to be independent such that

$$\sigma_g = \sigma_{res_g} + \sigma_{unres_g} + \sigma_{file\ 3_g} \qquad \text{VI-3}$$

This then allows the sensitivities for the resolved and unresolved to be computed independently, i.e.

$$\frac{\partial \sigma_g}{\partial q_{res}} = \frac{\partial \sigma_{res_g}}{\partial q_{res}} \ , \quad \frac{\partial \sigma_g}{\partial q_{unr}} = \frac{\partial \sigma_{unres_g}}{\partial q_{unr}} \ . \qquad \text{VI-4}$$

Point-wise Sensitivity Profiles

Several interesting effects can be seen from the study of point-wise resonance parameter sensitivity profiles. Shown in figure VI-3 are the zero-degrees K point-wise cross sections and resonance parameter sensitivities for ^{238}U capture to Γ_γ at 6.67 eV.

The pronounced dip in the point-wise resonance parameter sensitivity is very evident around the resonance peak at 6.67 eV. Similarly in figure VI-4 the resonance parameter (RP) sensitivity of ^{238}U capture cross section to Γ_γ at 36.7 eV is shown. Here the dip is not as pronounced and at points away from the dip the RP sensitivity is simply proportional to the cross section. This behavior can be explained by equation II-5. The RP sensitivity has two contributions, one positive and the other negative. For $\Gamma_\gamma < 1/2\Gamma_t$ the positive term dominates as seen in figure VI-4. For $\Gamma_\gamma > 1/2\Gamma_t$ the negative term dominates only near the resonance peak, with the positive term

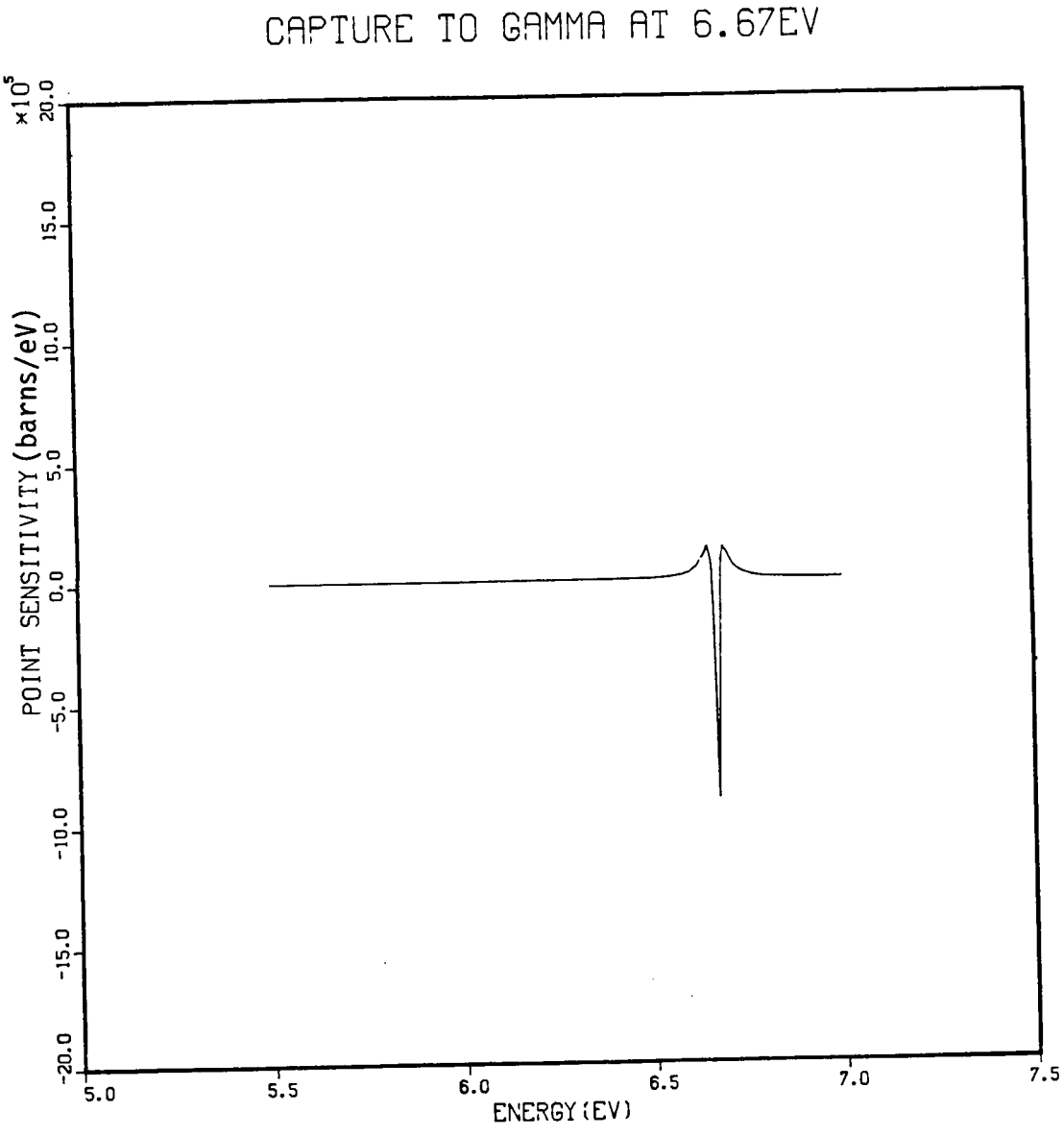

Figure VI-3. Pointwise Resonance Parameter Sensitivities of the U-238 Capture Cross Section to Γ_γ at 6.67 eV

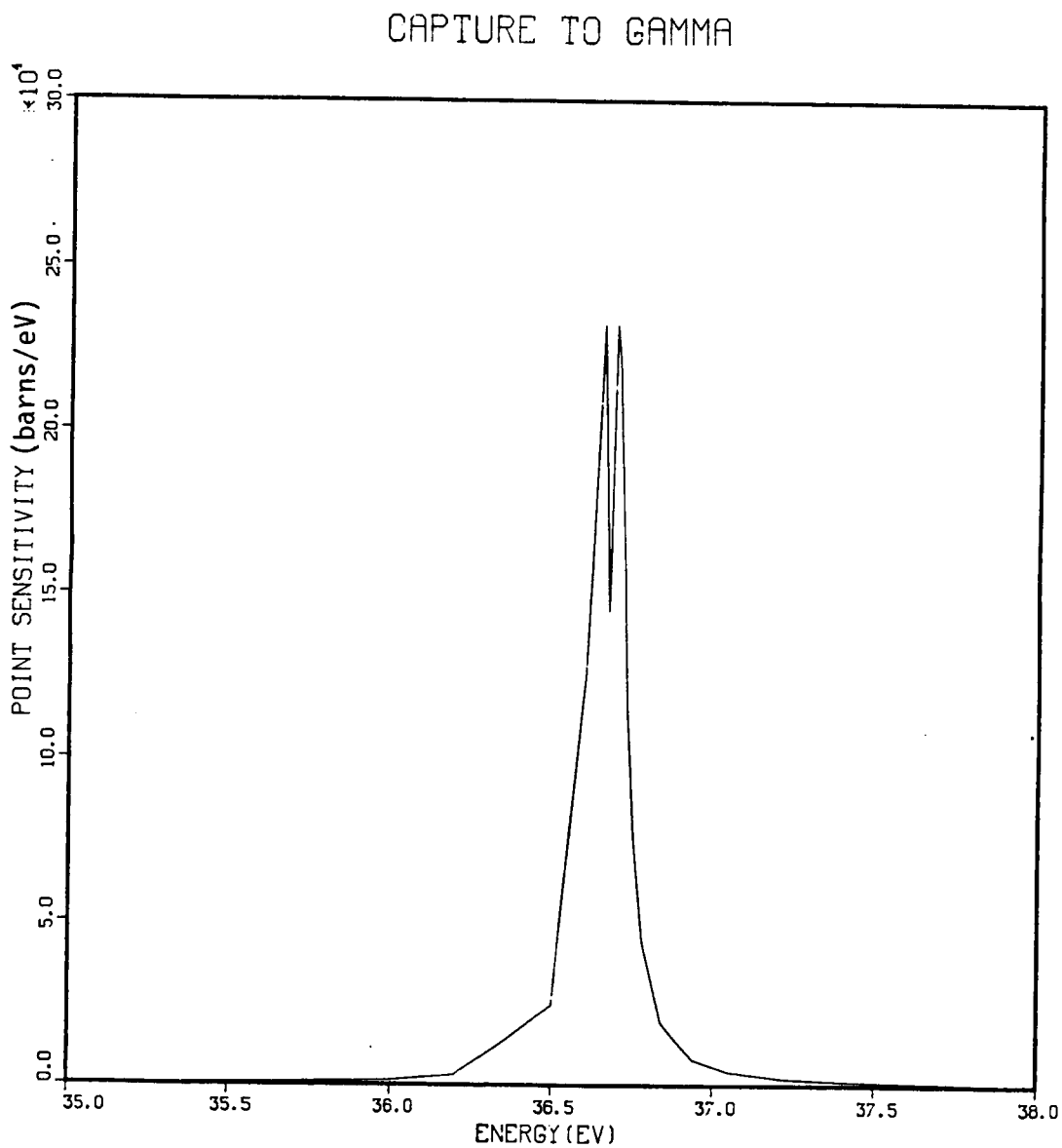

Figure VI-4. Pointwise Resonance Parameter Sensitivities of the U-238 Capture Cross Section to Γ_γ at 36.7 eV

dominating elsewhere. For $\Gamma_\gamma = 1/2\Gamma_t$ the RP sensitivity dip has a minimum of 0 at the resonance peak energy. It can also be seen from equation II-5 that the proportionality constant between the cross section and the RP sensitivity profile in figure VI-4 is Γ_γ. In figure VI-5 the RP sensitivity of ^{238}U elastic cross section to Γ_n at 6.67 eV is shown. This sensitivity has a shape similar to the cross section and goes negative at energies below the resonance energy.

Resolved Resonance Region Validation

In order to validate the results of the DEFUNCT code calculations, a dummy ^{238}U ENDF/B-like file (^{28}DUM) was created using 36 resolved resonances (see Chapter VIII). The validations were performed by making direct perturbations in the resonance parameters and using the NJOY cross section processing code to obtain reference and perturbed ^{28}DUM cross section values. The perturbations in the resolved resonance parameters were in all cases 10%. In Tables VI-1 and VI-2 comparisons between NJOY "actual" and DEFUNCT "predicted" RP sensitivities are shown for the 6.67 eV and 20.9 eV resonances of ^{28}DUM, respectively, at a temperature of 300°K and σ_0 = 100 barns. The agreement ranges from less than 1% to 5% for capture to Γ_γ, 4% to 15% for capture to Γ_n RP sensitivities, and 1% to 70% for elastic to Γ_n. The 70% discrepency in the elastic to Γ_n RP sensitivity in the group from 29.0 to 37.3 eV for the 20.9 eV resonance is not of major concern since it is not a significant contributor to the total group sensitivity. This error is attri-

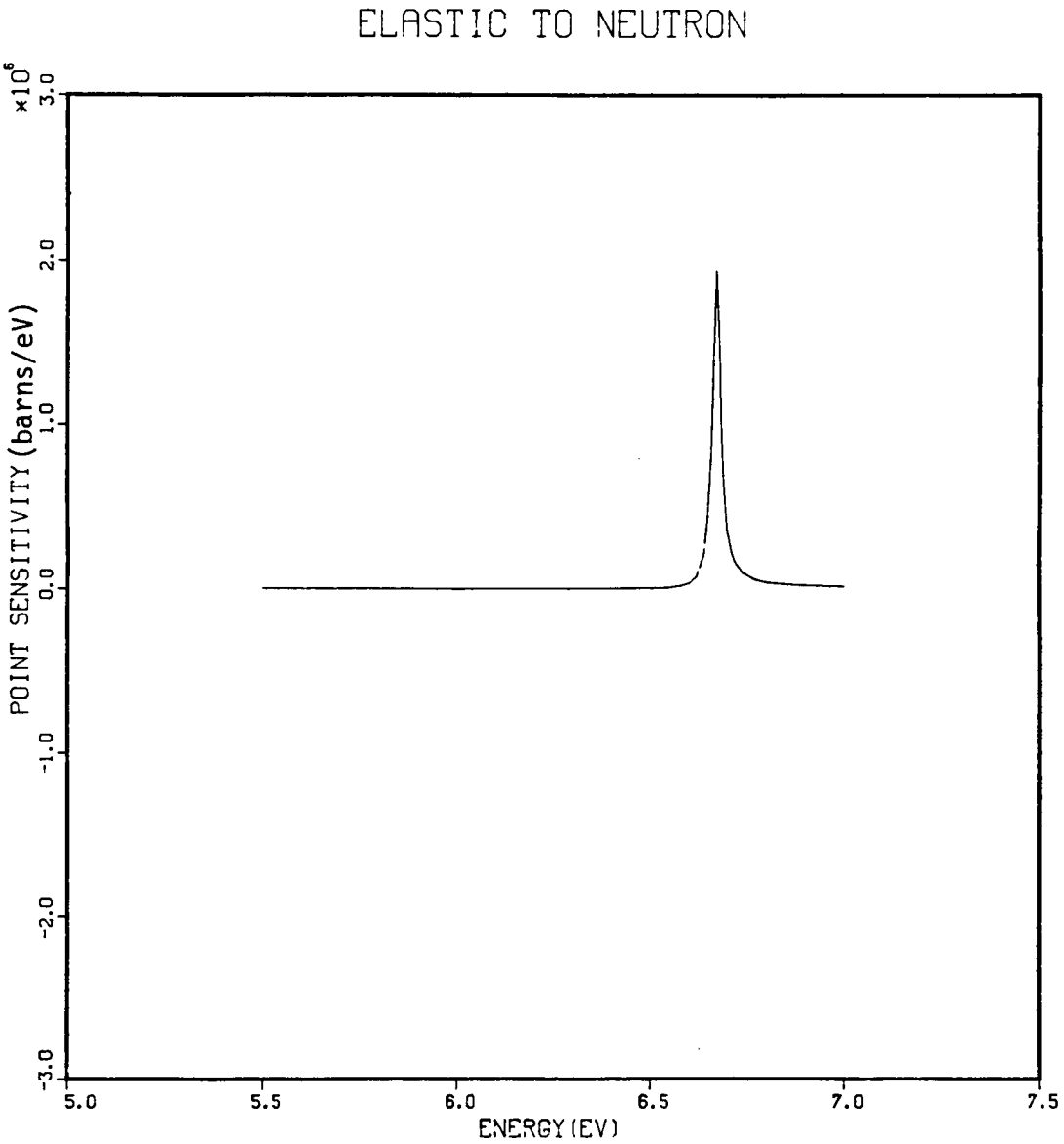

Figure VI-5. Pointwise Resonance Parameter Sensitivities of the U-238 Elastic Cross Section to Γ_n at 6.67 eV

Table VI-1

Resonance Parameter Sensitivity Comparisons for 6.67 eV Resonance in ^{28}DUM Cross Sections

Group Boundaries (eV)	capture to Γ_γ sensitivity		capture to Γ_n sensitivity		elastic to Γ_n sensitivity	
	actual[a]	predicted[b]	actual[a]	predicted[b]	actual[a]	predicted[b]
3.06	20.51	20.54	306.0	306.6	-562.9	-632.6
3.93	39.50	39.80	596.0	594.2	-794.7	-909.5
5.04	345.3	361.4	5172.	5431.	-1603.	-1964.
6.48	639.1	665.3	8874.	9355.	4570.	4972.
8.32	20.15	20.30	300.0	302.3	755.0	855.8
10.7	4.083	4.080	60.93	60.88	344.4	406.4
13.7	1.332	1.308	19.87	19.53	192.1	243.7
17.6						

a- the sensitivity obtained from a direct recalculation using NJOY
b- the sensitivity as calculated using DEFUNCT

Table VI-2

Resonance Parameter Sensitivity Comparisons for 20.9 eV Resonance in ^{28}DUM Cross Sections

Group Boundaries (eV)	capture to Γ_n sensitivity		elastic to Γ_n sensitivity	
	actual[a]	predicted[b]	actual[a]	predicted[b]
3.06	5.93	5.90	-58.3	-66.2
3.93	5.93	5.86	-59.3	-70.1
5.04	4.94	5.57	-54.3	-75.6
6.48	-9.88	-8.41	-98.8	-87.0
8.32	8.40	8.37	-94.9	-99.6
10.7	12.7	12.9	-119.	-129.
13.7	34.6	35.2	-187.	-211.
17.6	524.	613.	632.	634.
22.6	48.6	53.6	287.	350.
29.0	9.88	10.2	69.2	118.
37.3	<.988	1.10	79.1	56.9
47.9				

a- the sensitivity obtained from a direct recalculation using NJOY
b- the sensitivity as calculated using DEFUNCT

buted to the difficulty in adequately representing the rapid variations in the point-wise resonance profiles in this range as shown in figure VI-5.

In Table VI-3 a similar comparison is made, with actual and predicted values of capture to $\hat{a}$, elastic to $\hat{a}$, and capture to σ_0 relative RP sensitivities shown. Here as before the agreement is reasonably good with the most important values generally within 1-10% of the actual values.

As an additional verification of the methodology developed herein and to evaluate a proposed alternative resonance parameter sensitivity method, additional results for ^{238}U are given in Tables VI-4 to VI-9 for two different values of self-shielding, $\sigma_0 = 10^{10}$ and 22 barns, and two temperatures, T = 0,300°K. Table VI-4 gives relative sensitivity results for ^{238}U capture for all resonances in a group spanning 167eV to 214eV, Table VI-5 results for ^{238}U capture for all resonances in a group spanning 275eV to 354eV, and Tables VI-6 to VI-9 results for ^{238}U capture for all resonances in a group spanning 1.58keV to 2.03 keV. The Perey method was developed by F.G. Perey and is briefly described in reference 28 and Appendix F. The method is designed to operate on resonances with energies greater than 100eV as described in reference 28. Tables VI-4 to VI-9 compare the results of our method (labeled DEFUNCT), Perey's method, and direct recalculations using the MINX code for the sensitivities of ^{238}U capture cross sections to the Γ_γ and Γ_n resonance parameters. The resonances selected for direct recalculations were chosen first, on their high sensitivity and second, on apparent discrepencies between the Perey and DEFUNCT results. In Tables VI-4 to VI-9 a

Table VI-3

Resonance Parameter Sensitivity Comparisons
for σ_0 and $\hat{a}$ in ^{28}DUM Cross Sections

Group Boundaries (eV)	capture to $\hat{a}$ rel. sens.		elastic to $\hat{a}$ rel. sens.		capture to σ_0 rel. sens.	
	actual[a]	predicted[b]	actual[a]	predicted[b]	actual[a]	predicted[b]
5.04	.049	.044	2.97	3.10	.101	.104
6.48	.132	.124	1.71	1.58	.519	.516
8.32	-.001	-.001	2.30	2.16	.002	.003
10.7	0.0	0.0	2.42	2.31	0.0	0.0
13.7	.003	.003	2.64	2.56	-.001	-.002
17.6	.091	.083	1.32	1.24	.458	.445
22.6	-.008	-.012	2.16	1.95	.011	.023
29.0	.131	.120	1.09	0.97	.505	.496
37.3	-.037	-.038	1.47	1.37	.172	.173
47.9	-.002	.004	2.12	2.00	-.002	-.004
61.4	.144	.125	1.53	1.38	.493	.449
78.9	.081	.067	2.26	2.05	.370	.338
101.3	.203	.185	1.28	1.22	.500	.495
130.1						

a- the sensitivity obtained from a direct recalculation using NJOY
b- the sensitivity as calculated using DEFUNCT

Table VI-4

Relative Sensitivity Comparisons for ^{238}U Capture Group Cross Section (167eV to 214eV) to all Resonances Contained in the Group

Resonance Energy (eV)	Γ_γ (D)+ rel. sens.	Γ_γ (P)+ rel. sens.	Γ_n (D)+ rel. sens.	Γ_n (P)+ rel. sens.
189.6	.534	.543	.0753	.0761
			(.0654)*	
208.5	.266	.258	.123	.119
			(.114)*	
173.2			1.68-3	1.78-3
194.8			1.41-3	1.41-3
			(1.31-3)*	
200.7			1.57-3	1.54-3
203.1				
		$\sigma_0 = 10^{10}$, T = 0.0 °K		
189.2	.499	.469	.0388	.0515
			(.0346)*	
208.5	.314	.274	1.70-3	.0102
			(-.0113)*	
173.2			.0255	.0328
194.8			.0133	.0261
			(.0139)*	
200.7			.0186	.0283
203.1			.0122	.0173
		$\sigma_0 = 22.2$, T = 300°K		

* direct recalculation
\+ (D) = DEFUNCT method, (P) = Perey method

Table VI-5

Relative Sensitivity Comparisons for ^{238}U Capture Group Cross Section (275eV to 354eV) to all Resonances Contained in the Group

Resonance Energy (eV)	Γ_γ (D)+ rel. sens.	Γ_γ (P)+ rel. sens.	Γ_n (D)+ rel. sens.	Γ_n (P)+ rel. sens.
291.0	.174	.181	.239	.249
	(.156)*		(.228)*	
311.3	1.95-3	1.57-3	.0355	.0358
347.8	.418	.402	.118	.112
			(.106)*	
282.4			4.73-3	5.02-3
306.2			1.94-3	1.97-3
322.9			1.51-3	1.50-3
332.0			1.77-3	1.72-3
337.3			3.34-3	3.24-3
351.9			6.42-3	6.11-3
	$\sigma_0 = 10^{10}$, T = 0.0 °K			
291.0	.218	.134	-.0015	.114
	(.200)*		(-.0065)*	
311.3	.0109	.0100	.115	.209
347.8	.254	.199	-.0307	.0505
			(-.0264)*	
282.4			.0274	.0369
306.2			.0115	.0151
322.9			9.24-3	.0116
332.0			.0109	.0132
337.3			.0201	.0242
351.9			.0287	.0430
	$\sigma_0 = 22.2$, T = 300°K			

* direct recalculation
+ (D) = DEFUNCT method, (P) = Perey method

Table VI-6

Relative Sensitivity Comparisons at Infinite Dilution for ^{238}U Capture Cross Section (1.58keV to 2.03keV) to all s-wave Resonances Contained in the Group

Resonance Energy (eV)	Γ_γ (D)+ rel. sens.	Γ_γ (P)+ rel. sens.	Γ_n (D)+ rel. sens.	Γ_n (P)+ rel. sens.
1598	.0732	.0783	4.54-3	4.68-3
1623	.0544	.0571	.0126	.0125
1638	.0400	.0410	.0186	.0182
1662	.0676	.0704	7.94-3	7.72-3
1689	.0526	.0541	.0123	.0121
1710	.0534	.0544	.0172	.0169
1723	.0145	.0139	.0182	.0178
1756	.0581	.0588	.0120	.0116
1783	.0652	.0658	2.72-3	2.42-3
1808	.0153	.0134	.0143	.0123
	(.0127)*		(.0115)*	
1846	8.03-3	7.09-3	.0110	.0100
1868			2.34-3	2.19-3
			(1.74-3)*	
1903	.0274	.0260	.0155	.0145
	(.0259)*		(.0138)*	
1913			5.07-3	4.67-3
1917	.0246	.0232	.0147	.0135
1954	1.84-3	1.29-3	7.92-3	7.22-3
1969	.0680	.0654	2.80-3	2.48-3
1975	.0513	.0492	3.15-3	2.71-3
2024	.0444	.0420	5.02-3	4.47-3
2030	.0247	.0233	.0129	.0121

* direct recalculation
+ (D) = DEFUNCT method, (P) = Perey method

Table VI-7

Relative Sensitivity Comparisons at Infinite Dilution for ^{238}U Capture Cross Section (1.58keV to 2.03keV) to all p-wave Resonances Contained in the Group

Resonance Energy (eV)	Γ_γ (D)+ rel. sens.	Γ_γ (P)+ rel. sens.	Γ_n (D)+ rel. sens.	Γ_n (P)+ rel. sens.
1592			3.92-3	4.15-3
1612			1.43-3	1.50-3
				(1.16-3)*
1673			3.29-4	3.25-4
1682			1.35-3	1.34-3
1696			1.37-3	1.34-3
1707			4.16-3	4.11-3
				(4.07-3)*
1746			4.79-3	4.65-3
1769			1.52-3	1.47-3
1776			2.05-3	1.97-3
1781			3.33-3	3.22-3
				(2.90-3)*
1797			6.91-3	6.57-3
1824			2.04-3	1.91-3
1834			1.18-3	1.13-3
				(<1.16-3)*
1867	1.12-3	7.60-4	6.59-3	6.15-3
				(5.80-3)*
1870	1.01-3	6.27-4	6.06-3	5.64-3
				(5.22-3)*
1881			3.57-3	3.35-3
1894			3.83-3	3.54-3
1925			2.36-3	2.17-3
1933			1.03-3	9.50-4
1943			1.67-3	1.53-3
1990			3.23-3	2.91-3
2001			1.17-3	1.06-3

* direct recalculation
+ (D) = DEFUNCT method, (P) = Perey method

Table VI-8

Relative Sensitivity Comparisons at σ_0 = 22.2 barns for ^{238}U Capture Group Cross Section (1.58keV to 2.03keV) to all s-wave Resonances Contained in the Group

Resonance Energy (eV)	Γ_γ (D)+ rel. sens.	Γ_γ (P)+ rel. sens.	Γ_n (D)+ rel. sens.	Γ_n (P)+ rel. sens.
1598	.0378	.0326	8.31-3	1.93-3
1623	.0447	.0406	-.0103	7.95-3
1638	.0470	.0472	-4.76-3	.0194
1662	.0403	.0281	-6.66-3	2.68-3
1689	.0433	.0393	-.0125	7.91-3
1710	.0473	.0448	-.0108	.0126
1723	.0262	.0205	.0176	.0279
1756	.0444	.0367	-.0117	6.49-3
1783	.0313	.0286	-7.54-4	1.04-3
1808	.0279	.0194	.0151	.0190
	(.0223)*		(9.37-3)*	
1846	.0176	.0165	.0150	.0237
1868			5.88-3	7.38-3
			(5.13-3)*	
1903	.0378	.0375	-1.23-3	.0200
	(.0364)*		(-4.26-3)*	
1913	2.76-3	1.41-3	.0139	.0150
1917	.0361	.0354	1.49-3	.0200
1954	5.47-3	3.85-3	.0207	.0216
1969	.0360	.0298	-3.90-3	1.12-3
1975	.0208	.0226	-3.95-3	1.24-3
2024	.0289	.0214	-.0144	2.05-3
2030	.0290	.0341	-1.22-3	.0171

* direct recalculation
+ (D) = DEFUNCT method, (P) = Perey method

Table VI-9

Relative Sensitivity Comparisons at σ_0 = 22.2 barns for ^{238}U Capture Group Cross Section (1.58keV to 2.03keV) to all p-wave Resonances Contained in the Group

Resonance Energy (eV)	Γ_γ (D)+ rel. sens.	Γ_γ (P)+ rel. sens.	Γ_n (D)+ rel. sens.	Γ_n (P)+ rel. sens.
1592			.0134	.0137
1612			3.75-3	5.12-3
			(3.42-3)*	
1673			8.68-4	1.13-3
1682			3.75-3	4.61-3
1696			3.53-3	4.59-3
1707	1.48-3	7.88-4	.0111	.0135
			(.0133)*	
1746	1.75-3	1.08-3	.0119	.0151
	(1.57-3)*			
1769			4.39-3	5.02-3
1776			6.66-3	6.69-3
1781	9.10-4	5.35-4	6.00-3	.0107
	(1.28-3)*		(6.56-3)*	
1797	2.93-3	2.42-3	.0139	.0204
1824			5.31-3	6.49-3
1834			3.24-3	3.87-3
			(1.85-3)*	
1867	3.40-3	2.36-3	.0154	.0192
			(.0157)*	
1870	3.41-3	1.97-3	.0135	.0178
	(2.14-3)*		(.0145)*	
1881	1.29-3	6.75-4	9.20-3	.0110
1894	1.43-3	7.70-4	.0105	.0116
1925	1.04-3	2.93-4	7.01-3	7.29-3
1933			2.99-3	3.27-3
1943			5.38-3	5.22-3
1990			7.40-3	9.65-3
2001			2.79-3	3.63-3

* direct recalculation
+ (D) = DEFUNCT method, (P) = Perey method

cut-off of 1.0×10^{-3} is used for all the relative sensitivities so that insignificant sensitivities are omitted from the comparison. Shown in the top half of Table VI-4 are the relative sensitivities for ^{238}U infinitely dilute capture cross sections (i.e. $\sigma_0 = 10^{10}$). In the case for infinitely dilute cross sections the Perey method is nearly exact. This is verified by the good agreement between the DEFUNCT, Perey, and the direct recalculation (for a 10% variation) relative sensitivity values. Two comparisons can be made here, (1) agreement between the DEFUNCT and Perey methods partially validate the DEFUNCT methodology since the Perey method is nearly exact for the infinitely dilute case, (2) comparison of the DEFUNCT and Perey methods with direct recalculations can also be used to validate both methods. However, in some cases as shown later, the direct perturbations contain non-linear terms so that a direct comparison is not possible.

A good example of this is seen in the bottom half of Table VI-4 for ^{238}U capture cross sections at a self-shielding value of $\sigma_0 = 22$ barns (the value for TRX-1) and temperature of 300°K. The relative sensitivities for Γ_n at the 208.5 eV resonance show wide variation between the three values shown. The presence of non-linear terms is confirmed by making a -10% direct recalculation and again estimating the relative sensitivity value. In this case the predicted relative sensitivity value is -1.73×10^{-3} which is quite different from the positive 10% value. At $\sigma_0 = 100$ barns and a temperature of 300°K, this effect is not seen and the DEFUNCT result agree very well with the direct recalculations (i.e. DEFUNCT = -6.1×10^{-2} ; 10% direct recalculation = -6.2×10^{-2} ; -10% direct recalculation = -6.5×10^{-2}). For other resonances in Table VI-4

it appears that the DEFUNCT values agree very well with the direct recalculations, while the Perey value agreements are much less satisfactory.

The same effects as are seen in Table VI-4 are duplicated in Table VI-5 for the group spanning 275eV to 354eV. Close agreement is seen for all three methods for the infinitely dilute and 0°K case and fairly close agreement between the DEFUNCT method and direct recalculations for the σ_0 = 22.2 barns and temperature = 300°K case. One exception is the apparent discrepency between the DEFUNCT and direct recalculation values for Γ_n at 291eV for the σ_0 = 22.2 barns and temperature = 300°K case. The cause of this discrepency was not investigated further due to the relatively small contribution to the total.

In Tables VI-6 and VI-7 relative sensitivity values for ^{238}U capture cross sections in the group spanning 1.58keV to 2.03keV are given for the s-wave and p-wave resonance parameters, respectively, at a value of $\sigma_0 = 10^{10}$ barns and a temperature of 0°K. In all cases the agreement between the DEFUNCT, Perey, and direct recalculation values is good. In Table VI-8 for the σ_0 = 22.2 barns and temperature = 300°K case for the s-wave resonance parameters, the agreement between the DEFUNCT, Perey, and direct recalculation methods is worse than the infinitely dilute case (approximately 20% discrepency), but in most cases still acceptable (with the exception of the 1662 and 1954eV resonances). For the Γ_n relative sensitivities the Perey method appears to be unable to predict any of the negative values. This should be due in part to the approximation made in the derivation of the denominator term as seen in Appendix F. Even the DEFUNCT values appear to give poor results for

the 1808eV and 1903eV resonances. However, if a -10% direct recalculation is performed for the 1808eV resonance case a value of .0123 for the relative sensitivity is obtained. This value is much closer to the value predicted by DEFUNCT and thus this apparent error can be attributed to non-linearities. Concerning the 1903eV resonance, it is felt that even though a difference of a factor of 3-4 is seen between the predicted and actual values, the magnitude of the sensitivilty is such that very little consequences result from this apparent discrepency.

In Table VI-9 the p-wave relative sensitivities are given for the ^{238}U capture cross section at σ_0 = 22.2 barns and a temperature of 300°K. Again, in most cases, fairly good (less than 20%) agreement is seen between DEFUNCT and the direct recalculations. In one case at the 1870eV value for Γ_γ, the Perey method seems to give a better answer than the DEFUNCT method, but this is clearly the exception rather than the rule. Also, it seems that although both the DEFUNCT and Perey methods agree at 1834eV for Γ_n, the direct recalculation is about a factor of 2 lower. It is felt that this discrepency can also be attributed to non-linearities.

In summary, the simple and very quick Perey method seems to give quite good results at infinite dilution. For heavily self-shielded cases the Perey method gives excellent to good results for the most important Γ_γ relative sensitivities and in general very poor results for the Γ_n relative sensitivities. Also as a caution, these results are given only for the capture cross sections. Other cross sections have not been tested and the results could possibly be different. This section has also not compared any σ_0 and $\hat{a}$ sensitivities.

Unresolved Resonance Region Validation

In Tables VI-10 to VI-12, actual vs. predicted values are displayed to validate the unresolved region processing portion of the DEFUNCT code. In these tables the "actual" column represents the fractional change in the indicated group cross section obtained by a direct recalculation using a 1% change in average resonance parameters for all sequences (j,ℓ values) at a given resonance energy (E* point). Comparisons are made for both capture and elastic cross section changes due to $\langle\Gamma_n\rangle$ and $\langle\Gamma_\gamma\rangle$ changes at both 4.25 kev (Table VI-10) and 6.5 kev (Table VI-11) as well as $\langle D\rangle$ changes at 6.5 kev (Table VI-12). In most cases agreement is good with some degradation in agreement seen for the smaller σ_0 values.

RP Sensitivity Results for ^{238}U Cross Sections

The relative RP sensitivity of the ^{238}U capture group cross section from 1 eV to 100 eV to Γ_γ at 6.67 eV is shown in Figure VI-6 for several degrees of self-shielding. At approximately 7 eV a pronounced dip is seen for the infinitely dilute sensitivity value. This dip is due to the fact that Γ_γ at 6.67 eV is 94% of Γ_t, thus with a flat weighting (i.e. $\sigma_0=\infty$) a cancellation between Γ_γ and Γ_t occurs such that the cross section is dominated by Γ_n (see Figure VI-13). However, this depression vanishes as one tends toward lower σ_0 values due to the cancellation of the resonance peak by the flux depression. Similar depressions followed by subsequent filling for lower σ_0 values are also seen in other groups containing resonances.

Table VI-10

Resonance Parameter Sensitivity Comparisons for Capture and Elastic Group Cross Sections (4 keV-5.53 keV) to Γ_γ and Γ_n Average Parameters at 4.25 keV

Fractional change in Capture Cross Section

σ_0 value	1% Γ_γ change actual(a)	predicted(b)	1% Γ_n change actual(a)	predicted(b)
∞	.00120	.00110	.00076	.00069
100	.00101	.00100	.00113	.00128
50	.00095	.00094	.00176	.00192
10	.00082	.00086	.00229	.00256

Fractional change in Elastic Cross Section

σ_0 value	1% Γ_n change actual(a)	predicted(b)	1% Γ_γ change actual(a)	predicted(b)
∞	.00069	.00069	-.00006	-.00006
100	.00079	.00088	-.00005	-.00005
50	.00090	.00089	-.00005	-.00005
10	.00038	.00077	-.00003	-.00004

a-obtained by direct recalculation

b-obtained by DEFUNCT sensitivity calculation

Table VI-11

Resonance Parameter Sensitivity Comparisons for Capture and Elastic Group Cross Sections (5.53 keV-9.12 keV) to Γ_γ and Γ_n Average Parameters at 6.5 keV

Fractional change in Capture Cross Section

σ_0 value	1% Γ_γ change actual(a)	predicted(b)	1% Γ_n change actual(a)	predicted(b)
∞	.00180	.00170	.00140	.00141
100	.00166	.00162	.00262	.00285
50	.00159	.00158	.00391	.00436
10	.00149	.00148	.00496	.00580

Fractional change in Elastic Cross Section

σ_0 value	1% Γ_n change actual(a)	predicted(b)	1% Γ_γ change actual(a)	predicted(b)
∞	.00102	.00103	-.00009	-.00009
100	.00135	.00149	-.00008	-.00008
50	.00161	.00154	-.00007	-.00007
10	.00082	.00125	-.00006	-.00007

a-obtained by direct recalculation

b-obtained by DEFUNCT sensitivity calculation

Table VI-12

Resonance Parameter Sensitivity Comparisons for Capture and Elastic Group Cross Sections (5.53 keV-9.12 keV) to D Average Parameter at 6.5 keV

	Fractional change in Capture Cross Section			
	Capture change due to 1% D		Elastic change due to 1% D	
σ_0 value	actual(a)	predicted(b)	actual(a)	predicted(b)
∞	-.00317	-.00312	-.00093	-.00094
100	-.00317	-.00327	-.00074	-.00075
50	-.00333	-.00336	-.00064	-.00048
10	-.00314	-.00357	-.00039	-.00005

a-obtained by direct recalculation

b-obtained by DEFUNCT sensitivity calculation

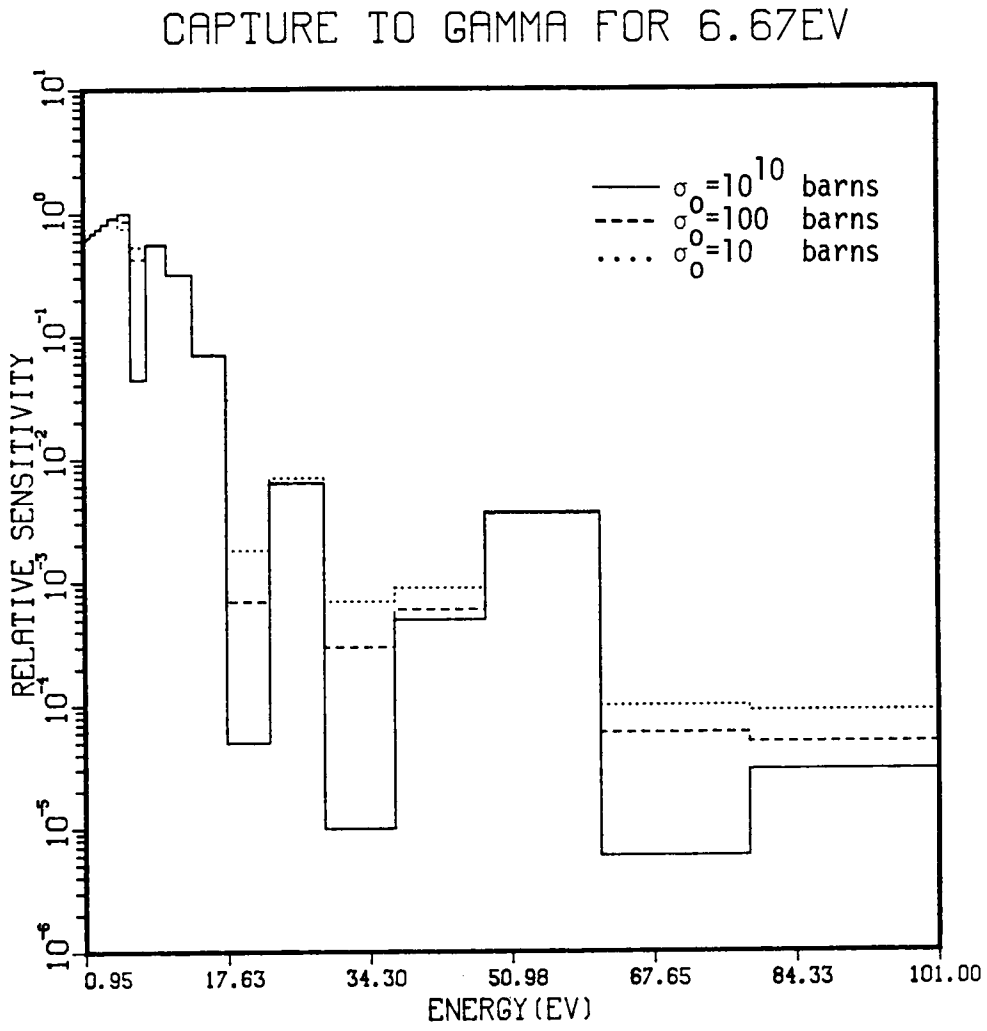

Figure VI-6. Relative Sensitivity Values for U-238 Capture Cross Section to Γ_γ at 6.67 eV for Various Values of Energy Self-Shielding

In Figure VI-7 the overall behavior of the relative RP sensitivity of ^{238}U capture group cross section to the Γ_n value at 6.67 eV is very similar to the capture cross section to Γ_γ plot in Figure VI-6. However, the opposite effect is seen in the group containing the 6.67 eV resonance. As stated before, at infinite dilution the influence of Γ_γ on the cross section cancels out leading to the dominance of Γ_n on the capture cross section. As the degree of self-shielding increases the influence of the Γ_n value decreases due to the increasing importance of Γ_γ. A very interesting phenomenom occurs as can be seen in figure VI-7 when the value of the relative sensitivity of the capture group cross section containing the 6.67eV resonance first decreases then increases as the value of σ_0 decreases from 10^{10} to 10 barns. This reversal is actually due to the varying rates of decrease of the absolute sensitivity and the self-shielded cross sections. The absolute sensitivity reaches its asymptotic value before the cross section, hence the continued decrease of the cross section with decreasing σ_0 makes the relative sensitivity 'turn around' or begin increasing in magnitude.

In figure VI-8 the relative sensitivity of the ^{238}U capture cross section from 1eV to 100eV to Γ_γ at 20.86eV is plotted. The same 'dip' is seen in the group containing the 20.86eV resonance as was seen for the 6.67eV resonance, however it is not as deep since in this case Γ_γ is only 70% of Γ_t. The wings of the 20.86eV resonance also have a slight effect on the group containing the 6.67eV resonance since an increase in the wing from the 20.86eV resonance is seen as an increase in the background cross section and hence an increase in the total capture

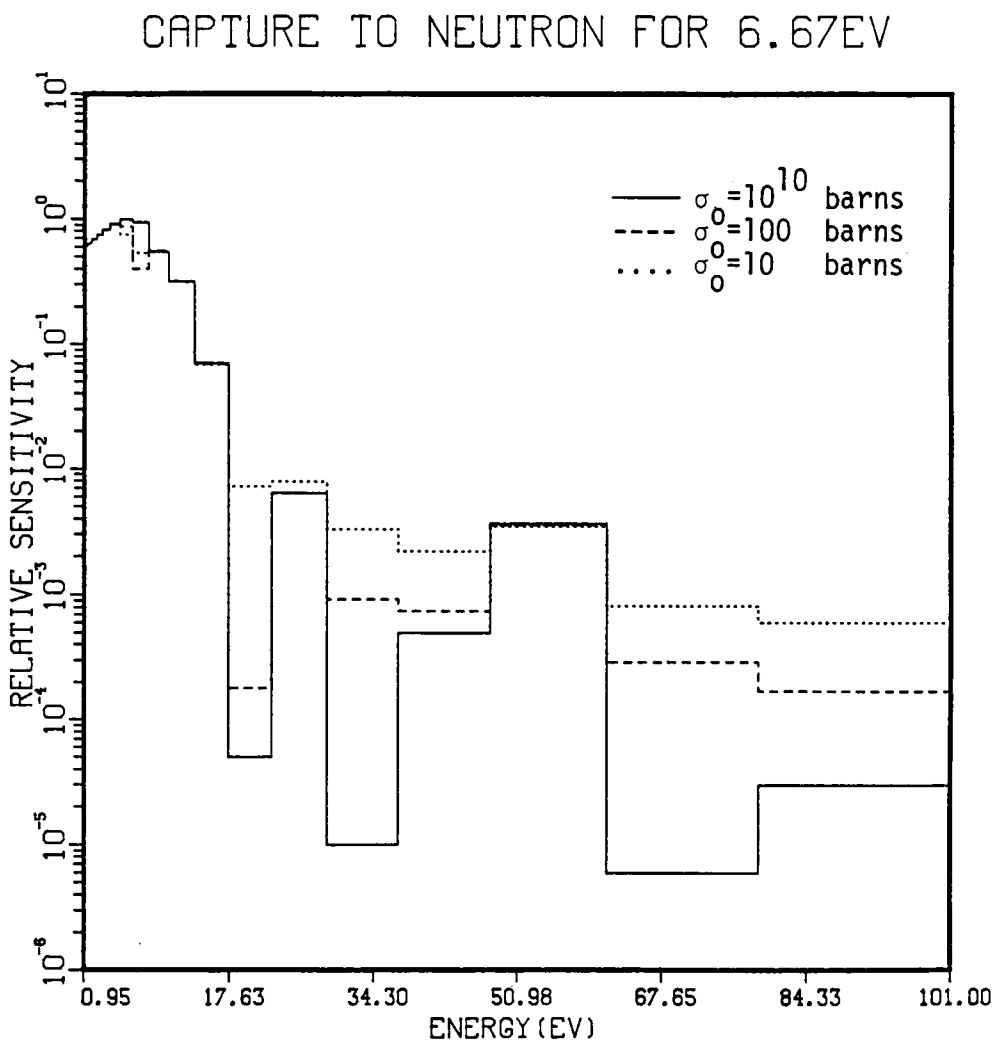

Figure VI-7. Relative Sensitivity Values for U-238 Capture Cross Sections to Γ_n at 6.67 eV for Various Values of Energy Self-Shielding

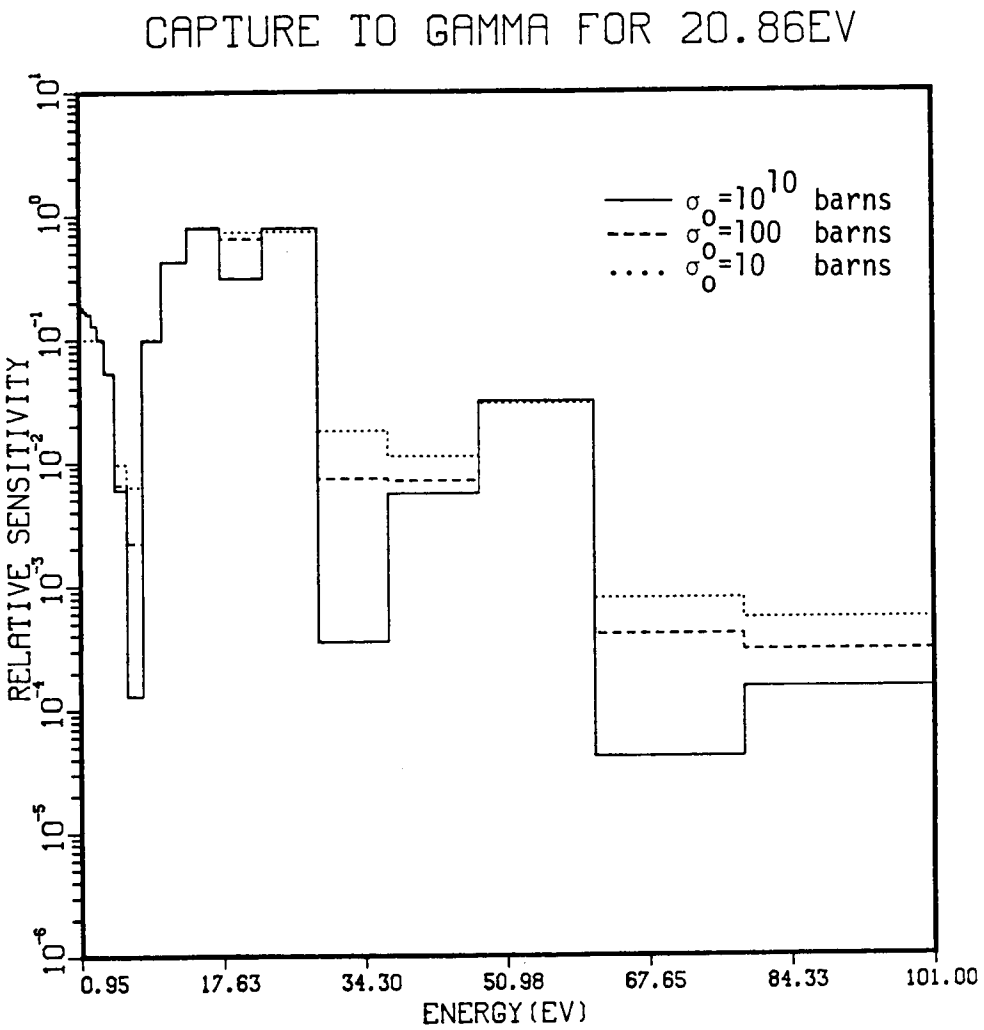

Figure VI-8. Relative Sensitivity Values for U-238 Capture Cross Sections to Γ_γ at 20.86 eV for Various Values of Energy Self-Shielding

cross section due to the decreased self-shielding.

The relative sensitivity of the ^{238}U elastic cross section to Γ_n at 6.67eV is shown in figure VI-9 from 1eV to 100eV. The relative sensitivity at $\sigma_0 = 10^{10}$ barns is quite high and decreases monotonically with decreasing σ_0 values. Note that below this group the relative sensitivity values are negative. This is due to the fact that below the resonance energy the resonant portion of the elastic cross section becomes negative and thus increasing Γ_n actually decreases the elastic cross section in this region.

In the unresolved regions the range of RP sensitivities is much shorter than the resolved region. For this reason the results are presented in a different manner. Tables VI-13 to VI-17 show relative RP sensitivities of the capture and elastic group (5.53keV - 9.12keV) cross sections to the first few sequences ((J,l)=0,1/2;1,1/2;1,3/2) of the $\langle\Gamma_\gamma\rangle$, $\langle\Gamma_n\rangle$, and $\langle D\rangle$ average resonance parameters. Table VI-13 shows relative RP sensitivities at four different σ_0 values for capture cross section to $\langle\Gamma_\gamma\rangle$ for the first three levels at five E^* points. As expected all s-wave relative RP sensitivities decrease with decreasing σ_0. Also the 6.5 keV and 7.5 keV points exhibit the largest sensitivities since they are completely contained in the group. Somewhat surprising is that the p-wave relative RP sensitivities increase with decreasing σ_0 values. This is due not to the increasing absolute sensitivity, but due to the increasing fractional contribution to the total capture cross section caused by self-shielding of the s-wave contribution. An interesting observation with respect to uncertainty analysis is that at low σ_0 values the p-wave uncertainty contributions

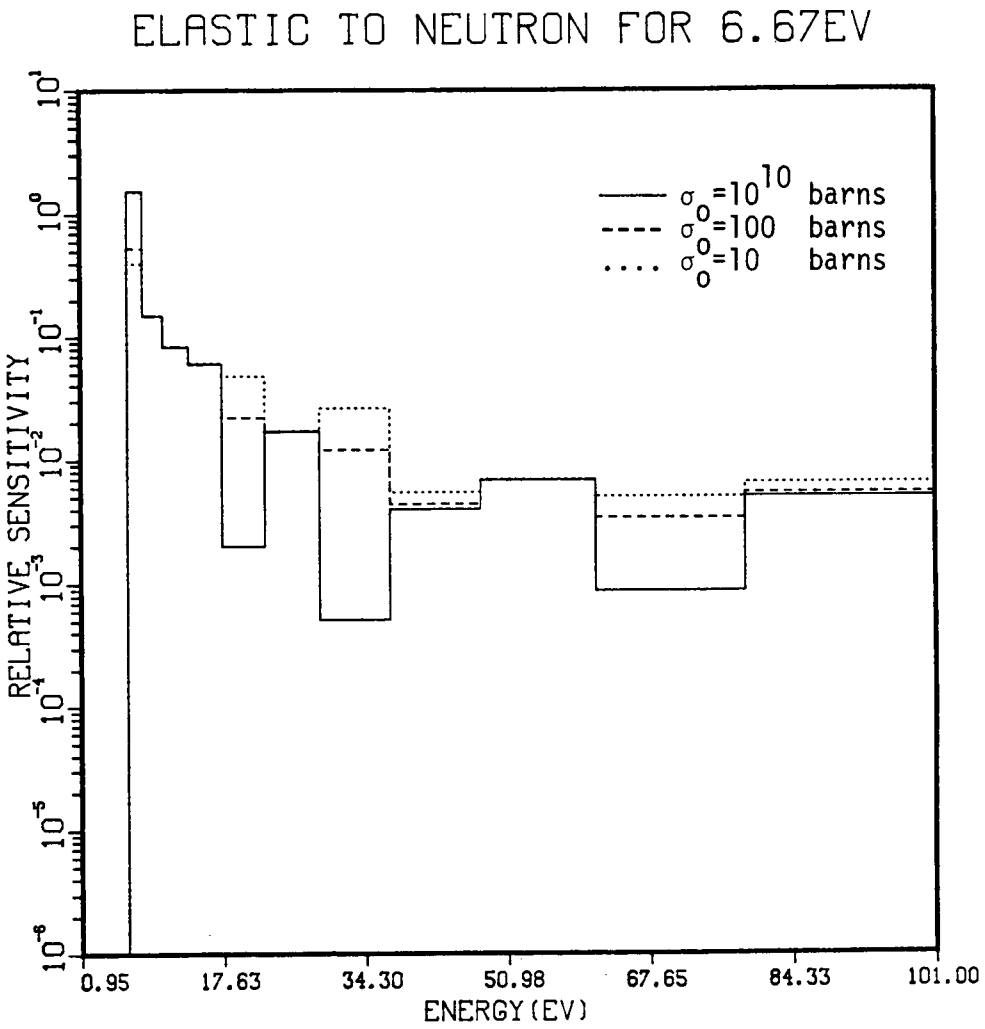

Figure VI-9. Relative Sensitivity Values for U-238 Elastic Cross Sections to Γ_n at 6.67 eV for Various Values of Energy Self-Shielding

Table VI-13

Unresolved Resonance Parameter Relative Sensitivities for ^{238}U Capture Group Cross Section (5.53 keV to 9.12 keV) to Γ_γ Average Resonance Parameters at Various Degrees of Energy Self-Shielding

σ_0 value*	5.5 keV resonance	6.5 keV resonance	7.5 keV resonance	8.5 keV resonance	9.25keV resonance
			(J,l)=0,1/2		
∞	.086	.142	.108	.074	.019
100	.077	.131	.102	.072	.019
50	.073	.125	.099	.070	.018
10	.062	.109	.088	.063	.017
			(J,l)=1,1/2		
∞	.005	.011	.011	.008	.003
100	.006	.012	.012	.008	.003
50	.006	.013	.012	.009	.003
10	.007	.014	.014	.010	.003
			(J,l)=1,3/2		
∞	.008	.017	.018	.013	.005
100	.009	.019	.019	.014	.005
50	.010	.020	.020	.015	.005
10	.011	.024	.024	.017	.006

*All temperatures are 300° K except for infinitely dilute where the temperature is 0° K.

Table VI-14

Unresolved Resonance Parameter Relative Sensitivities for ^{238}U Capture Group Cross Section (5.53 keV to 9.12 keV) to Γ_n Average Resonance Parameters at Various Degrees of Energy Self-Shielding

σ_0 value*	5.5 keV resonance	6.5 keV resonance	7.5 keV resonance	8.5 keV resonance	9.25keV resonance
			(J,l)=0,1/2		
∞	.023	.037	.027	.018	.005
100	.017	.030	.025	.018	.005
50	.015	.028	.024	.017	.005
10	.007	.016	.015	.012	.004
			(J,l)=1,1/2		
∞	.016	.028	.023	.016	.005
100	.017	.030	.025	.018	.005
50	.018	.032	.026	.018	.005
10	.019	.035	.029	.021	.006
			(J,l)=1,3/2		
∞	.041	.075	.064	.045	.013
100	.044	.080	.069	.048	.014
50	.045	.083	.072	.050	.015
10	.049	.091	.078	.056	.017

*All temperatures are 300° K except for infinitely dilute where the temperature is 0° K.

Table VI-15

Unresolved Resonance Parameter Relative Sensitivities for ^{238}U Elastic Group Cross Section (5.53 keV to 9.12 keV) to Γ_n Average Resonance Parameters at Various Degrees of Energy Self-Shielding

σ_0 value*	5.5 keV resonance	6.5 keV resonance	7.5 keV resonance	8.5 keV resonance	9.25keV resonance
			(J,l)=0,1/2		
∞	.057	.099	.079	.057	.015
100	.038	.070	.059	.044	.012
50	.026	.048	.041	.031	.009
10	.017	.033	.028	.021	.006
			(J,l)=1,1/2		
∞	7.2×10^{-4}	1.5×10^{-3}	1.5×10^{-3}	1.1×10^{-3}	4.2×10^{-4}
100	8.5×10^{-4}	1.8×10^{-3}	1.8×10^{-3}	1.3×10^{-3}	4.8×10^{-4}
50	5.0×10^{-4}	1.1×10^{-3}	1.2×10^{-3}	8.6×10^{-4}	3.3×10^{-4}
10	-2.1×10^{-4}	-2.7×10^{-4}	-9.3×10^{-5}	-4.3×10^{-5}	-3.1×10^{-5}
			(J,l)=1,3/2		
∞	9.6×10^{-4}	2.1×10^{-3}	2.2×10^{-3}	1.6×10^{-3}	6.2×10^{-4}
100	1.2×10^{-3}	2.6×10^{-3}	2.6×10^{-3}	1.9×10^{-3}	7.3×10^{-4}
50	5.0×10^{-4}	1.2×10^{-3}	1.4×10^{-3}	1.0×10^{-3}	4.3×10^{-4}
10	-9.1×10^{-4}	-1.5×10^{-3}	-1.1×10^{-3}	-7.7×10^{-4}	-1.6×10^{-4}

*All temperatures are 300° K except for infinitely dilute where the temperature is 0° K.

Table VI-16

Unresolved Resonance Parameter Relative Sensitivities for ^{238}U Capture Group Cross Section (5.53 keV to 9.12 keV) to D Average Resonance Parameters at Various Degrees of Energy Self-Shielding

σ_0 value*	5.5 keV resonance	6.5 keV resonance	7.5 keV resonance	8.5 keV resonance	9.25keV resonance
			(J,l)=0,1/2		
∞	-.109	-.179	-.136	-.092	-.024
100	-.108	-.183	-.142	-.099	-.026
50	-.108	-.185	-.146	-.102	-.027
10	-.104	-.184	-.149	-.107	-.029
			(J,l)=1,1/2		
∞	-.021	-.039	-.034	-.024	-.007
100	-.023	-.043	-.037	-.026	-.008
50	-.024	-.045	-.039	-.027	-.008
10	-.028	-.052	-.045	-.032	-.010
			(J,l)=1,3/2		
∞	-.049	-.092	-.082	-.057	-.018
100	-.053	-.100	-.089	-.063	-.020
50	-.056	-.105	-.094	-.066	-.021
10	-.063	-.119	-.106	-.075	-.024

*All temperatures are 300° K except for infinitely dilute where the temperature is 0° K.

Table VI-17

Unresolved Resonance Parameter Relative Sensitivities for ^{238}U Elastic Group Cross Section (5.53 keV to 9.12 keV) to D Average Resonance Parameters at Various Degrees of Energy Self-Shielding

σ_0 value*	5.5 keV resonance	6.5 keV resonance	7.5 keV resonance	8.5 keV resonance	9.25keV resonance
			(J,l)=0,1/2		
∞	-.052	-.092	-.074	-.053	-.014
100	-.040	-.073	-.061	-.045	-.012
50	-.025	-.047	-.040	-.030	-.008
10	-.004	-.009	-.008	-.006	-.002
			(J,l)=1,1/2		
∞	-4.4×10^{-4}	-9.6×10^{-4}	-1.0×10^{-3}	-7.2×10^{-4}	-2.8×10^{-4}
100	-5.7×10^{-4}	-1.2×10^{-3}	-1.2×10^{-3}	-8.9×10^{-4}	-3.4×10^{-4}
50	-2.1×10^{-4}	-5.2×10^{-4}	-6.0×10^{-4}	-4.5×10^{-4}	-1.9×10^{-4}
10	5.5×10^{-4}	9.4×10^{-4}	7.4×10^{-4}	5.1×10^{-4}	1.3×10^{-4}
			(J,l)=1,3/2		
∞	-5.5×10^{-4}	-1.2×10^{-3}	-1.3×10^{-3}	-9.5×10^{-4}	-3.8×10^{-4}
100	-7.8×10^{-4}	-1.7×10^{-3}	-1.7×10^{-3}	-1.3×10^{-3}	-4.9×10^{-4}
50	-6.1×10^{-5}	-2.7×10^{-4}	-4.5×10^{-4}	-3.5×10^{-4}	-1.8×10^{-4}
10	1.5×10^{-3}	2.7×10^{-3}	2.3×10^{-3}	1.6×10^{-3}	4.5×10^{-4}

*All temperatures are 300° K except for infinitely dilute where the temperature is 0° K.

can equal or surpass the s-wave contributions since p-wave values are usually much less well known than s-wave values.

The capture cross section in the group from 5.53 keV to 9.12 keV is less sensitive to the $\langle\Gamma_n\rangle$ values than in $\langle\Gamma_\gamma\rangle$ values as can be seen in Table VI-14. However, once again at low σ_0 values the p-wave relative RP sensitivities are increasing and become nearly as large as those for the s-wave $\langle\Gamma_\gamma\rangle$.

The elastic cross section is almost entirely sensitive to the S-wave $\langle\Gamma_n\rangle$ value as seen in Table VI-15. The p-wave contributions are in general at least a factor of ten below the s-wave values. Here, the s-wave relative RP sensitivities decrease in value as σ_0 decreases, while the p-wave values fluctuate.

The effects of changes in the value of $\langle D\rangle$ for the capture and elastic cross sections can be seen in Tables VI-16 and VI-17, respectively. The capture relative RP sensitivity values all increase in absolute value with decreasing σ_0 value except for the 5.5 keV s-wave values. In all cases these changes with σ_0 are fairly small. All relative sensitivities shown in Table VI-16 are negative due to the fact that increasing the average width of a resonance without changing the energy limits or number of resonances in a "statistical group" of resonances will naturally result in a decrease in the average cross section for that "statistical group." Again it is noted that for small values of σ_0 the relative sensitivities of the p-waves are almost as large as the s-wave relative sensitivities.

In Table VI-17 the effects of changes in $\langle D\rangle$ to the ^{238}U elastic cross section are given as a function of several σ_0 values. In this

case the s-wave components clearly dominate those of the p-waves. These relative sensitivities are fairly small due to the fact that the potential cross sections do not change and hence very little effect is seen from changing a resonance value. At very low σ_0 values this effect is clearly evident by the very small relative sensitivities. At these low values of σ_0 the elastic cross section is almost entirely the potential cross section.

Table VI-18 contains rankings of the five most important resolved resonance parameters with respect to the capture cross sections for groups 41-63 of the 77 group structure. Also included for comparison are the relative sensitivities to both $\hat{a}$ and σ_0. These values correspond to a σ_0 value of 22.2 barns which is the value for TRX-1.

Table VI-18

^{238}U Capture Cross Section Resonance Parameter Sensitivity Rankings at σ_0 = 22 barns

Group Rank	#1 (749-583eV) A	#1 (749-583eV) B	#2 (583-454eV) A	#2 (583-454eV) B	#3 (454-354eV) A	#3 (454-354eV) B
1	.237	G410.2	.262	G291.0	.415	G237.3
2	.208	N376.9	.237	G347.8	.258	G273.5
3	.195	N397.6	.183	N311.3	.128	N237.3
4	.155	G397.6	.091	N291.0	.030	N189.6
5	.097	N410.2	.080	N273.5	.030	N208.5
$\hat{a}$	.225		.280		.382	
σ_0	.192		.250		.324	

Group Rank	#4 (354-275eV) A	#4 (354-275eV) B	#5 (275-214eV) A	#5 (275-214eV) B	#6 (214-167eV) A	#6 (214-167eV) B
1	.516	G189.6	.234	N145.6	.399	G102.5
2	.343	G208.5	.177	N165.3	.392	G116.9
3	.067	N189.6	.153	G165.3	.147	N116.9
4	.032	N208.5	.075	G145.6	.040	N102.5
5	.029	N165.3	.012	G189.6	-.010	N189.6
$\hat{a}$	.374		.321		.442	
σ_0	.291		.318		.282	

Group Rank	#7 (167-130eV) A	#7 (167-130eV) B	#8 (130-101eV) A	#8 (130-101eV) B	#9 (101-78.9eV) A	#9 (101-78.9eV) B
1	.338	G102.5	.724	G66.01	.569	N66.01
2	.287	N102.5	.378	N66.01	.561	G66.01
3	.210	N80.73	.019	N63.50*	.378	G36.67
4	.157	G80.73	.015	N36.67	.377	N36.67
5	.080	N89.29*	.009	G80.73	.046	N102.5
$\hat{a}$	.234		.327		.006	
σ_0	.226		.238		-.009	

Group Rank	#10 (78.9-61.4eV) A	#10 (78.9-61.4eV) B	#11 (61.4-47.9eV) A	#11 (61.4-47.9eV) B	#12 (47.9-37.3eV) A	#12 (47.9-37.3eV) B
1	.897	G36.67	.761	G36.67	.759	G20.86
2	.599	N36.67	.174	N36.67	.709	N20.86
3	.015	N20.86	.031	N20.87	.203	G36.67
4	.013	N45.17*	.014	G20.86	.190	N36.67
5	.012	N72.78*	-.005	N66.01	.008	G66.01
$\hat{a}$	.070		.390		-.004	
σ_0	.189		.322		.051	

TABLE VI-18 (Continued)

Group Rank	#13 (37.3-29.0eV) A	B	#14 (29.0-22.6eV) A	B	#15 (22.6-17.6eV) A	B
1	.711	G20.86	.800	N20.86	.420	G20.86
2	.448	N20.86	.794	G20.86	.420	N20.86
3	-.015	N36.67	.107	N36.67	.323	N6.67
4	.009	N19.52*	.107	G36.67	.323	G6.67
5	.008	G36.67	.070	G6.67	.148	N11.31*
$\hat{a}$	.235		.005		.001	
σ_o	.302		-.005		.003	

Group Rank	#16 (17.6-13.7eV) A	B	#17 (13.7-10.7eV) A	B	#18 (10.7-8.3eV) A	B
1	.560	G6.67	.494	G6.67	.776	N6.67
2	.560	N6.67	.485	N6.67	.769	G6.67
3	.262	N10.24*	-.013	N36.67		
4	.100	G20.87	-.009	N20.86		
5	.099	N20.87	.005	G20.86		
$\hat{a}$	.013		.346		.158	
σ_o	.016		.351		.142	

Group Rank	#19 (8.3-6.5eV) A	B	#20 (6.5-5.0eV) A	B	#21 (5.0-3.9eV) A	B
1	.917	N6.67	.826	N6.67	.736	N6.67
2	.917	G6.67	.826	G6.67	.736	G6.67
3	.081	N4.40*	.103	N20.86	.134	N20.86
4			.103	G20.86	.134	G20.86
5			.071	N36.67	.096	N36.67
$\hat{a}$	.002		0.0		0.0	
σ_o	.001		0.0		0.0	

Group Rank	#22 (3.9-3.1eV) A	B	#23 (3.1-2.4eV) A	B
1	.680	N6.67	.650	N6.67
2	.680	G6.67	.650	G6.67
3	.155	N20.86	.165	N20.86
4	.155	G20.86	.165	G20.86
5	.115	N36.67	.124	N36.67
$\hat{a}$	0.0		0.0	
σ_o	0.0		0.0	

A - relative sensitivity value
B - G is for a Γ_γ parameter, N is for a Γ_n parameter, followed by the resonance energy, and an * indicated a p-wave resonance

CHAPTER VII

COVARIANCE GENERATION

Credible covariances form the foundation of any Uncertainty Analysis or Nuclear Data Adjustment. This Chapter will describe the generation and processing of covariance information necessary for the demonstration adjustment given in Chapter VIII. Considerable effort has been expended in the development of covariance matrices for ENDF/B-V[29] for quite a number of materials. Several special application libraries of processed multigroup covariances have been generated.[30,31] These processed libraries contain variance-covariance information for the infinitely-dilute multigroup cross sections only. Only the PUFF-2[30,32] covariance processor has resonance processing capabilities and it is somewhat crude.

The resonance parameter sensitivities developed in Chapter II can be used to obtain detailed resonance region covariances as well as covariances for self-shielded cross sections. This Chapter describes the generation of the infinitely dilute, the energy-shielded, and spatial-shielded cross section covariances followed by a description of the methods uncertainty procedures used in this study.

The cross section covariances for all TRX-1 constituent materials except ^{238}U (i.e. ^{235}U, ^{1}H, ^{27}Al, ^{16}O) were processed using standard methods and the PUFF-2 covariance processor. The governing equations are presented in reference 32. These covariances were processed into the 77 group structure using Vitamin-E[33] cross sections and weight function. Plots of the most important reactions are shown in figures

VII-1 to VII-3. Figure VII-3 shows a representation of the ENDF/B-V covariance file of ^{238}U capture cross section. Note the resolved resonance range (1 eV-4 keV) is zero. The ENDF/B-V description for ^{238}U refers the reader to reference 34 containing resolved resonance parameter covariance information. If we represent this covariance information as $COV(q_k,q_{k'})$, the covariance of resonance parameter q_k with resonance parameter $q_{k'}$, then we can calculate the multigroup infinite dilution cross section covariance as

$$COV(\sigma_{\infty g},\sigma_{\infty h}) = \sum_{k,k'} \frac{\partial f_g}{\partial q_k} COV(q_k,q_{k'}) \frac{\partial f_h}{\partial q_{k'}} . \qquad \text{VII-1}$$

This processed covariance file can then be added back into the file processed from the information in figure VII-3.

As will be shown in the next section $COV(q_k,q_{k'})$ can be used to incorporate self-shielding effects into an uncertainty analysis directly or via an f-factor covariance matrix, given in a similar manner to the infinitely-dilute cross section value as

$$COV(f_g,f_h) = \sum_{k,k'} \frac{\partial f_g}{\partial q_k} COV(q_k,q_{k'}) \frac{\partial f_h}{\partial q_{k'}} . \qquad \text{VII-2}$$

Currently the recommended procedure in ENDF/B for representing covariances in the unresolved region is to include the uncertainty data in the "smooth" part or file 33. However, this once again can only represent the infinite-dilution cross section covariance. Thus, it was felt that uncertainties in the average resonance parameters themselves would be a superior representation.

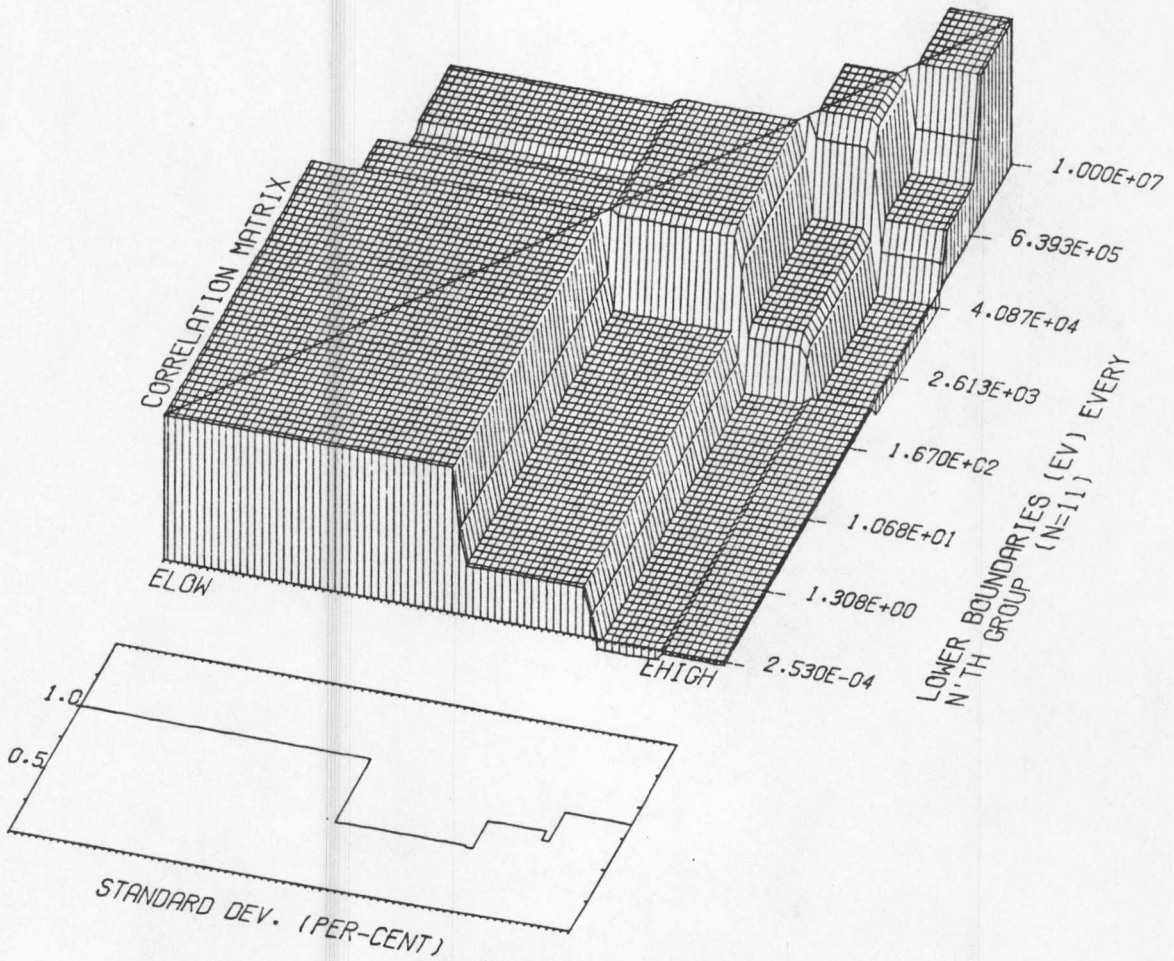

MAT'L 1301 77 GROUPS REACT 2 TO REACT 2

Figure VII-1. Correlation Matrix and Standard Deviation Plots for H-1 Elastic Scattering Cross Sections

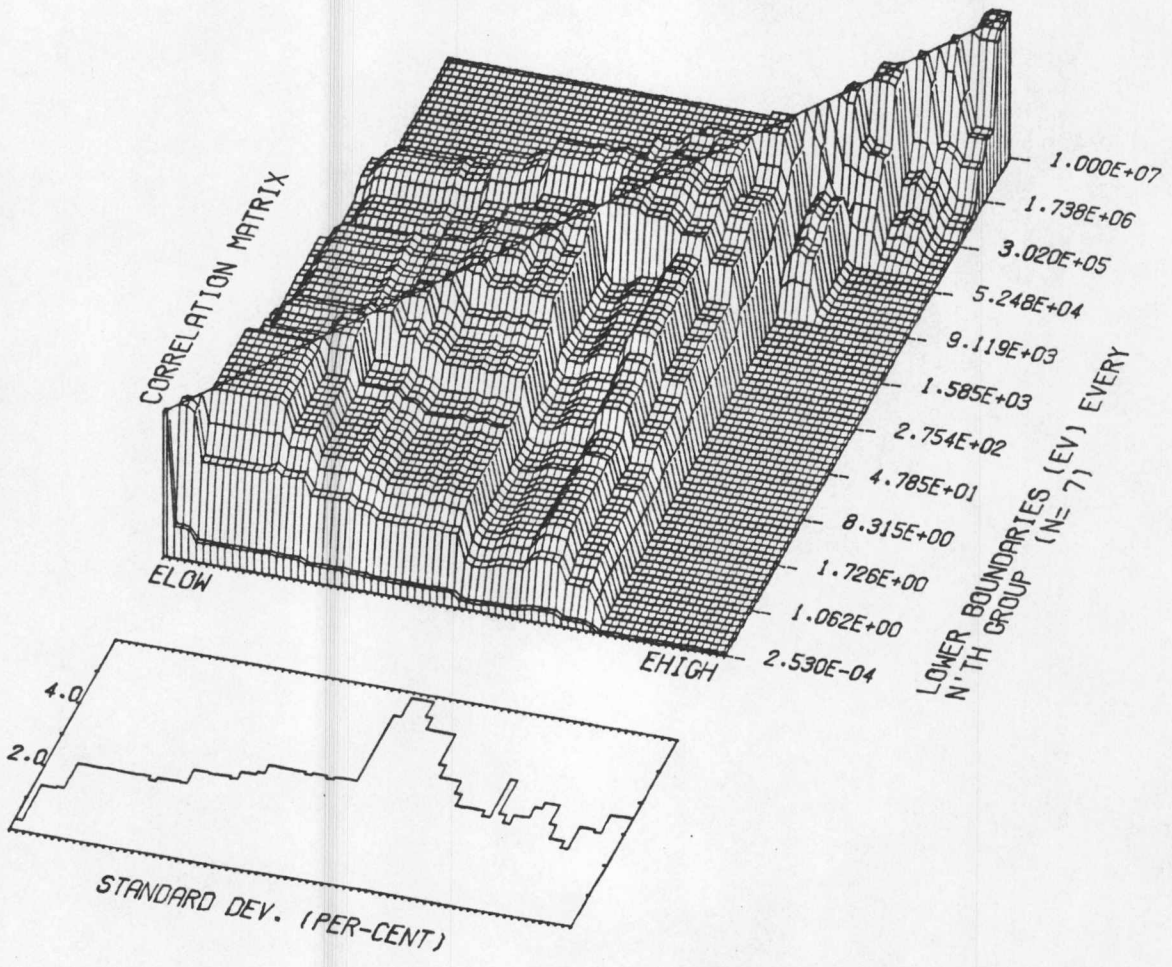

Figure VII-2. Correlation Matrix and Standard Deviation Plots for U-235 Fission Cross Sections

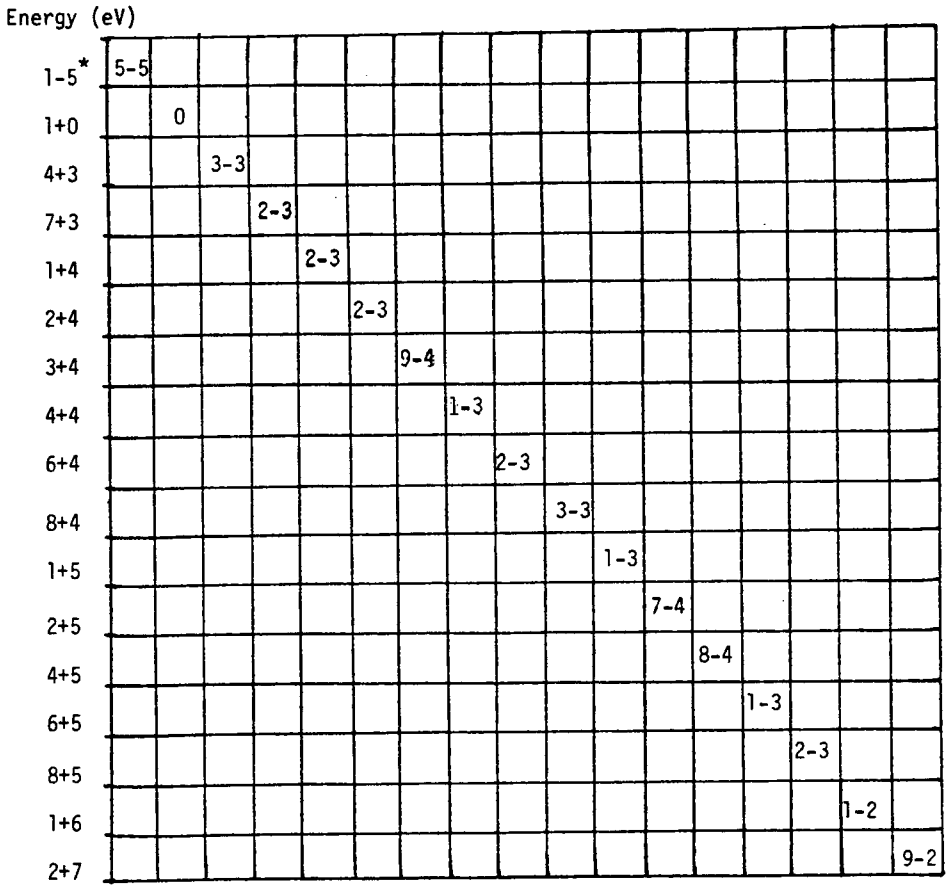

* 1-5 represents 1 x 10^{-5}

Figure VII-3. ENDF/B-V Representation of U-238 Capture Cross Section Covariance

deSaussure and Marable[35] have produced a set of covariances for the first 19 unresolved resonances in ^{238}U. Thus, for the infinite dilute cross sections equation VII-1 once again can be used in the unresolved region. However, for consistency the values in figure VII-3 currently in ENDF/B-V are set to zero and replaced with this new representation.

Sensitivities are now available for both the infinitely dilute and energy self-shielded cross sections to the resonance parameters. The final step in this covariance generation is to obtain sensitivities of the spatial self-shielded cross sections to the resonance parameters. The reader is referred to equations IV-1 and IV-2 in Chapter IV. The group flux in equation IV-2 was calculated using XSDRNPM, calculating the flux derivative does not appear very economical using a transport calculation. However, if we use an approximation to equation IV-2 that is analytic the analysis should be greatly simplified. The following equation has been derived[36] using several approximations, among them: (1) absorbers only in the fuel, (2) narrow resonance approximation for moderator, (3) isolated resonance approximation in the fuel, and (4) wide resonance approximation for resonance scattering;

$$\Sigma_{cg}^{j} = f_{\phi g}^{j} f_{\sigma g}^{j} \sigma_{\infty g}^{j} \quad , \qquad \text{VII-3}$$

where

$$f_{\phi g} = \left[1 + \left(\frac{V_m}{V_c}\right) \frac{(1-\beta)}{\sum_{i \neq j} \lambda_i \Sigma_{pf}^{i} + \Sigma_e} \Sigma_{ag}\right]^{-1} \quad ,$$

V_m = moderator volume ,

V_c = cell volume ,

λ_i = wide resonance parameter ,

$\Sigma_{pf}{}^i$ = potential scattering cross section for fuel material i ,

Σ_e = escape cross section ,

$\beta = V_f \Sigma_e / V_m \Sigma_{pm}$,

V_f = fuel volume,

Σ_{pm} = potential scattering cross section for the moderator.

Taking derivatives of equation VII-3 with respect to q_k ,

$$\frac{q_k}{f_{\phi g}} \frac{\partial f_{\phi g}}{\partial q_k} = (f_{\phi g} - 1) \frac{q_k}{\Sigma_{ag}} \frac{\partial \Sigma_{ag}}{\partial q_k} . \qquad \text{VII-4}$$

Once again we can use equation VII-2 to obtain the covariance matrix for the $f_{\phi g}$ (i.e. $COV(f_{\phi g}, f_{\phi h})$).

The final uncertainty we shall look at is that of the calculational method used in the $^{28}\rho$ response calculation. The normal procedure involves the quantification of the uncertainty in the final response to the various methods or modelling approximations (i.e. 1-D to 2-D,2-D to 3-D, cross section processing methods,etc.) used in the calculation. However, such a study is beyond the scope of this work. The method utilized herein is less rigorous; however, it is felt to be sufficient since the adjustment is primarily for the purpose of demonstrating the methodology. The approach is to simply obtain the methods uncertainty via a spread in the calculated responses using several different methods (i.e. transport, diffusion, Monte Carlo, etc.).

Calculated values of TRX-1 $^{28}\rho$ by various analysts are presented in Table IV-2 (p.27). The calculated value in Table VII-1 represents a mean of these four calculations. The method error shown is simply the spread

of these four calculations. This method error is an attempt to provide an estimate of the inaccuracy of the method (i.e. transport, diffusion, etc.) used to calculate the $^{28}\rho$ response. The "modelling" errors (i.e. mesh size, actual constituent material number densities, etc.) are assumed to be negligible.

Table VII-1

TRX-1 $^{28}\rho$ Response Values

experimental value	experimental standard dev.(%)	calculated value	method error standard dev.(%)
1.32	1.59	1.35	0.80

CHAPTER VIII

FINAL DATA PREPARATION AND ADJUSTMENT

This section describes two ways in which the various input data can be assembled into the actual adjustment module and gives a demonstration adjustment for one method. The first method involves the use of the resonance parameter covariances directly in the adjustment while the second involves using them indirectly through an f-factor covariance matrix.

For convenience, the equation for Data Adjustment is repeated here;

$$p' - \bar{p} = MG^{+}(N+V)^{-1}(r_0 - \bar{r}) \ . \qquad \text{VIII-1}$$

In the first method we allow the p vector to contain only resonance parameters and group-wise cross sections in the resonance region and only group-wise cross sections outside of the resonance region. Thus, p can be written;

$$p = \begin{pmatrix} q_1 \\ q_2 \\ \cdot \\ \cdot \\ \sigma_1 \\ \sigma_2 \end{pmatrix} \qquad \text{VIII-2}$$

$$M = \begin{pmatrix} \text{var}(q_1,q_1) & & & & \\ \text{cov}(q_2,q_1) & \text{var}(q_2,q_2) & & & \\ & & \cdot & & \\ & & & \cdot & \\ & & & \text{var}(\sigma_1,\sigma_1) & \\ & & & \text{cov}(\sigma_2,\sigma_1) & \text{var}(\sigma_2,\sigma_2) \end{pmatrix}$$

Using the linear model as in Chapter III,

$$r = \bar{r} + G(p-\bar{p})$$

we can see that $G = \{\frac{\partial R_i}{\partial p_j}\}$ VIII-3

Thus for $p_j = q_k$, $\frac{\partial R_i}{\partial q_k} = \sum_g \frac{\partial R_i}{\partial \sigma_g} \frac{\partial \sigma_g}{\partial q_k}$.

For $p_j = \sigma_g$ only generalized perturbation theory results are needed. Thus the adjusted parameters p' include both the resonance parameters and group-wise cross section. Sensitivity plots obtained using generalized perturbation theory as needed for both adjustment methods were given in Chapter V. Table VIII-1 contains the s-wave resonance parameter sensitivities that will be utilized in the demonstration adjustment using method 1. Table VIII-2 gives the complete list of resonances included in the demonstration adjustment. In Table VIII-1 sensitivity values are included for three cases to emphasize various effects. First the Γ_γ relative sensitivities are given for each resonance with both energy and spatial self-shielding accounted for, followed by cases where only energy shelf-shielding is included and finally no self-shielding included. The same comparison is then made for the Γ_n relative sensitivities.

As expected the first three resonances dominate the others with respect to the TRX-1 $^{28}\rho$ response for both the Γ_γ and Γ_n parameters. It would be very helpful to have direct recalculations for each of the values in Table VIII-1, however, these runs are quite expensive and only one run was performed as part of this work. The relative sensitivity value for TRX-1 $^{28}\rho$ to Γ_γ at 6.67eV was determined to be .14. This is within about 20% of the predicted value shown in Table VIII-1.

Table VIII-1

S-wave Resonance Relative Sensitivities to be Used in the Demonstration Adjustment

Res. energy	28_ρ sens. to Γ_γ (spatial+ energy)	28_ρ sens. to Γ_γ (energy)	28_ρ sens. to Γ_γ (none)	28_ρ sens. to Γ_n (spatial+ energy)	28_ρ sens. to Γ_n (energy)	28_ρ sens. to Γ_n (none)
6.67eV	.172	.200	.150	.172	.200	.290
20.86	.093	.110	.061	.068	.076	.100
36.67	.078	.082	.071	.035	.036	.060
66.01	.031	.033	.025	.018	.019	.024
80.73	.0047	.0047	.0025	.0058	.0058	.021
102.5	.031	.032	.028	.017	.016	.017
116.9	.015	.016	.0098	.0073	.0076	.0085
145.6	.0012	.0012	.0005	.0035	.0036	.0041
165.3	.031	.0031	.0020	.0034	.0035	.0097
189.6	.029	.029	.029	.018	.018	.021
208.5	.012	.013	.011	.0061	.0061	.0081
237.3	.010	.010	.0086	.0052	.0052	.0082
273.5	.0084	.0086	.0072	.0039	.0040	.0067
291.0	.0057	.0057	.0047	.0033	.0033	.0055
311.3	.00069	.0070	.0002	.0025	.0026	.0007
347.8	.018	.018	.021	.015	.015	.017
376.9	.00083	.0009	.0004	.0032	.0032	.0013
397.6	.0039	.0040	.0030	.0045	.0045	.0053
410.2	.010	.010	.011	.0082	.0083	.0012
2.598keV	.027	.028	.027	.012	.012	.013
3.110	.015	.015	.015	.0014	.0014	.0042
3.858	.0019	.0019	.0021	.0014	.0014	.0016
3.873	.0009	.0009	.0010	.0005	.0005	.0006
4.041	.0002	.0002	.0002	.0001	.0001	.0002

Table VIII-2

Complete Listing of 36 Resonances Utilized
in Demonstration Adjustment Problem

S-wave Resonance Energies	P-wave Resonance Energies
6.672 eV	4.404 eV
20.86	10.24
36.67	11.31
66.01	16.29
80.73	19.52
102.5	45.17
116.9	49.63
145.6	63.50
165.3	72.78
189.6	74.38
208.5	83.68
237.3	89.29
273.5	
291.0	
311.1	
347.8	
376.9	
397.6	
410.2	
2.598 keV	
3.110	
3.858	
3.873	
4.041	

Note that this discrepency would have been much larger if the spatial self-shielding had not been taken into account. The importance of spatial self-shielding is only seen at the 6.67eV resonance and to a lesser extent at the 20.86eV resonance. A previous study by Tomlinson et.al.[37] obtained the following ^{238}U relative sensitivities for TRX-2 $^{28}\rho$ to Γ_γ and Γ_n for the first four resonances.

Table VIII-3

Comparison of TRX-1 and TRX-2 $^{28}\rho$
Relative Sensitivities

Resonance	TRX-1 rho-28 to Γ_γ	TRX-2 rho-28 to Γ_γ	TRX-1 rho-28 to Γ_n	TRX-2 rho-28 to Γ_n
6.67 eV	.172	.147	.172	.149
20.86	.093	.066	.068	.068
36.67	.078	.055	.035	.055
66.01	.031	.020	.018	.020

The Γ_n values are in most cases in pretty good agreement with about the same 20%-30% differences seen for the Γ_γ relative sensitivities.

Also, it should be pointed out that at resonances greater than or equal to 410.2eV the contributions are somewhat exagerated. This is due to the missing resonances in-between the ones actually considered, which usually "share" these contributions.

Lastly, some very interesting phenomonem can be seen by comparing the infinitely dilute, the energy self-shielded, and the spatial self-

shielded values. In general, the Γ_γ relative sensitivities increase and the Γ_n relative sensitivity values decrease with increased energy self-shielding and both the Γ_n and Γ_γ sensitivity values decrease with increased spatial self-shielding. The energy self-shielding effect is due to the same causes seen in Chapter VI (see fig. VI-6) although the magnitude is less since most Γ_γ values are only 50% or more of Γ_t. The spatial self-shielding in essence causes the Γ_γ and Γ_n parameters to be less important with respect to $^{28}\rho$ as can easily be seen in equation VII-4.

There are several ways to represent the second method, however only the one that appears most suitable will be shown here. If we represent the p vector with multigroup infinitely dilute cross sections, energy shielding factors, f_σ, and spatial shielding factors, f_ϕ, as

$$p = \begin{pmatrix} \sigma_\infty \\ \cdot \\ \cdot \\ f_\sigma \\ \cdot \\ \cdot \\ f_\phi \end{pmatrix}, \quad M = \begin{pmatrix} \mathrm{var}(\sigma_\infty,\sigma_\infty) & & & & \\ & \cdot & & & \\ & & \cdot & & \\ & & & \mathrm{var}(f_\sigma,f_\sigma) & \\ & & & & \cdot \\ & & & & \cdot \\ & & & & \mathrm{var}(f_\phi,f_\phi) \end{pmatrix} \qquad \text{VIII-4}$$

Again using the linear model we obtain

$$p_j = \sigma_g^\infty \ , \quad G = \left\{\frac{\partial R_i}{\partial \sigma_g}\right\}_\infty \ ,$$

$$p_j = f_{\sigma g} \ , \ G = \left\{\frac{\partial R_i}{\partial f_{\sigma g}}\right\} \ , \qquad \text{VIII-5}$$

$$p_j = f_{\phi g} \ , \ G = \left\{\frac{\partial R_i}{\partial f_{\phi g}}\right\} \ ,$$

and since $\sigma_g = \sigma_g^{\infty} f_{\sigma g} f_{\phi g}$,

$$\frac{\sigma_g}{R_i}\frac{\partial R_i}{\partial \sigma_g} = \frac{\sigma_g^{\infty}}{R_i}\frac{\partial R_i}{\partial \sigma_g^{\infty}} = \frac{f_{\sigma g}}{R_i}\frac{\partial R_i}{\partial f_{\sigma g}} = \frac{f_{\phi g}}{R_i}\frac{\partial R_i}{\partial f_{\phi g}} \ . \qquad \text{VIII-6}$$

Thus, the sensitivities needed are obtained through Generalized Perturbation Theory and are given for the most important materials in Chapter V. The $COV(f_{\sigma_g}, f_{\sigma_h})$ is calculated as shown in Chapter VII and repeated here as follows:

$$COV(\sigma_g^{\infty}, \sigma_h^{\infty}) = \sum_{k,k'} \frac{\partial \sigma_g^{\infty}}{\partial q_k} COV(q_k, q_{k'}) \frac{\partial \sigma_h^{\infty}}{\partial q_{k'}} \ ,$$

$$COV(f_{\sigma g}, f_{\sigma h}) = \sum_{k,k'} \frac{\partial f_{\sigma g}}{\partial q_k} COV(q_k, q_{k'}) \frac{\partial f_{\sigma h}}{\partial q_{k'}} \ , \qquad \text{VIII-7}$$

$$COV(f_{\phi g}, f_{\phi h}) = \sum_{k,k'} \frac{\partial f_{\phi g}}{\partial q_k} COV(q_k, q_{k'}) \frac{\partial f_{\phi h}}{\partial q_{k'}} \ .$$

And similarly for the cross terms:

$$COV(\sigma_g^{\infty}, f_{\sigma h}) = \sum_{k,k'} \frac{\partial \sigma_g^{\infty}}{\partial q_k} COV(q_k, q_{k'}) \frac{\partial f_{\sigma h}}{\partial q_{k'}} \ ,$$

$$COV(\sigma_g^{\infty}, f_{\phi h}) = \sum_{k,k'} \frac{\partial \sigma_g^{\infty}}{\partial q_k} COV(q_k, q_{k'}) \frac{\partial f_{\phi h}}{\partial q_{k'}} \ , \qquad \text{VIII-8}$$

$$COV(f_{\sigma g}, f_{\phi h}) = \sum_{k,k'} \frac{\partial f_{\sigma g}}{\partial q_k} COV(q_k, q_{k'}) \frac{\partial f_{\phi h}}{\partial q_{k'}} \ .$$

The covariance matrices represented by equation VIII-7 are shown in

figures VIII-1 to VIII-3. Tables VIII-4 and VIII-5 show the various covariance matrices needed and their dimensions for the demonstration problem on TRX-1 $^{28}\rho$ response. These covariances as well as the previously generated sensitivity coefficients are then read by the module COVERS[25] which then prepares the proper input to the adjustment module UNCOVER[25]. The following section contains the results of such an adjustment using the first method as described earlier in this chapter. This method results in adjustments in the actual resonance parameters.

The value of $^{28}\rho$ for TRX-1 before and after adjustment and it's uncertainty are shown in Table VIII-6. The value of chi-squared[1] for this adjustment is 0.1 indicating the consistency between the calculated and experimental values as seen in Table VIII-6. The effect of the adjustment procedure is to reduce the uncertainty in $^{28}\rho$ to 0.796% or very slightly below the experimental uncertainty. Generally, this uncertainty reduction is more usually pronounced than in this simple demonstration problem with only one response. The reduction in the uncertainty of the calculated valued is more obvious since the 8.02% uncertainty is reduced to 0.796% by the adjustment procedure. This uncertainty reduction in the calculated value is not superficial. It is a direct result of the reduced uncertainties in the parameters used to calculate $^{28}\rho$. Several of the most important parameter uncertainty reductions are shown in Tables VIII-7 to VIII-9.

The changes in each of the parameters and their uncertainties is quite small, however, the net effect of these uncertainty reductions is

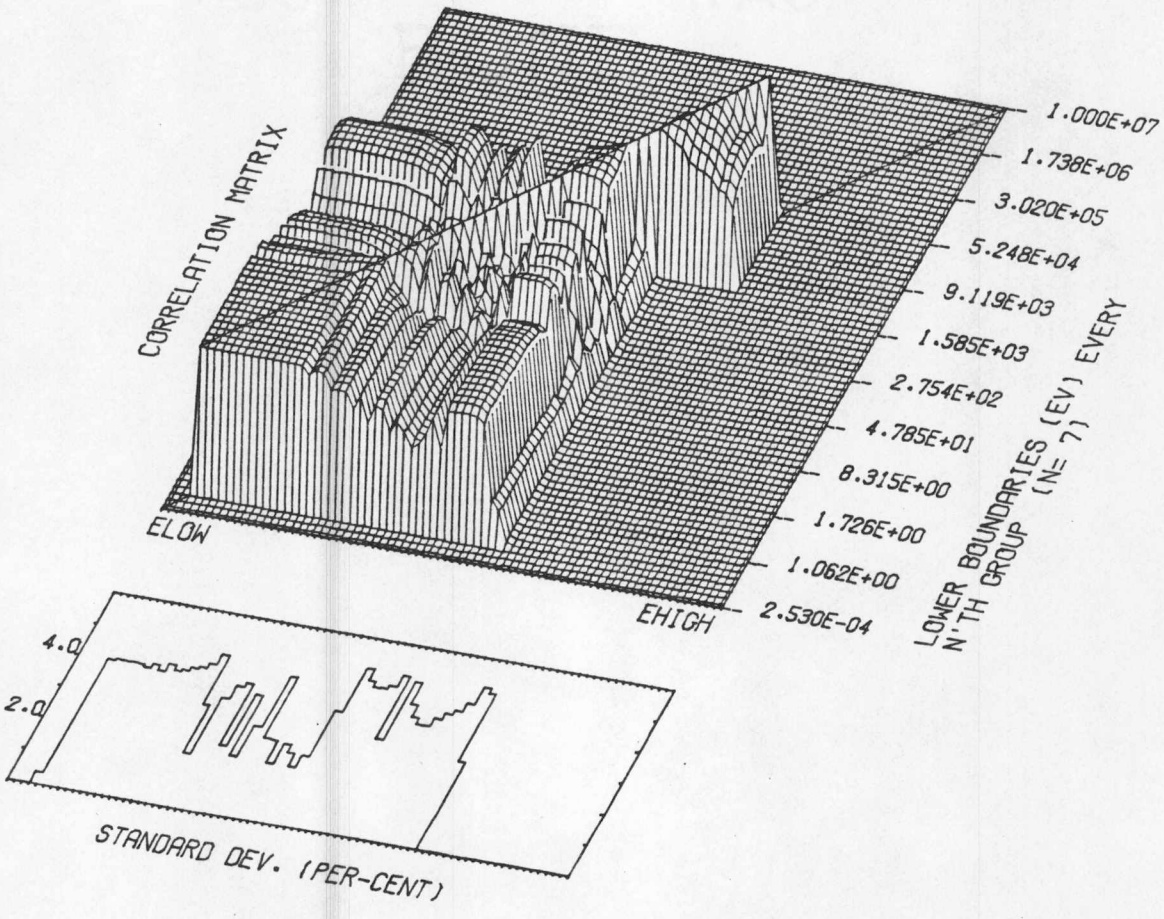

Figure VIII-1. Correlation Matrix and Standard Deviation Plots for U-238 Infinite Dilute Capture Cross Sections in the Resolved and Unresolved Ranges

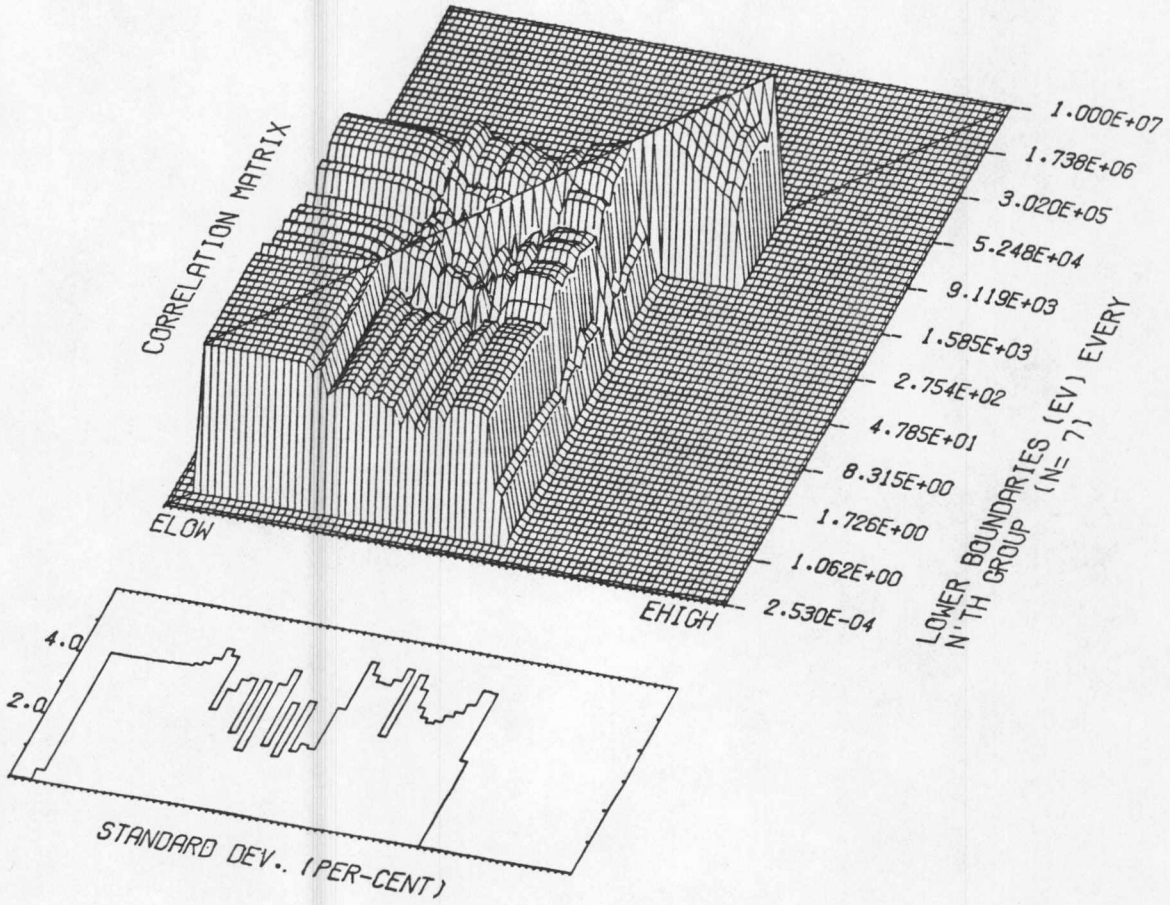

MAT'L 1398 77 GROUPS REACT2102 TO REACT2102

Figure VIII-2. Correlation Matrix and Standard Deviation Plots for U-238 Energy Self-Shielding Factors in the Resolved and Unresolved Ranges

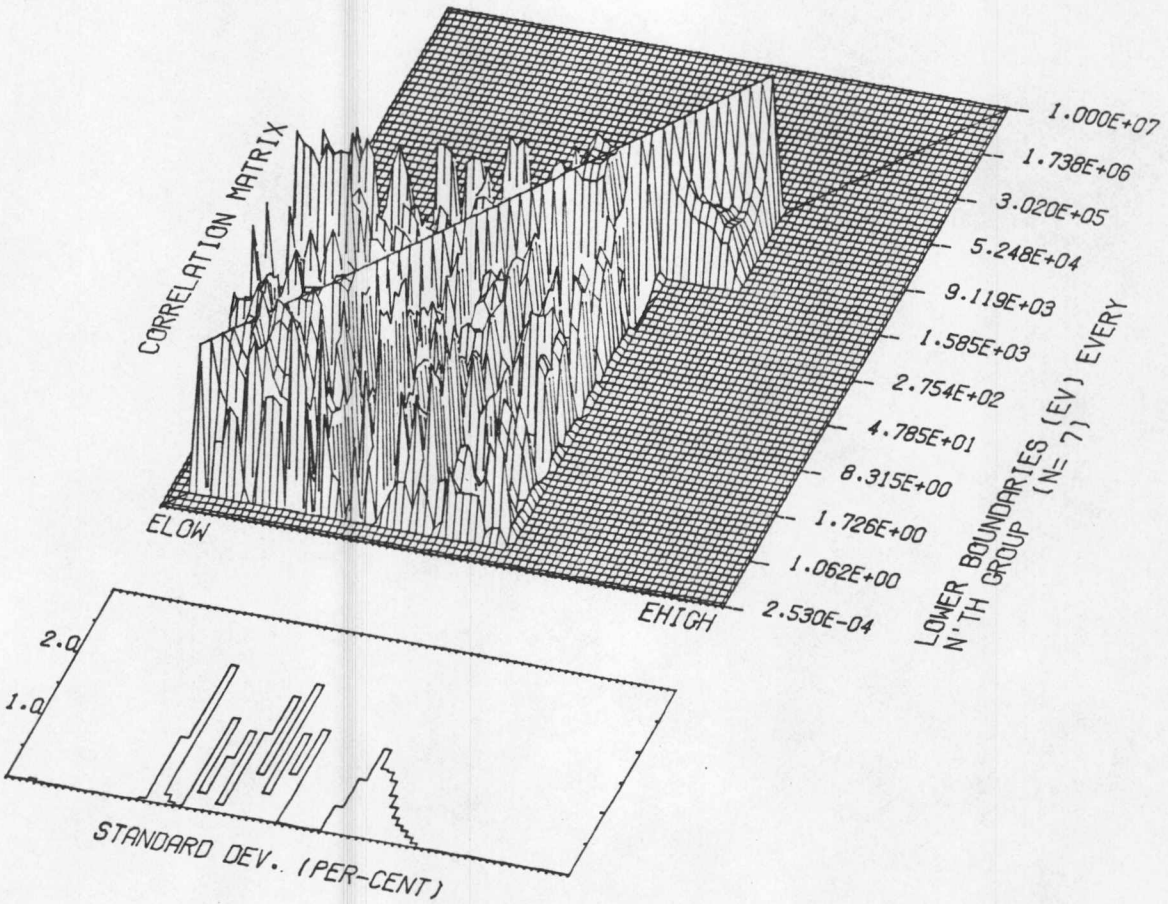

Figure VIII-3. Correlation Matrix and Standard Deviation Plots for U-238 Spatial Self-Shielding Factors in the Resolved and Unresolved Ranges

Table VIII-4

Extended Covariance Matrix (F-factor method)

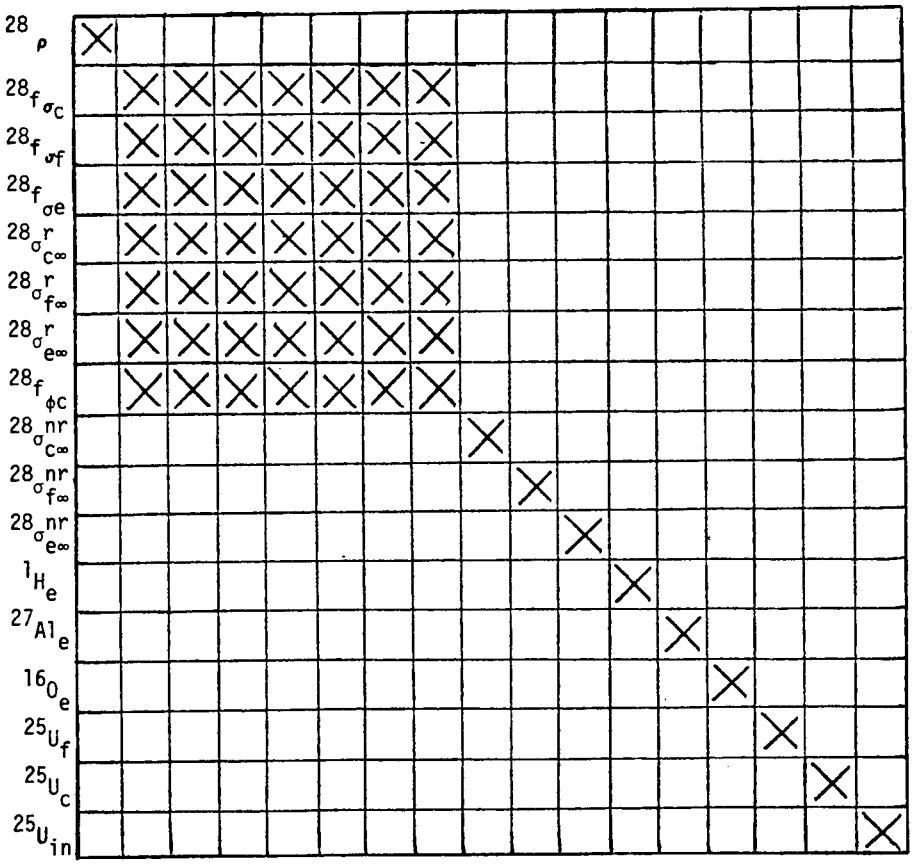

r = resonance part
nr = non-resonance part

Table VIII-5

Extended Covariance Matrix (Resonance Parameter method)

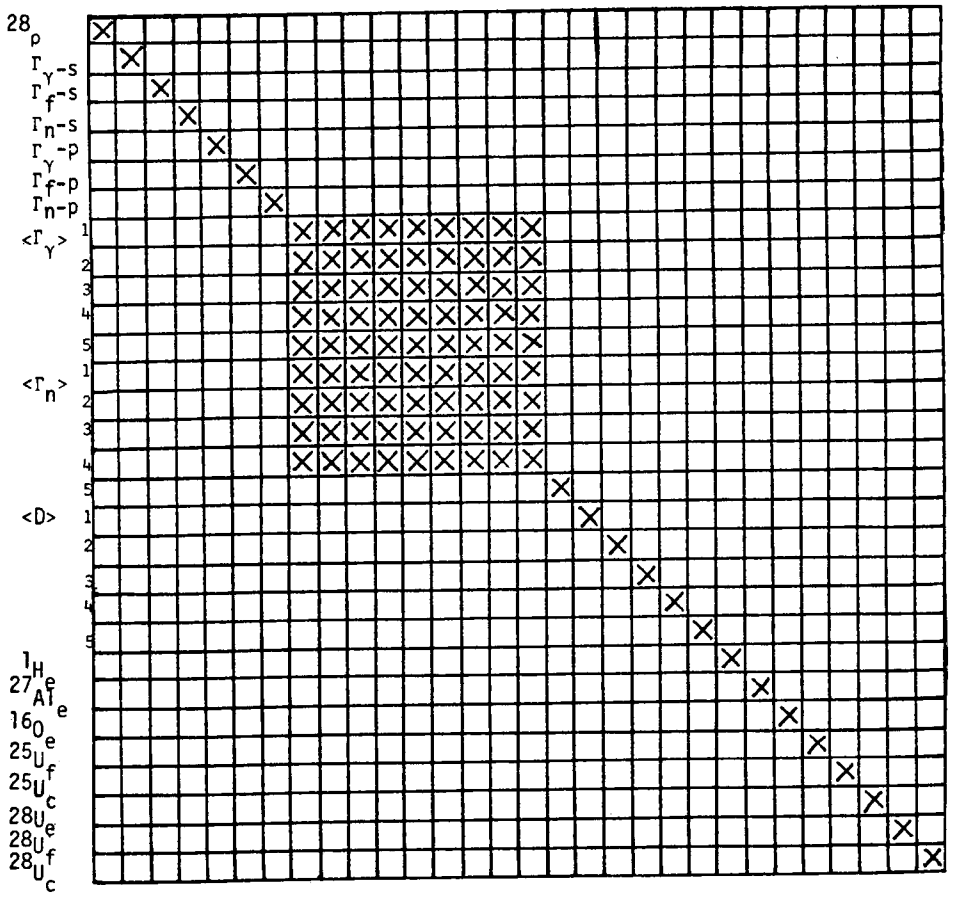

Table VIII-6

TRX-1 $^{28}\rho$ Adjustment Values

Experimental value	Calculated value	Adjusted value	Exp. Std.Dev.	Calc. Std.Dev.	Adj. Std.Dev.
1.32	1.35	1.32	0.800%	8.02%	0.796%

Table VIII-7

Γ_γ Adjustments for Demonstration Problem

Resonance Energy	Change (%)	Stand. Dev. old (%)	Stand. Dev. new (%)
6.672 eV	-.14	3.421	3.39
20.86	-.11	2.80	2.78
36.67	-.10	2.33	2.31
66.01	-.10	2.46	2.44
80.73	-.10	5.17	5.16
102.5	-.10	2.46	2.44
116.9	-.10	2.79	2.77
145.6	-.10	15.89	15.77
165.3	-.18	8.85	8.83
189.6	-.10	2.91	2.89
208.5	-.09	2.68	2.67
237.3	-.09	2.75	2.73
273.5	-.09	2.97	2.96
291.0	-.09	3.11	3.09
311.3	-.10	10.20	10.19
347.8	-.09	2.37	2.35
376.9	-.10	10.20	10.19
397.6	-.13	16.61	16.61
410.2	-.09	2.99	2.97
2.598 keV	-.10	3.15	3.14
3.110	-.11	5.48	5.47
3.858	-.10	10.20	10.19
3.873	-.09	2.92	2.90
4.041	-.09	2.33	2.31

Table VIII-8

Γ_n Adjustments for Demonstration Problem

Resonance Energy	Change (%)	Stand. Dev. old (%)	Stand. Dev. new (%)
6.672 eV	-.14	3.18	3.14
20.86	-.17	3.23	3.18
36.67	-.17	3.37	3.33
66.01	-.18	3.61	3.56
80.73	-.18	3.98	3.94
102.5	-.18	3.46	3.41
116.9	-.19	3.64	3.59
145.6	-.19	4.14	4.09
165.3	-.20	4.26	4.21
189.6	-.20	3.90	3.84
208.5	-.21	4.15	4.09
237.3	-.21	4.30	4.25
273.5	-.22	4.40	4.34
291.0	-.22	4.66	4.60
311.3	-.23	5.15	5.10
347.8	-.24	4.57	4.51
376.9	-.24	4.97	4.91
397.6	-.25	5.12	5.06
410.2	-.25	4.88	4.81
2.598 keV	-.26	5.09	5.02
3.110	-.26	5.55	5.48
3.858	-.26	5.48	5.42
3.873	-.27	5.29	5.22
4.041	-.28	5.41	5.33

Table VIII-9

^{1}H Adjustments for Demonstration Problem

Energy Range	Change (%)	Stand. Dev. old (%)	Stand. Dev. new (%)
10.0--1.05 MeV	-.0054	.866	.866
1.05--0.82	-.0010	.638	.637
0.82--0.11	-.0126	.707	.706
0.11--0.087	.0234	.486	.481
0.087Mev--1.23keV	.0531	.500	.470
1.23--0.96	.0882	.497	.407
0.96--2.53E-4 eV	.300	1.000	.270

as seen in Table VIII-6 (i.e. 8% to 0.8%). Tables VIII-7 to VIII-9 also give the major changes in the parameters for this adjustment. These parameter changes are also quite small and are intended, as is this entire exercise, for demonstration purposes only. However, a close look at the values in Table VIII-7 and VIII-8 reveal the power in this method. The result of applying this adjustment procedure is that adjustments are obtained on the basic parameters (i.e. Γ_γ and Γ_n for various resonances) as opposed to the more conventional group cross section adjustments. Also, unlike earlier adjustment methods, both spatial and energy self-shielding have been included in this adjustment.

Identical results would be obtained using method 2 as described earlier in this chapter. In this case both spatial and energy self-shielding would be accounted for and the resulting adjustments would be for the group cross sections and both the energy and spatial self-shielding factors.

CHAPTER IX

CONCLUSIONS

This work has dealt with the development and demonstration of a Nuclear Data Adjustment Methodology that allows inclusion of both energy and spatial self-shielding into the adjustment procedure. The adjustments are given for the basic parameters in the resonance range and for group cross sections outside the resonance range. The majority of this development effort has consisted of producing and validating the resonance parameter sensitivity information which allows the linkage between the responses of interest and the basic parameters.

The resonance parameter sensitivity methodology developed herein usually provides accurate results as compared to direct recalculations using well-known cross section processing codes. However, several caveats are appropriate concerning the use of this methodology. It has been shown in several cases that the shielding cross sections can be very non-linear functions of the basic parameters. For this reason, caution must be used in any undertaking which assumes a linear relationship exists between a given group cross section and its corresponding basic data parameters.

Additionally, caution is advised when processing materials with a large number of resolved resonances(>100). Considerable computer time is expended in such an operation and the pitfalls (e.g. errors that appear only after considerable CPU time has elapsed) that occur for production cross section processing codes also occur in these cases.

A method of including the spatial self-shielding into the adjust-

ment process is also introduced in this study. The usefulness of this method appears to be limited to the low eV range as seen in ^{238}U. The method does, however, provide a quick and useful method for treating the spatial self-shielding for a given reactor configuration if it is significant.

CHAPTER X

RECOMMENDATIONS FOR FUTURE WORK

The results of this study have pointed to the need for work in several different areas. They include (1) finding ways to speed up the calculational procedure used by the DEFUNCT code, (2) developing improved approximations similar to the Perey method, and (3) further development of the resonance parameter covariances to include new materials and improve the ones currently available.

Requarding the first area of further study, a good start would be to allow different methods to be used at different energies. Perhaps the single most time consuming step is the calculation of resonance parameter sensitivities for all groups to a given resonance. This procedure is useful for low-lying resonances whose wings span groups that contain no resonances. However, in the higher energy resonances many resonances generally lie within a single group such that group-to-group interactions for a given resonance are not needed. Another possible improvement is the use of an approximation at high energies. An approximation similar to that of Perey (i.e. no overlapping resonances at high energies) could also speed up computations considerably.

The second and perhaps most promising area for future study is the area of simple methods similar to that of Perey. Although the method is very simple, surprisingly good results have been obtained in some cases. If the causes of some discrepencies can be isolated and corrected easily a very quick and generally useful method should result.

Lastly, for meaningful data adjustment studies utilizing the reso-

nance parameters explicitely, the covariance information must be available. To date only a few of these have been reported.

LIST OF REFERENCES

LIST OF REFERENCES

(1.) C.R. Weisbin, E.M. Oblow, J.H. Marable, R.W. Peelle, and J.L. Lucius, Nucl. Sci. Eng.,66, 307(1978).

(2.) J.B. Dragt, J.W. Dekker, H. Gruppelaar, and A.J. Janssen, Nucl. Sci. Eng.,62, 117(1977).

(3.) F.G. Perey, "Least-Squares Dosimetry Unfolding: The Program STAY'SL", ORNL/TM-6062, ENDF-254(1977).

(4.) A. Gandini, "Nuclear Data and Integral Measurements Correlation for Fast Reactors," Parts I, II, and III, RT/FI(73)5,RT/FI(73)22, and RT/FI(74)3, Comitato Nazionale Energia Nucleare, Casaccia, Italy (1973 and 1974).

(5.) E. Greenspan, Y. Karni, and D. Gilai, "Spectral Fine-Structure Effects in Cross Section Sensitivity Analysis," Proceedings of a Seminar-Workshop on Theory and Application of Sensitivity and Uncertainty Analysis, ORNL/RSIC-42, August 22-24, 1978.

(6.) E. Greenspan, Y. Karni, "Spectral Fine-Structure Effects in Cross Section Sensitivity Analysis," unpublished. (note: Expanded version of reference 5)

(7.) ENDF-102 Data Formats and Procedures for the Evaluated Nuclear Data File, ENDF, BNL-NCS-50496 (October 1975).

(8.) G.I. Bell and Samuel Glasstone, Nuclear Reactor Theory, Van Nostrand Reinhold Company, 1970.

(9.) C.R. Weisbin, P.D. Soran, R.E. MacFarlane, D.R. Harris, R.J. LaBauve, J.S. Hendricks, J.E. White, and R.B. Kidman, "MINX: A Multigroup Interpretation of Nuclear X-Sections," LA-6486-MS (ENDF-237) (1976).

(10.) I.I. Bondarenko, (ed.) Group Constants for Nuclear Reactor Calculations (Consultants Bureau, New York 1964).

(11.) Personal Communication, N.M Greene.

(12.) H. Henryson, II, B.J. Toppel, and C.G. Stenberg, "MC^2-2: A Code to Calculate Fast Neutron Spectra and Multigroup Nuclear Cross Section Processing," ANL-8144(ENDF-239) (June 1976).

(13.) G.E.P. Box and G.C. Tiao, Bayesian Interference in Statistics, 3rd edition, MacMillian Publishing Co., New York (1970).

(14.) ENDF-202 Cross Section Evaluation Working Group Benchmark Specifications, BNL 19302 (November 1974).

(15.) R.E MacFarlane and R.M. Boicourt, "NJOY: A Neutron and Photon Cross Section Processing System," Trans. Am. Nucl. Soc. 22, 702 (1975).

(16.) N.M. Greene, J.L. Lucius, L.M. Petrie, W.E. Ford, III, J.E. White, and R.Q. Wright, "AMPX: A Modular Code System for Generating Coupled Multigroup Neutron-Gamma Libraries from ENDF/B," ORNL/TM-3706 (March 1976).

(17.) Additional information on EPRI-CELL can be obtained from the Electric Power Research Institute, P.O. Box 10402, Palo Alto, CA 94304.

(18.) N.M. Greene and C.W. Craven, Jr., "XSDRN: A Discrete Ordinates Spectral Averaging Code," ORNL-TM-2500 (July 1969).

(19.) M.L. Williams, personal communication.

(20.) Thermal Reactor Subcommittee of the CSEWG Data Testing and Applications Committee, "Benchmark Testing of ENDF/B Data for Thermal Reactors, Archival Volume," ENDF-313, BNL-NCS-29891, July 1981.

(21.) ENDF-311 Benchmark Data Testing of ENDF/B-V, BNL-NCS-31531, August 1982.

(22.) L.N. Usachev, J. Nucl. Energy, Part A/B, 18, 571 (1964).

(23.) A. Gandini, J. Nucl. Energy, 21, 755 (1967).

(24.) H. Greenspan, C.N. Kelber, and D. Okrent, Computing Methods in Reactor Physics, Gordon and Breach, New York (1968).

(25.) J.L. Lucius, C.R. Weisbin, J.H. Marable, J.D. Drischler, R.Q. Wright, and J.E. White, "A Users Manual for the FORSS Sensitivity and Uncertainty Analysis Code System," ORNL-5316 (ENDF-291) (January 1981).

(26.) R.E. Schenter, J.L. Baker, and R.B. Kidman, "ETOX, A Code to Calculate Group Constants for Nuclear Reactor Calculations," Battelle Northwest Laboratory report BNWL-1002 (ENDF-127) (1969).

(27.) J. Barhen and D.G. Cacuci, "Cross Section Processing for the Unresolved Energy Region," Oak Ridge National Laboratory Internal Memorandum, December 4, 1978.

(28.) F.G. Perey, "Estimated Uncertainties in Nuclear Data--An Approach," Proc. Conf. Nucl. Cross Sections and Tech., R.A. Schrack and C.D. Bowman, Editors, p.842, NBS Special Publication 425 (1975).

(29.) Information and tapes for ENDF/B-V can be obtained from the National Nuclear Data Center, Brookhaven National Laboratory, Upton, NY, 11973.

(30.) J.D. Smith, III, and B.L. Broadhead, "Multigroup Covariance Matrices for Fast Reactor Studies," ORNL/TM-7389 (April 1981).

(31.) R.E. Maerker, J.J. Wagschal, and B.L. Broadhead, "Development and Demonstration of an Advanced Methodology for LWR Dosimetry Applications," EPRI NP-2188 (December 1981).

(32.) J.D. Smith, III, "Processing ENDF/B-V Uncertainty Data in Multigroup Covariance Matrices," ORNL/TM-7221 (June 1980).

(33.) C.R. Weisbin, R.W. Roussin, J.J. Wagschal, J.E. White, and R.Q. Wright, "VITAMIN-E: An ENDF/B-V Multigroup Cross-Section Library for LMFBR Core and Shield, LWR Shield, Dosimetry and Fusion Blanket Technology," ORNL-5055 (ENDF-274).

(34.) G. deSaussure, D.K. Olsen, R.B. Perez, and F.C. Difilippo, "Evaluation of the ^{238}U Neutron Cross-Sections for Incident Neutron Energies up to 4 keV," Progress in Nuclear Energy, Vol. 3, pp.87-124, Pergamon Press Ltd. (1979).

(35.) Intra-Laboratory Correspondence from G. deSaussure and J.H. Marable to Bryan Broadhead, March 30, 1981.

(36.) R.E. MacFarlane, "ENDF/B-IV and V Cross Section Libraries for Thermal Power Reactor Analysis," Nuclear Cross Sections for Technology Proceedings, NBS Special Publication 594 (1979).

(37.) E.T. Tomlinson, G. deSaussure, and C.R. Weisbin, "Sensitivity Analysis of TRX-2 Lattice Parameters with Emphasis on Epithermal ^{238}U Capture," EPRI NP-346 (March 1977).

APPENDICES

APPENDIX A

GENERALIZED LINEAR LEAST SQUARES SIMPLIFIED

This Appendix is intended for the reader that is not familiar with the concept of Generalized Linear Least Squares. A comparison is made to Standard Least Squares since it is more widely known than Generalized Least Squares. In Standard Least Squares using a linear model for simplicity we write:

$$y(x) = ax + b, \qquad \text{A-1}$$

where we desire to obtain estimates of the values of a and b. We do so by obtaining by some observation the quantities y_i and x_i, for i=1, N. If we let the so-called chi-squared (χ^2) be:

$$\chi^2 = \sum_N (y(x_i)-y_i)^2 \qquad \text{A-2}$$

$$= \sum_N (ax_i+b-y_i)^2$$

We then take the partial derivatives of χ^2 with respect to a and b and set them to zero, then solve for a and b. This gives us a linear model that "best" fits our data points based on our definition of "best" as being the minimum of the squares of the differences of y(x) and y.

The Generalized Linear Least Squares technique seeks to minimize chi-squared given as,

$$\chi^2 = (y_1' - y_1)^2/\sigma_{y1}^2 + (x_1' - x_1)^2/\sigma_{x1}^2 \qquad \text{A-3}$$

with the constraint that

$$y_1' = \bar{y}_1 + a(x_1' - x_1) \ ,$$

where,

$$\bar{y}_1 = f(x_1) \ ,$$

and y_1' and x_1' are the resulting adjusted or new best estimates of x_1 and y_1. These equations are valid only for scalar quantities, however.

Generalizing the previous equations to vectors of differing order, we now minimize:

$$\chi^2 = (r' - r)^{+}V^{-1}(r' - r) \ + \ (p' - p)^{+}M^{-1}(p' - p) \ , \qquad \text{A-4}$$

with the constraint that

$$r' = \bar{r} + G(p' - p),$$

$$\bar{r} = f(p),$$

where,

$$r' = \begin{pmatrix} y_1' \\ y_2' \\ \cdot \\ \cdot \\ y_n' \end{pmatrix}, \quad \bar{r} = \begin{pmatrix} \bar{y}_1 \\ \bar{y}_2 \\ \cdot \\ \cdot \\ \bar{y}_n \end{pmatrix}, \quad V = \begin{pmatrix} \sigma_{y1}^2 & & & & \\ \cdot & \sigma_{y2}^2 & & & \\ \cdot & \cdot & \cdot & & \\ \cdot & \cdot & \cdot & \cdot & \\ \cdot & \cdot & \cdot & \cdot & \sigma_{yn}^2 \end{pmatrix} \ ,$$

$$p' = \begin{pmatrix} x_1' \\ x_2' \\ \cdot \\ \cdot \\ x_m' \end{pmatrix}, \quad p = \begin{pmatrix} x_1 \\ x_2 \\ \cdot \\ \cdot \\ x_m \end{pmatrix}, \quad M = \begin{pmatrix} \sigma_{x1}^2 & & & & \\ \cdot & \sigma_{x2}^2 & & & \\ \cdot & \cdot & \cdot & & \\ \cdot & \cdot & \cdot & \cdot & \\ \cdot & \cdot & \cdot & \cdot & \sigma_{xm}^2 \end{pmatrix},$$

$$G = \begin{pmatrix} a_{11} & & & & \\ a_{21} & a_{22} & & & \\ \cdot & \cdot & \cdot & & \\ \cdot & \cdot & \cdot & \cdot & \\ \cdot & \cdot & \cdot & \cdot & a_{nm} \end{pmatrix},$$

where the dots indicate additional elements and all matrices are symmetric.

To see the motivation behind this procedure we apply it to the evaluation or adjustment of nuclear cross sections. We begin by giving meanings to each of the variables above. The p values correspond to differential cross section measurements, and the r values correspond to integral parameter measurements (i.e. K_{eff}, breeding ratio, reactivity worth, etc.). The G matrix corresponds to sensitivity coefficients of the integral parameters to the differential cross sections. The integral measurements can thus be combined with the cross section measurements to obtain "best" estimates of both the differential cross sections and the integral parameters based on the definitions of "best" as implied in χ^2.

APPENDIX B

BASIC DOPPLER BROADENING FOR RESONANCE PARAMETER SENSITIVITY EQUATIONS

Doppler Broadening the resonance parameter sensitivities follows closely that of the MINX algorithm for cross sections. First, we write the basic equation:

$$\sigma_x(E,T_2) = \frac{1}{2E}\sqrt{\alpha/\pi}\int_0^\infty dE_r E_r^{1/2}\sigma_x(E_r,T)$$

$$\cdot\left[e^{-\alpha(E^{1/2}-E_r^{1/2})^2} - e^{-\alpha(E^{1/2}+E_r^{1/2})^2}\right] , \qquad \text{B-1}$$

with

$$\alpha = A/k(T_2-T_1) ,$$

then differentiate with respect to the resonance parameter, q_k;

$$\frac{\partial\sigma_x(E,T_2)}{\partial q_k} = \frac{1}{2E}\sqrt{\alpha/\pi}\int_0^\infty dE_r E_r^{1/2}\frac{\partial\sigma_x(E_r,T_1)}{\partial q_k} \qquad \text{B-2}$$

$$\cdot\left[e^{-\alpha(E^{1/2}-E_r^{1/2})^2} - e^{-\alpha(E^{1/2}+E_r^{1/2})^2}\right] .$$

Next, we assume a linear form of the sensitivity functions,

$$\frac{\partial\sigma(E)}{\partial q_k} = A_n + B_n E , \qquad \text{B-3}$$

where

$$A_n = \frac{E_{n+1}\left.\frac{\partial\sigma}{\partial q_k}\right|_n}{E_{n+1}-E_n} - \frac{E_n\left.\frac{\partial\sigma}{\partial q_k}\right|_{n+1}}{E_{n+1}-E_n} ,$$

$$B_n = \frac{\frac{\partial\sigma}{\partial q_k}\Big|_{n+1}}{E_{n+1} - E_n} - \frac{\frac{\partial\sigma}{\partial q_k}\Big|_{n}}{E_{n+1} - E_n} \quad .$$

Changing variables, let

$$x^2 = \alpha E_r \ ,$$

$$y^2 = \alpha E \ .$$

Then equation B-3 becomes:

$$\frac{\partial\sigma(x,T_1)}{\partial q_k} = A_n' + C_n x^2 \qquad \text{B-4}$$

Break the integral in equation B-2 into two integrals,

$$\frac{\partial\sigma(y,T_2)}{\partial q_k} = \frac{\partial\sigma^*(y,T_2)}{\partial q_k} - \frac{\partial\sigma^*(-y,T_2)}{\partial q_k} \quad ,$$

with, B-5

$$\partial\sigma^*(y,T_2) = \frac{1}{y^2}\sqrt{1/\pi}\int_0^\infty x^2 \frac{\partial\sigma(x,T_1)}{\partial q_k} e^{-(x-y)^2} dx.$$

Break the x integration into x_k pieces, and insert equation B-4 into equation B-2.

$$\frac{\partial\sigma^*(y,T_2)}{\partial q_k} = \frac{1}{y^2}\sqrt{1/\pi}\sum_n \int_{x_n}^{x_{n+1}} x^2(A_n' + C_n x^2)\, e^{-(x-y)^2} dx \ , \qquad \text{B-6}$$

Changing variables, let z=x-y,

$$\frac{\partial\sigma^*(y,T_2)}{\partial q_k} = \frac{1}{y^2}\sqrt{1/\pi}\sum_n \int_{x_n-y}^{x_{n+1}-y} [C_n'z^4 + 4C_n'yz^3 + (A_n' + 6C_n'y^2)z^2 +$$

$$(2A_n'y + 4C_n'y^3)z + (A_n'y^2 + C_n'y^4)]\, e^{(-z^2)}\, dz \quad . \qquad \text{B-7}$$

The above expression can be written exactly in terms of the functions,

$$H^n(a,b) = F^n(a) - F^n(b) \ ,$$
$$F^n(a) = 2/\sqrt{\pi} \int z^n\, e^{(-z^2)}\, dz \ , \ n=0,1,2,3,... \quad . \qquad \text{B-8}$$

It has been determined that n=0,1,2,3,4 is sufficient for Doppler broadening. Thus, writing equation B-7 in terms of H^n,

$$\frac{\partial\sigma^*(y,T_2)}{\partial q_k} = \frac{1}{2y^2}\sum_n C_n'H^4(z_{n+1},z_n) + 4C_n'yH^3(z_{n+1},z_n)$$
$$+ (A_n' + 6C_n'y)H^2(z_{n+1},z_n) + (2A_n'y + 4C_n'y^3)H^1(z_{n+1},z_n)$$
$$+ (A_n'y^2 + C_n'y^4)H^0(z_{n+1},z_n) \ , \qquad \text{B-9}$$

where,

$$z_{n+1} = x_{n+1} - y \ ,$$
$$z_n = x_n - y \ ,$$
$$F^0(a) = \mathrm{erf}(a) \ ,$$
$$F^1(a) = \sqrt{1/\pi}\ [\ 1 - e^{(-a^2)}\ ] \ ,$$
$$F^2(a) = 1/2\ \mathrm{erf}(a) - a/\sqrt{\pi}\, e^{(-a^2)} \ ,$$
$$F^3(a) = \sqrt{1/\pi}\ [\ 1 - (\ 1 + a^2\ )\, e^{(-a^2)}\ ] \ ,$$
$$F^4(a) = 3/4\ \mathrm{erf}(a) - \sqrt{1/\pi}\ (3/2\ a + a^3)\, e^{(-a^2)} \ .$$

APPENDIX C

J FUNCTION DERIVATIVES FOR Γ_γ

For the case of Γ_γ, $P_\nu(\Gamma_\gamma)$ is a delta function such that,

$$\frac{\partial \langle \Gamma_\gamma J \rangle}{\partial \Gamma_\gamma(E^*)} = \int_0^\infty P_\mu(\Gamma_\chi) d\Gamma_\chi \left[\Gamma_\gamma(E^*) \frac{\partial J(\Gamma_\chi, \Gamma_\gamma)}{\partial \Gamma_\gamma(E^*)} + J(\Gamma_\chi, \Gamma_\gamma) \right] \qquad \text{C-1}$$

Thus it is necessary to evaluate the derivatives of the J function with respect to Γ_γ. We first write the generalized J function as:

$$J(\beta,\theta,a,b) = J(\beta,\theta) + I(\beta,\theta,a) - bM(\beta,\theta,a), \qquad \text{C-2}$$

where,

$$J(\beta,\theta,a,b) = 1/2 \int_{-\infty}^{\infty} dx \frac{T\psi + b\chi}{\beta + s\psi + a\chi} ,$$

$$J(\beta,\theta) = T \int_0^\infty dx \frac{\psi}{\beta + S\psi} ,$$

$$M(\beta,\theta,a) = a \int_0^\infty dx \frac{\chi^2}{(\beta + S\psi)^2 - a^2\chi^2} ,$$

$$I(\beta,\theta,a) = Ta^2 \int_0^\infty dx \frac{\psi}{\beta + S\psi} \frac{\chi^2}{(\beta + S\psi)^2 - a^2\chi^2} ,$$

and T = S = 1 for single level resonances, and b = 0 for capture or fission and b = a for total.

It is important to point out that $J(\beta,\theta)$ is the function needed for the ETOX algorithm, while $J(\beta,\theta,a,b)$ is needed for both UXS and MC^2-2 algorithms. Thus, the derivatives for $J(\beta,\theta,a,b)$ will suffice for all three methods.

First using the chain rule,

$$\frac{\partial J(\beta,\theta,a,b)}{\partial \Gamma_\gamma} = \frac{\partial J(\beta,\theta,a,b)}{\partial \beta}\frac{\partial \beta}{\partial \Gamma_\gamma} + \frac{\partial J(\beta,\theta,a,b)}{\partial \theta}\frac{\partial \theta}{\partial \Gamma_\gamma} , \qquad \text{C-3}$$

where

$$\frac{\partial \beta}{\partial \Gamma_\gamma} = \frac{\Gamma_\gamma}{\beta} ,$$

$$\frac{\partial \theta}{\partial \Gamma_\gamma} = \frac{\Gamma_\gamma}{\theta} .$$

The basic algorithm for the evaluation for $J(\beta,\theta,a,b)$ is taken from reference 12 and the reader is referred there for further considerations.

We begin our derivation by defining:

$$T1 = \frac{\beta + \psi(\theta,0)}{\psi(\theta,0)} . \qquad \text{C-4}$$

For $T1 < 4.5$ J, M, and I are evaluated using a Gauss-Jacobi integration scheme[12]. Thus for $T1 < 4.5$ we simply take derivatives of J, M, and I with respect to β and θ, and evaluate them using the same numerical procedure as the J function. The derivatives are as follows:

$$\frac{\partial J}{\partial \beta} = -T \int_0^\infty dx \, \frac{\psi}{(\beta + S\psi)^2} \quad , \qquad \text{C-5}$$

$$\frac{\partial J}{\partial \theta} = T \int_0^\infty dx \, \left[\frac{1}{\beta + S\psi} \frac{\partial \psi}{\partial \theta} - \frac{\psi}{(\beta + S\psi)^2} \frac{\partial \psi}{\partial \theta} \right] \quad , \qquad \text{C-6}$$

$$\frac{\partial M}{\partial \beta} = -a \int_0^\infty dx \, \frac{\chi^2 [2(\beta + S\psi)]}{[(\beta + S\psi)^2 - a^2\chi^2]^2} \quad , \qquad \text{C-7}$$

$$\frac{\partial M}{\partial \theta} = a \int_0^\infty \frac{2[(\beta + S\psi)^2 - a^2\chi^2]\chi \frac{\partial \chi}{\partial \theta} - \chi^2 [2(\beta + S\psi)\frac{\partial \psi}{\partial \theta} - 2a^2 \chi \frac{\partial \chi}{\partial \theta}]}{[(\beta + S\psi)^2 - a^2\chi^2]^2} \quad ,$$

with

$$\frac{\partial \chi}{\partial \theta} = \frac{\theta}{2} \left[\left(\frac{2}{\theta^2} - \chi^2 + 1 \right) \chi(x,\theta) + 4x\psi(x,\theta) + 2x \right] \quad ,$$

$$\frac{\partial \psi}{\partial \theta} = \frac{\theta}{2} \left[\left(\frac{2}{\theta^2} - \chi^2 + 1 \right) \psi(x,\theta) + x\chi(x,\theta) - 1 \right] \quad ,$$

Since the integrand of I is equal to the product of the integrand of J and M, the I derivatives follow.

For T1 > 4.5, J and its derivatives can be approximated as follows:

$$J(\beta,\theta) \cong \frac{\pi}{2(\beta + \rho)} + \frac{1}{(\beta + \rho)^3} \left[\int_0^\infty \psi^3 dx - (\pi/2)\rho^2 \right] \quad , \qquad \text{C-8}$$

$$\frac{\partial J}{\partial \beta} \cong \frac{-2\pi}{4(\beta + \rho)^2} - \frac{3}{(\beta + \rho)^4} \left[\int_0^\infty \psi^3 dx - (3\pi/2)\rho^2 \right] \quad , \qquad \text{C-9}$$

$$\frac{\partial J}{\partial \theta} \cong \frac{-2\pi}{4(\beta + \rho)^2} \frac{\partial \rho}{\partial \theta} + \frac{\frac{\partial}{\partial \theta} \int \psi^3 dx - \pi\rho \frac{\partial \rho}{\partial \theta}}{(\beta + \rho)^3} \qquad \text{C-10}$$

$$- \frac{3 \int_0^\infty \psi^3 dx - (3\pi/2)\rho^2}{(\beta + \rho)^4} \frac{\partial \rho}{\partial \theta} \quad ;$$

$$M(\beta, \theta, a) = \frac{\pi a \rho}{(\beta + \rho)^2} + \frac{4a/3 \int_0^\infty \psi^3 dx - (\pi/2)\rho^2}{(\beta + \rho)^3} \quad , \qquad \text{C-11}$$

$$\frac{\partial M}{\partial \beta} = \frac{-2\pi a \rho}{(\beta + \rho)^3} - \frac{4a \int_0^\infty \psi^3 dx - (3\pi/2)\rho^2}{(\beta + \rho)^4} \quad , \qquad \text{C-12}$$

$$\frac{\partial M}{\partial \theta} = \frac{\pi a}{(\beta + \rho)^2} \frac{\partial \rho}{\partial \theta} - \frac{2\pi a \rho}{(\beta + \rho)^3} \frac{\partial \rho}{\partial \theta} + \frac{4a/3 \frac{\partial}{\partial \theta} \int_0^\infty \psi^3 dx - \pi\rho \frac{\partial \rho}{\partial \theta}}{(\beta + \rho)^3} \qquad \text{C-13}$$

$$- \frac{4a \int_0^\infty \psi^3 dx - (3\pi/2)\rho^2}{(\beta + \rho)^4} \frac{\partial \rho}{\partial \theta} \quad ;$$

$$I(\beta, \theta, a) \cong \frac{4a^2/3 \int_0^\infty \psi^3 dx}{(\beta + \rho)^3} \quad , \qquad \text{C-14}$$

$$\frac{\partial I}{\partial \beta} = \frac{-4a^2 \int_0^\infty \psi^3 dx}{(\beta + \rho)^4} \quad , \qquad \text{C-15}$$

$$\frac{\partial I}{\partial \theta} = \frac{4a^2/3 \frac{\partial}{\partial \theta} \int_0^\infty \psi^3 dx}{(\beta + \rho)^3} - \frac{4a^2 \int_0^\infty \psi^3 dx}{(\beta + \rho)^4} \frac{\partial \rho}{\partial \theta} \quad , \qquad \text{C-16}$$

where

$$\rho = 1/2\psi(\sqrt{2\theta},0) \quad ,$$

$$\frac{\partial \rho}{\partial \theta} = \frac{\theta}{2} \left(\frac{1}{\theta^2} + 1\right) \psi(\sqrt{2\theta},0) - 1] \quad .$$

We now need to evaluate $\int_0^\infty \psi^3 dx$ and its derivatives.

$$\int_0^\infty \psi^3 dx = 3\xi \quad , \qquad \text{C-17}$$

for $\theta \leq \sqrt{6}$,

$$\xi = \frac{\pi}{2}\{\rho[\psi(0,\sqrt{2\theta/3}) - \sqrt{\pi/6}\,\theta \exp(\theta^2/6)] + \frac{\theta^2}{2}\left(\frac{1}{4} + \sum_{n=1}^{\infty} \left[\frac{1}{4} + \sum_{m=1}^{n} B_m (\theta^2)^m\right] A_n\right)\}, \qquad \text{C-18}$$

$$A_n = \frac{n!}{(1 \cdot 3 \cdot 5 \cdots (2n+1)} \quad ,$$

$$B_m = \frac{(2/3)^m}{4m!} \quad ,$$

$$\frac{\partial \xi}{\partial \theta} = \frac{\pi}{2} \left\{ \frac{\partial \rho}{\partial \theta} \left[\psi(0, \sqrt{2/3}\theta) - \sqrt{\pi/6}\,\theta \exp(\theta^2/6) \right] \right. \qquad \text{C-19}$$

$$+ \rho \left[\frac{\partial \psi(0, \sqrt{2/3}\theta)}{\partial \theta} - \sqrt{\pi/6} \left[\exp(\theta^2/6) + \frac{1}{3}\theta^2 \exp(\theta^2/6) \right] \right.$$

$$\left. \left. + \theta \left(\frac{1}{4} + \sum_{n=1}^{\infty} \left[\frac{1}{4} + \sum_{m=1}^{n} B_m (\theta^2)^m \right] A_n + \frac{1}{2}\theta^2 \left[\sum_{n=1}^{\infty} A_n \sum_{m=1}^{n} B_m 2m \theta^{2m-1} \right] \right) \right\} .$$

For $\theta > \sqrt{6}$,

$$\xi = \frac{\pi}{8} \left[\frac{3}{2}\varepsilon - \sum_{n=1}^{\infty} h_n \right] , \qquad \text{C-20}$$

$$\varepsilon = 2\theta^2/3 \exp(2/3\theta^2) E_1(2\theta^2/3) ,$$

$$h_1 = 1 - \varepsilon ,$$

$$h_2 = 3\theta^2/2 - h_1 ,$$

$$h_3 = 5/9 \left[9/\theta^4 - 2h_2 \right] ,$$

$$h_4 = 7/2 \left[15\theta^4/2 - h_3/3 \right] ,$$

Note: the series is truncated at n=4.

$$E_1(x) \cong \frac{\left[x(x + 4.03640) + 1.15198 \right]}{x(x + 5.03637) + 4.19160} \qquad \text{for } x \geq 10 , \qquad \text{C-21}$$

$$\cong \frac{x(x + 2.334733) + 0.250621}{x(x + 3.330657) + 1.681534} \qquad \text{for } x < 10.$$

$$\frac{\partial \xi}{\partial \theta} = \frac{\pi}{8}\left[\frac{3}{2}\frac{\partial \varepsilon}{\partial \theta} - \sum_{n=1}^{\infty}\frac{\partial h_n}{\partial \theta}\right] , \qquad \text{C-22}$$

$$\frac{\partial \varepsilon}{\partial \theta} = \frac{2x + 2.334733}{2x + 3.330657} \quad \text{for } x < 10 , \qquad \text{C-23}$$

with $x = 2\theta^2/3$,

$$\frac{\partial h_1}{\partial \theta} = -\frac{\partial \varepsilon}{\partial \theta} ,$$

$$\frac{\partial h_2}{\partial \theta} = -\frac{3}{\theta^3} - \frac{\partial h_1}{\partial \theta} ,$$

$$\frac{\partial h_3}{\partial \theta} = \frac{5}{9}\left[-\frac{36}{\theta^5} - 2\frac{\partial h_2}{\partial \theta}\right] ,$$

$$\frac{\partial h_4}{\partial \theta} = \frac{7}{2}\left[-\frac{30}{\theta^5} - \frac{1}{3}\frac{\partial h_3}{\partial \theta}\right] .$$

Finally, for $\beta > 10^{10}$,

$$J = \frac{\pi}{2}\frac{1}{\beta + \rho} , \qquad \text{C-24}$$

$$\frac{\partial J}{\partial \beta} = -\frac{\pi}{2}\frac{1}{(\beta + \rho)^2} , \qquad \text{C-25}$$

$$\frac{\partial J}{\partial \theta} = -\frac{\pi}{2}\frac{1}{(\beta + \rho)^2}\frac{\partial \rho}{\partial \theta} . \qquad \text{C-26}$$

APPENDIX D

GENERALIZED LINEAR LEAST SQUARES

We start with formula III-9 in Chapter III,

$$f(p_o/r_o) = \frac{g(r_o/p_o)f(p_o)}{\int_p g(r_o/p)f(p)dp} \qquad \text{D-1}$$

Placing the expressions for $g(r_o/p)$ and $f(p)$ into the numerator of equation D-1 yields,

$$g(r_o,p)f(p) = c_r c_p \exp\left[-\frac{1}{2}\{(r_o - \bar{r})^{+}V^{-1}(r_o - \bar{r}) - 2(p - \bar{p})^{+}G^{+}V^{-1} \cdot (r_o - \bar{r}) + (p - \bar{p})^{+}G^{+}V^{-1}G(p - \bar{p}) + (p - \bar{p})^{+}M^{-1}(p - \bar{p})\}\right] . \qquad \text{D-2}$$

In the evaluation of the denominator term the quantity $\exp[-.5(r_o - \bar{r})^{+}V^{-1}(r_o - \bar{r})]$ can be brought outside of the integral. The remaining expressions in the integral integrate to a normalization constant. Thus,

$$f(p/r_o) = c\cdot\exp\left[-\frac{1}{2}[(p - \bar{p})^{+}G^{+}V^{-1}G(p - \bar{p}) - 2(p - \bar{p})^{+}G^{+}V^{-1}(r_o - \bar{r}) + (p - \bar{p})^{+}M^{-1}(p - \bar{p})]\right] \qquad \text{D-3}$$

$$= c'\cdot\exp\left[-\frac{1}{2}(p - p')^{+}M'^{-1}(p - p')\right] ,$$

with p' the mean and M' the variance-covariance matrix of $f(p/r_o)$.

The above expression must hold for any p, thus the coefficients of terms quadratic in p on the LHS must equal the coefficients of terms quadratic in p on the RHS. The same holds for the coefficients of terms linear in p. First equating the coefficients of terms quadratic in p gives:

$$p^{+}M'^{-1}p = p^{+}G^{+}V^{-1}Gp + p^{+}M^{-1}p$$

$$= p^{+}(G^{+}V^{-1}G + M^{-1})\, p \quad . \qquad \text{D-4}$$

Therefore,

$$M'^{-1} = G^{+}V^{-1}G + M^{-1} \quad . \qquad \text{D-5}$$

Similarly for the terms linear in p,

$$-2[p^{+}M'^{-1}p'] = -2p^{+}[G^{+}V^{-1}(r_o - \bar{r}) + M'^{-1}\bar{p}] \quad , \qquad \text{D-6}$$

and thus,

$$M'^{-1}(p' - \bar{p}) = G^{+}V^{-1}(r_o - \bar{r}) \qquad \text{D-7}$$

Now substitute eq. D-5 into eq. D-7 to obtain,

$$M^{-1}(p' - \bar{p}) = G^{+}V^{-1}(r_o - \bar{r} - G(p' - \bar{p})) \qquad \text{D-8}$$

Now letting,

$$x = V^{-1}[r_o - \bar{r} - G(\bar{p} - p)] \quad , \qquad \text{D-9}$$

$$(p' - \bar{p}) = MG + x \qquad \text{D-10}$$

Multiplying eq. D-10 by G from the left,

$$G(p' - \bar{p}) = GMG^{+} + x$$

Now defining $N = GMG^{+}$,

$$G(p' - \bar{p}) = Nx \qquad \text{D-11}$$

Using eq. D-11 and eq. D-9 we obtain,

$$x = V^{-1}[r_o - \bar{r} - Nx] ,$$

$$x = (N + V)^{-1} (r_o - \bar{r}) . \qquad \text{D-12}$$

Now combine eq. D-12 and eq. D-10 to obtain,

$$p' - \bar{p} = MG^{+}(N + V)^{-1}(r_o - \bar{r}) \qquad \text{D-13}$$

For the reduction of the equation for M' we start with our previous result,

$$M'^{-1} = G^{+}V^{-1}G + M^{-1} ,$$

then we write

$$M' = (G^{+}V^{-1}G + M^{-1})^{-1} \qquad \text{D-14}$$

Beginning with an identity,

$$1 = MM^{-1} = MM^{-1} + MG^{+}V^{-1}G - MG^{+}V^{-1}G$$

$$= M(M^{-1} + G^{+}V^{-1}G) - MG^{+}V^{-1}G . \qquad \text{D-15}$$

Also,

$$MG^{+}V^{-1}G = MG^{+}(N + V)^{-1}(N + V)V^{-1}G$$

$$= MG^{+}(N + V)^{-1}(NV^{-1}G + G)$$

$$= MG^{+}(N + V)^{-1}(GMG^{+}V^{-1}G + GMM^{-1})$$

$$= MG^{+}(N + V)^{-1}GM(M^{-1} + G^{+}V^{-1}G) \qquad \text{D-16}$$

Substitute eq. D-15 into eq. D-14 to obtain

$$1 = M - MG^{+}(N + V)^{-1}GM(M^{-1} + G^{+}V^{-1}G) \quad .$$

Then we have

$$(M^{-1} + G^{+}V^{-1}G)^{-1} = M - MG^{+}(N + V)^{-1}GM \qquad \text{D-17}$$

Comparing eq. D-17 and eq. D-14 we immediately write down the result,

$$M' = M - MG^{+}(N + V)^{-1}GM \qquad \text{D-18}$$

Equations D-13 and D-18 are now the final results.

APPENDIX E

DEFUNCT USERS MANUAL

The DEFUNCT computer code was written to test the methodology developed herein and is not intended to be used as a production code. As is the case with many cross section processing codes, the user input is very simple and the successful processing of certain materials very difficult. This paradox is due mainly to the vast amount of computing time, input-output operations, and core storage needed and their resulting complexities. For these reasons the novice user is cautioned against use of the code without a good knowledge of the inherent complexities of cross section processing codes. A graphic example of this is the processing of ^{238}U. The author has yet to complete a run for all the resonance parameters of ^{238}U. In general, approximately 200 minutes of IBM 3033 CPU time are required in order to process the ^{238}U cross sections only. The sensitivity coefficient generation is then added onto the already mammouth problem. The only way to thus attack such a material is to process "groups" of resonances individually. There are many possible ways of speeding up these calculations, but these are to be parts of future studies.

The DEFUNCT code flow path can be broken into two distinct paths as shown in figure E.1. The resolved region is completely new programming while the unresolved region methodology has been incorporated into the MINX code. The following section gives a brief summary of the user input to the DEFUNCT code.

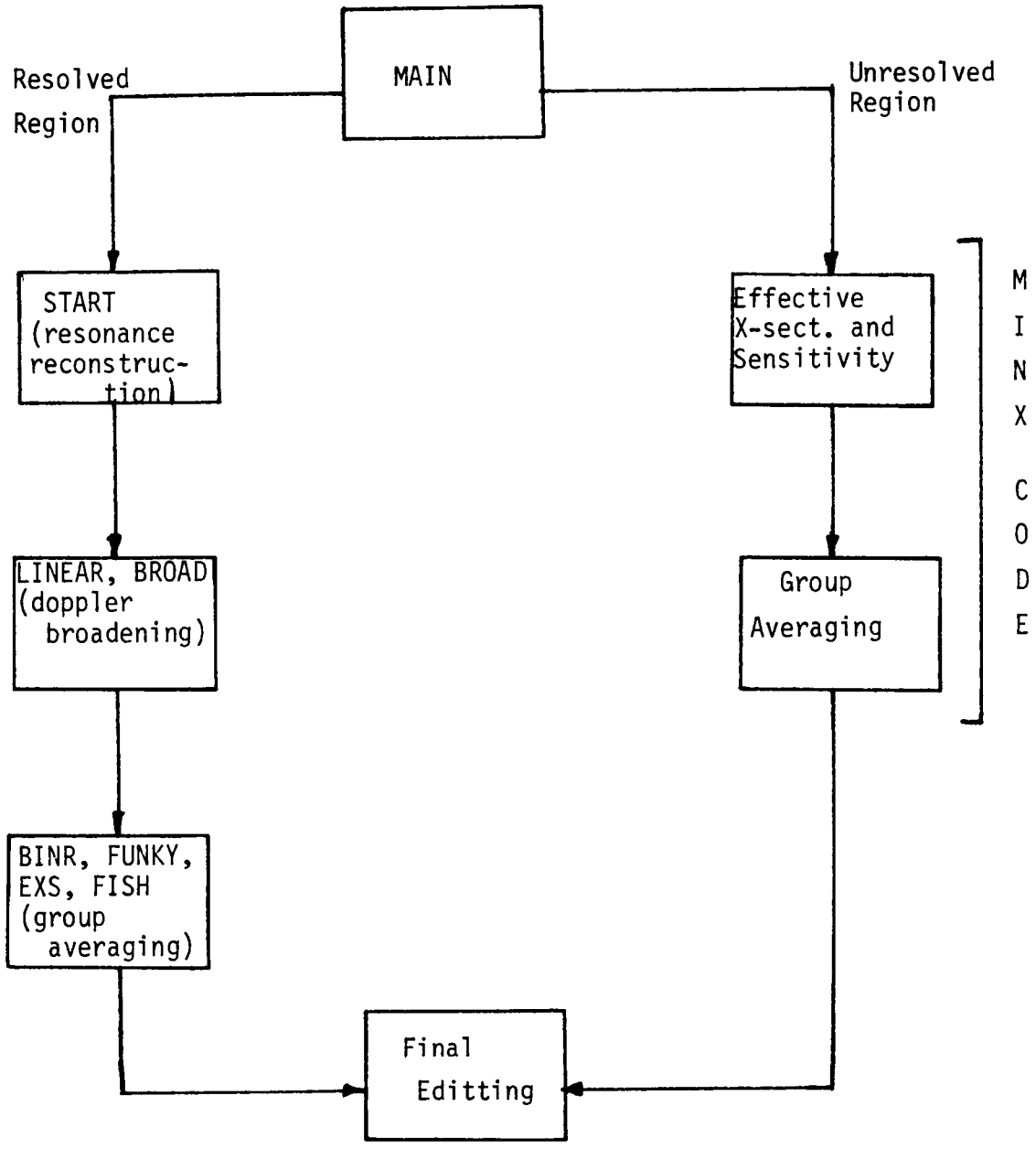

Figure E-1. DEFUNCT code flowpath

USER INPUT

Card 1 (9I5)

NGROUP - Number of user groups

MAT - material to be processed

DUM - not used enter 0

NSIG - Number of sigma zeroes to be processed (in addition to infinite dilution)

NTEMP - Number of temperatures to be processed (in addition to 0° K)

NOLVP - Sequence-sequence overlap option (0/1 - no/yes)

DUM1 - not used

ICODE - 1/2/3 - Option for unresolved calculations (ETOX/UXS/MC^2)

Card 2 (6E12.5)

Sigma zero values

Card 3 (6E12.5)

Temperatures

Card 4 (6E12.5)

User group structure (low-to-high energies)

This terminates the user input for DEFUNCT.

LOGICAL UNITS USED

File description	Logical Unit Number
Scratch	2-3
ENDF/B tape	10
Scratch	35-44
Scratch	50-52
Resolved resonance sens. output	60
Unresolved resonance sens. output	61

ERROR STOPS

STOP 1 - Number of user groups greater than 100 not allowed.

STOP 2 - Number of sigma zero values cannot exceed 5.

STOP 3 - Number of Temperatures cannot exceed 5.

STOP 4,6 - Number of points per resonance cannot exceed 1000.

STOP 5 - Number of Union points (i.e. for all resonances) cannot exceed 30,000 points.

STOP 1234 - Only single- and multi-level Breit-Wigner cross sections are allowed.

STOP 9999 - Number of ENDF/B file points cannot exceed 5000.

APPENDIX F

PEREY METHOD

Perey's expression for the contribution of a single resonance, i, to a given group cross section (assuming the resonance is wholly contained in that group) can be written as[28]:

$$\phi_g \sigma_{cg}{}^i = \frac{c_o{}^i}{\sigma_b{}^i} A_{\gamma i} f(\theta^i, \beta^i) \qquad \text{F-1}$$

with,

$c_o{}^i = c(E_o{}^i)$,

$\sigma_b{}^i$ = background cross section at $E_o{}^i$,

$A_\gamma{}^i$ = capture resonance area ,

$$\phi_g = \int_{E_g}^{E_{g+1}} \frac{C(E)dE}{\sigma_t(E)} \quad ,$$

$$f(\theta^i, \beta^i) \cong \sqrt{\beta^i/(1+\beta^i)} \quad \text{for } \beta^i < \theta^i\, 2/6 \quad ,$$

$$\cong \sum_\nu \frac{(-1)^r}{\sqrt{\nu+1}} \left(\frac{\theta^i\sqrt{\pi}}{2\beta^i}\right)^\nu \text{ for } \frac{\theta^i\pi}{2\beta^i} < 2 \quad ,$$

$$\cong 4\beta^i/\pi\theta^i \sqrt{\ln(\theta^i\sqrt{\pi}/2\beta^i)} \text{ for } \theta^i\sqrt{\pi}/2\beta^i > 2 \quad .$$

For this simple study the equation used is modified slightly to yield,

$$\sigma_{cg}{}^i = A_\gamma{}^i f(\theta^i, \beta^i)/(E_{g+1} - E_g) \; . \qquad \text{F-2}$$

VITA

Bryan Lamar Broadhead was born in New Orleans, Louisiana on September 5, 1955. He attended elementary school in Dothan, Alabama and Junior High Schools in Dothan, Alabama and Meridian, Mississippi and graduated from Meridian High School in May 1973. The following August he entered Mississippi State University and received a Bachelor of Science degree in Nuclear Enginnering in May 1977. In September 1977 he entered Graduate School at The University of Tennessee, Knoxville and received a Master's degree in Nuclear Engineering in March 1979. He continued his field of study at the University of Tennessee until March 1983 when he was awarded his Doctor of Philosophy degree with a major in Nuclear Engineering.

The author is a member of Tau Beta Pi, Phi Kappa Phi, and Lambda Chi Alpha. Dr. Broadhead is employed with Union Carbide at the Oak Ridge National Laboratory as a computing specialist.

He is married to the former Kathleen Skelton of Forest Park, Georgia and has one child, Kristen Marie born December 27, 1982.